Nanoscale Ordering at the Liquid-Solid Interface using Self-Assembly Principles

Lorenz Kampschulte
10. November 2006

Disputation: 23. April 2007

Referees: Prof. Dr. Wolfgang M. Heckl
                  Prof. Dr. Wolfgang Moritz

Abstract

The focus of this work is on the investigation and the understanding of molecular adsorption at the liquid-solid interface. The liquid-solid interface in this context, is basically defined as a relatively narrow volume between a crystalline solid substrate (e.g. a crystal) and a fluid (e.g. a droplet of solution providing the molecules to be adsorbed). Experiments prove to be an interesting field to investigate the mechanisms and requirements for interfacial self-assembly of molecules. The mobility of the compound within the fluid and the possibility of incessant exchange of structural molecules with the liquid phase above, result in a wealth of possibilities for structure formation, reorganization, and, in some cases subsequent degeneration. Unlike ultra high vacuum (UHV) conditions, this highly dynamic environment gives room for multiple ways controlling the structure formation, through adapting external parameters. Another whole new set of virtualities arises from the choice of solvent, often leading to different structural polymorphs.

Scanning Tunneling Microscopy (STM) has been proven as a very appropriate tool to investigate these self-assembled structures at the liquid-solid interface. STM provides real space images of the molecular networks with near atomic resolution.

In order to achieve self-assembled networks with a high degree of flexibility it was important to choose systems with weak to moderately strong binding behavior, both between molecule and substrate, and amongst the molecules. All selected molecules have mere van der Waals interaction with the substrate in common. In order to promote specific molecule-molecule interaction they are equipped with the ability to form hydrogen bonds. These bonds ideally meet the requirements for well ordered two-dimensional monolayers: On one hand, they are rendering a reorganization of networks possible due to easy connecting and disconnecting, i.e. a comparability between binding energy and thermal energy. On the other hand, they provide sufficient stability within the monolayer, and lead to a well defined geometry between neighboring molecules due to their high directionality.

For this thesis several different hydrogen bonded molecular systems were investigated at the liquid solid interface with scanning tunneling microscopy. Three main topics were targeted during the experiments:

First the attention was drawn to different polymorphic modifications of 1,3,5-Benzenetribenzoic acid (BTB) monolayers. Inspired by results of Lackinger et al. on a different but related molecule with similar symmetry[1], the formation of BTB monolayers was probed in eleven different solvents, resulting in two crystallographically different network structures. Later on, a third structure could be found for solutions older than three months, supposedly based on a degeneration of the solvent.

The second topic dealt with different bimolecular networks, i.e. networks comprised of two different molecules. It could be shown, that the adsorption of 1,3,5-Tris(4-pyridyl)-2,4,6-triazine (TPT) becomes possible at the liquid solid interface, when a second molecular species is provided as linker molecule. Probed under similar conditions the adsorption of TPT itself was not observed despite numerous attempts. Suitable linker molecules are for example trimesic acid (TMA), leading to a hexagonal structure with about 1.6 nm wide cavities, or terephthalic acid (TPA), resulting in a close-packed

bimolecular network. Different network structures could also be prepared using BTB and TMA molecules. Probing a two-dimensional concentration space it was possible to create a phase diagram of the system and to precisely address six different structures, three of them being bimolecular. Furthermore, it was possible to switch these structures in situ by adding solvent thereby diluting the solution.

The third issue addresses dynamic issues at the liquid-solid interface. First, two different molecules were investigated with regard to the stability of domain growth and the fluctuations of their boundaries. Significant differences were found for a one-dimensionally hydrogen bonded structure (TPA) versus a two-dimensionally linked one (TMA), resulting in a considerably higher stability of the latter one. Additionally, three more one-dimensionally hydrogen bound molecules were studied, all of them consisting of two benzoic acid groups, but with variable spacing in between. It was shown that there is no general size-stability relation (as intuitively expected due to the larger area feasible for van der Waals interaction), but the behavior being merely dominated by the local environment, namely the surrounding solution.

This thesis consists of four parts: Starting with an introduction and a brief review of the theory about scanning tunneling microscopy, the experimental details are described, including the characteristics of the adsorbate as well as the solvent molecules. In the following part (chapter 4) the experimental results are detailed. The first section (chapters 4.1 - 4.4) contains results already published in scientific journals (due to the form of this cumulative dissertation, in this section only summaries of the publications can be found, complete manuscripts are attached in the appendix). The second part of chapter 4 shows succeeding results not yet published. The dissertation ends with a conclusion of the investigations conducted.

Content

List of Abbreviations

AFM	Atomic Force Microscopy
BPDA	4,4'-Biphenyldicarboxylic acid
BTB	1,3,5-Benzenetribenzoic acid
EC-STM	Electrochemical STM
FFT	Fast Fourier Transformation
HOPG	Highly Oriented Pyrolytic Graphite
H-bond	Hydrogen bond
IVC	CurrentVoltage Converter
LDOS	Local Density of States
LEED	Low Energy Electron Diffraction
NDA	2,6-Naphthalenedicarboxylic acid
SDA	4,4'-Stilbenedicarboxylic acid
STM	Scanning Tunneling Microscope
TPD	Temperature Programmed Desorption
TMA	Trimesic acid
TPA	Terephthalic acid
TPT	1,3,5-Tris(4-pyridyl)-2,4,6-triazine
UHV	Ultra High Vacuum

1. Introduction

The liquid-solid interface provides an ideal environment to investigate self-assembly phenomena and to probe structures and properties of physisorbed monolayers at the nanoscale. The control of the lateral assembly and spatial arrangement of micro- and nano-objects at interfaces is often a prerequisite for potential applications, e.g. in areas such as lubrication, patterning of functional surfaces, and thin film based organic electronic devices. There are several ways to create two-dimensional patterns in the nanometer range. Basically one has to distinguish between two fundamentally different approaches: active patterning includes all techniques where the constituents of the structures are positioned through direct manmade guidance. This includes the well known lithography processes used in the semiconductor industry like optical lithography, interference lithography, and e-beam writing, but also scanning probe microscopy (SPM) manipulation techniques like AFM dip pen nanolithography[2-4], local oxidation with AFM[5-7], and atomic manipulation with STM, which was impressively shown by Don Eigler and coworkers[8-10], and many others[11-14]. The passive techniques include all approaches without guidance or management from an outside source to build defined structures with dimensions on the nanometer scale. This are for instance the lattice mismatch hetero-epitaxy[15-17] or overgrowth[18] methods used to produce quantum dots, self-ordered ligand stabilized nano-objects[19,20], and molecular self-assembly methods[21-25].

Self-assembly is a natural phenomenon that can be observed in many biological, chemical, and physical processes[26,27]. Moreover, it plays a crucial role in the emergence of life[28], since the basic coding of information in all living organisms is based on self-assembly methods. The self-assembly processes of single molecules at surfaces can be classified into two groups, in accordance to their binding properties: Chemisorption - where a adsorbate molecule adheres to a surface through the formation of a chemical bond, modifies substrate properties such that they significantly differ from those of the pristine substrate. Chemisorbed self-assembled monolayers[29] are thus of prime interest for technological applications. In contrast to chemisorption, physisorption (resulting from a weak physical force) is not very suitable for making 'permanent', i.e. highly stable structures. Nevertheless, physisorbed adsorbate layers are perfect model systems to investigate the interplay between molecular structure and the formation of ordered assemblies in two dimensions with high spatial resolution. The dynamical behavior of liquid-solid interfaces commonly observed for our systems – where molecules can adsorb on and desorb from the surface in equilibrium with the supernatant solvent – provides an environment in which two-dimensional crystals can be formed and dissolved depending on the surrounding conditions.

To preserve and further increase this flexibility and mobility of the structures it is obvious to use physical forces as intermolecular bonds within the monolayer networks likewise. They can reversibly be formed and broken during the organization process. An intensely investigated and for our systems perfectly suited type of intermolecular physical forces are so-called hydrogen bonds. Although stronger than van der Waals intermolecular forces, the typical hydrogen bond is much weaker than both the ionic bond and the covalent bond (hydrogen-bond: 4 … 40 kcal/mol)[30], furthermore hydrogen bonds feature a high degree of directionality (bond angles 175°-180° for strong H-bonds

(14 ... 40 kcal/mol))[30], and, depending on the system, selectivity. Carboxylic acid functionality plays a key role in this content, since it exhibits two robust hydrogen bonds with itself leading to an even higher degree of directionality. The hydroxyl group of the acid acts as a hydrogen bond donor, the carbonyl oxygen as an acceptor. In a symmetrical, polyfunctional disposition, the interplay of multiple hydrogen-bonds leads to well organized structures on surfaces and in bulk crystals. For instance, the para-position of the carboxylic groups in terephthalic acid (TPA) results in formation of hydrogen bonded linear chains on a surface.[31,32] Also, the relative position of functional groups attached to a core molecules can be exploited to steer the self-assembly process.[31,33] Among hydrogen bonded supramolecular structures, two-dimensional template structures enable ordering[23,34,35] and addressing of nanometer sized objects such as clusters[36-38] or functional molecules[39,40] on surfaces with subnanometer precision. These template structures exhibit a periodic arrangement of cavities of various size and shape, where the guest species can be confined in. As shown by our group several years ago, the archetypical supramolecular model system trimesic acid is well suited for this purpose. STM experiments in an UHV environment with evaporated TMA monolayers on graphite(0001) revealed two different polymorphs: chicken-wire and flower structure[41]. Both structures are governed by intermolecular hydrogen bonding and exhibit a periodic arrangement of approximately 1.0 nm wide circular cavities. Similarly, a TMA chicken-wire structure was found on Cu(100)[42]. However, due to stronger interaction with the metal substrate, the TMA lattice was slightly distorted and no large domains could be grown. Among others, a TMA chicken-wire structure was realized on Au(111) in an electrochemical STM study for suitable potential conditions[43]. Another EC-STM study of TMA, equally on Au(111) found various densely packed phases with upright molecules and potential driven phase transitions, revealing the influence of a stronger adsorbate-substrate interaction[44]. In addition, a more comprehensive EC-STM study of TMA on Au(111) complemented by ATR SEIRAS (attenuated total reflection surface enhanced infra red adsorption spectroscopy) found phases with upright TMA molecules and coadsorbed interfacial water molecules inhibiting intermolecular hydrogen bonds between TMA molecules[45]. Bai et al. succeeded in growing and characterizing a hexagonal two-dimensional host system, likewise on HOPG with an enlarged cavity diameter of 1.9 nm[46]. This study applied a molecule related to TMA, but with additional C-O-C spacers between the aromatic core and the three carboxylic groups, respectively. In UHV co-deposition experiments, the group of Prof. Beton combined PTCDI (perylene tetracarboxylic diimide) and melamine to form a hexagonal hetero-molecular host network with a fairly large lattice constant of 3.46 nm[21,22]. In this case 3-fold intermolecular hydrogen bonds were the driving force for the self-assembly process and the symmetry of the adlayer was governed by the 3-fold symmetry of melamine. As has been shown in this work, the cavities are large enough to incorporate up to seven C60 fullerene molecules within a single cell. Very recently Pawin and coworkers presented a hydrogen bond network with a cavity diameter of roughly 5 nm (about five times the size of the constituent molecules)[47]. The network was prepared under UHV conditions and originates from a delicate balance between substrate-mediated repulsion and intermolecular attraction.

An often underestimated, though obviously important factor at the liquid-solid interface is the role played by the solvent. Typical organic solvents used for scanning tunneling microscopy experiments have a low vapor pressure, are electrochemically inert and have a lower affinity for the substrate than for the compound of interest. However, there is increasing evidence for their effect on ordering. A part of this thesis is dedicated to

the influence of the solvent on the structure formation. For instance, we discovered two different polymorphic structures emerging from the same molecule using various solvents (cf. chapter 4.2), and dilution of a bimolecular system leading to different structures dependent on the local concentration on the sample (cf. chapter 4.3).

Scanning tunneling microscopy (STM) is one of the preferred techniques to investigate the ordering, the properties, and the dynamics of self-assembled monolayers, not only under ultrahigh vacuum conditions (UHV)[33,48-50], but also at the liquid-solid[51-53] or solid-solid interface[54,55]. Since the invention of the STM in 1982 by 1986-Nobel-laureates Binnig and Rohrer[56,57] there has been a great development to improve the instruments and adapt them to different experimental environments. Still there is no end in sight, e.g. for 2009 an experimental setup is scheduled to fly to the International Space Station ISS to conduct experiments under zero-gravity conditions. This could be interesting to investigate the influence of gravity e.g. on crystal growth. A feasibility study operating an STM in micro-gravity environment was successfully performed in 2001[58]. Today STM is not only a tool to take images at a nanometer scale, it is a powerful methodology to investigate self-assembly at the liquid-solid interface where it provides insight into the ordering, dynamics, reactivity, and electronic properties of adsorbates. Moreover, it can also be utilized as a tool for manipulation of matter on an atom by atom basis.

Compared to sample preparation and characterization under UHV conditions, the liquid-solid interface offers a number of advantages[53]: (1) The experimental approach is straightforward and does not require a complicated or as expensive infrastructure. (2) Though the UHV environment provides excellent control leading to unprecedented high resolution (especially when cooling to low temperatures), not all species can be adapted to UHV, such as those with relatively low thermal stability or large compounds. The requirements posed on the properties (size and function) for the investigation of molecules at the liquid-solid interface are easier to meet. (3) The choice of solvent can be adapted to the function of the particular solute and/or substrate. (4) The dynamic exchange of molecules adsorbed on the surface and dissolved in the liquid phase above promotes healing of defects in the self-assembled layers. As a result, the liquid/solid interface approach in combination with STM imaging is becoming increasingly popular to investigate self-assembly on surfaces.

Additional control of the monolayer formation can be achieved under potential control in electrolytes. Under electrochemical conditions, adsorbate-substrate interactions can be modulated by the surface charge density. Electrochemical STM therefore offers additional possibilities to control surface dynamics and monolayer structures via the surface charge[59-61].

2. Theory of STM

Principle of the Scanning Tunneling Microscope (STM)

The development of the STM began in 1981 with the experimental proof of stable vacuum tunneling by Binnig, Rohrer, Gerber, and Weibel[56]. This discovery paved the way for a real space imaging instrument with the capability of atomic resolution, and soon the first STM was introduced[57]. For the first time it was possible to image electrical conductive surfaces in real space on an atomic scale. One of the early great profits of the new system was the enlightenment of the so far misunderstood Si(111)-7×7 reconstruction[62]. In 1986 the Nobel Price in Physics was awarded to Gerd Binnig and Heinrich Rohrer for their invention.

The functional principle is based on the eponymous quantum mechanic tunneling effect, which states that electrons can pass potential barriers which they were not allowed to by classical mechanics. Figure 1 shows a schematic drawing of a STM setup.
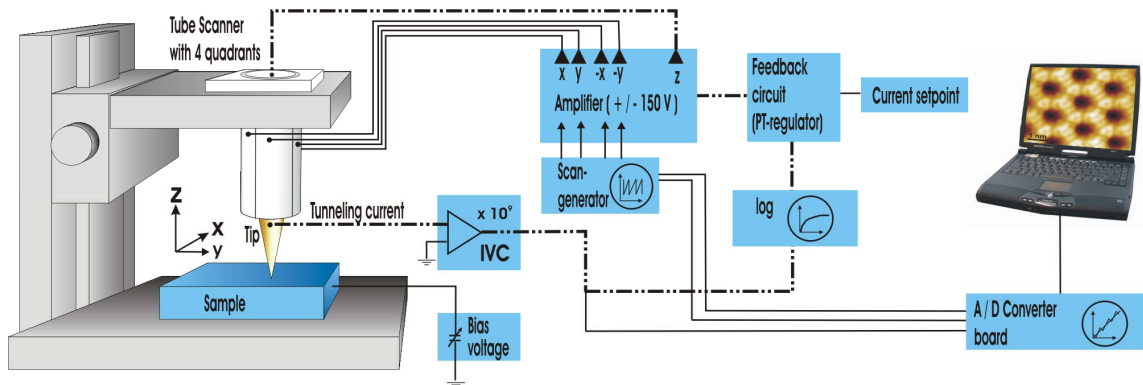

Figure 1: Schematic drawing of a scanning tunneling microscope: The dashed line indicates the feedback circle.

The functional principle of STM is as follows. A very sharp metallic needle is placed very close to the probed surface so the wave functions of the closest tip atom and the surface atoms already overlap. This occurs for tip-sample distances in the order of ~ 5 … 10 Å. If one applies a small bias voltage (~ 0.01 … 1 V) between the tip and the sample, a tunneling current will flow through the gap. This current is detected with a highly sensitive current-voltage converter (IVC). In simplified form, the dependence of the tunneling current I from the distance d is given by:

$$I \propto e^{-2d\sqrt{\frac{2m\Phi}{\hbar^2}}}$$

(2.1)

where m is the electron mass, Φ the work function (= barrier height), $\hbar = h/2\pi$ with h being Planck's constant, and d the width of the tunneling barrier (cf. Figure 2).
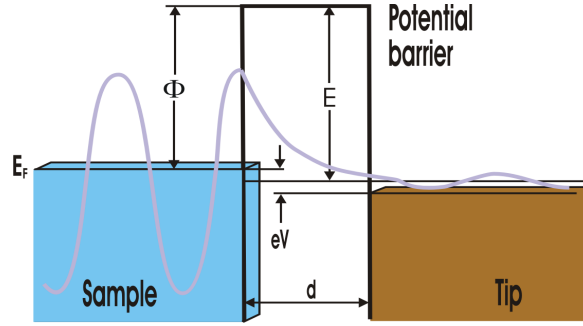
Figure 2: A one dimensional metal-vacuum-metal tunneling junction. The potential barrier is located between sample, left, and tip, right. The overlapping wave functions of tip and indicated by the gray line. Tip and sample are modeled as semi-infinite pieces of free-electron metal.

The effective change in the tunneling current as function of the distance is about an order of magnitude for $\Delta d = 1$ Å[63]. This strong distance dependency explains why atomic resolution is also possible from tips with a mesoscopic radius of curvature. The main part of the tunneling current is carried by those tip atoms being closest to the sample surface.

To image the surface the tip is moved meander like over the surface (x/y) and the tunneling current is measured simultaneously. Typical tunneling currents are in the range of 10 pA to 10 nA. For most samples the STM is operated in the so-called constant-current mode, where the tunneling current is kept constant by a feed back loop, i.e. the distance between tip and sample is fix on each point on the surface. The image information is contained in the z control signal of the tip. In this operating mode the control loop for the tip movement limits the scanning speed. For atomically flat samples it is also possible to keep the distance between tip and an averaged surface level constant (constant-height mode). This allows faster scanning speeds since there is no movement of the tip in z direction. In this mode the tunneling current contains the image signal.

Theoretical Model of the Tunneling Process (Tersoff-Hamann, s-wave-tip model)

The first theoretical model still being the standard for modeling the three-dimensional tunneling process leading to STM topographs was developed by Tersoff and Hamann[64,65]. Although it is based on several simplifying assumptions and therefore seems not to be valid for all experimental conditions, it can be used to derive some fundamental statements.

In first-order perturbation theory, the tunneling current is specified by the following expression (Bardeen's formalism[66]):

$$I = \frac{2\pi |e|}{\hbar} \sum_{\mu,v} \left[f(E_v) - f(E_\mu) \right] \left| M_{\mu v} \right|^2 \delta\left(E_v + |e|V - E_\mu \right) \tag{2.2}$$

where $f(E)$ is the Fermi function, V is the applied voltage, $M_{\mu v}$ is the tunneling matrix element between states Ψ_μ of the probe and Ψ_v of the surface (calculated independently), E_μ is the energy of Ψ_μ relative to the Fermi level of the tip, and E_v is the energy of Ψ_v relative to the Fermi level of the surface. The delta function ensures that only elastic

tunneling processes are taken into account with $E_v = E_\mu$. Since most experiments take place at room temperature or below, the Fermi functions (E_F) can be approximated by their zero-temperature values, i.e. unit step functions. In the range of small voltages this expression then further simplifies to

$$I = \frac{2\pi}{\hbar} e^2 V \sum_{\mu,v} |M_{\mu v}|^2 \delta(E_\mu - E_F) \delta(E_v - E_F)$$

(2.3)

Bardeen[66] has shown, that under certain assumptions the matrix element in (2.3) can be evaluated using the following equation:

$$M_{\mu v} = \frac{\hbar^2}{2m} \int dS \cdot \left(\Psi_\mu^* \nabla \Psi_v - \Psi_v \nabla \Psi_\mu^* \right)$$

(2.4)

where the integral is to be taken over any surface lying entirely within the vacuum (barrier) region separating the two sides.

Now the ideal STM tip would consist of a mathematical point source of current, whose position we denote r_T. In that case, (2.3) for the current at small voltages would reduce to

$$I \infty \sum_\mu |\Psi_\mu(r_T)|^2 \delta(E_\mu - E_F) \equiv \rho(r_T, E_F)$$

(2.5)

Thus the ideal STM would simply measure $\rho(r_T, E_F)$, the local density of states (LDOS) at E_F. This means, that the LDOS of the sample surface is evaluated in absence of the tip, but at the position where the center of the spherical tip is be located. Thus, this model gives a relatively simple interpretation of measuring the bare sample surface, without taking the complex tip-sample interaction into account. Despite it's simplicity the Tersoff Haman approach is still used as a zero order model for explanation of STM iamge contrast.

Although this model was successfully used for different examples (e.g. Au(110) 2×1 or Au(110) 3×1 reconstruction[65]) it is not generally valid. C. Julian Chen has exceeded the Tersoff-Hamann model to the so called Modified Bardeen Approach[67]. Besides others this model includes different and more complex tip wave functions (not only s-type wave functions) and a much better agreement with experimental data was achieved.

3. Experimental

This part of the thesis briefly describes the instruments and experimental methods used for the investigations. Also relevant properties of the used substrates, solvents, and compounds are characterized in brief.

3.1. STM

3.1.1. Liquid-Solid STM

All experiments included in this work were carried out at the liquid-solid interface under ambient conditions (e.g. room temperature and standard pressure). To investigate the interfacial monolayer between the substrate and the liquid phase above, the STM tip is immersed into the droplet. To achieve atomic resolution inside the liquid it has to be assured that the totel current between probe and sample is carried by the foremost part of the tip only (ideally the foremost atom of the tip). This would not be the case for conductive liquids, even small leakage currents would easily exceed the tunneling current, so one has to either use solvents with zero electrical conductance, or isolated tips.
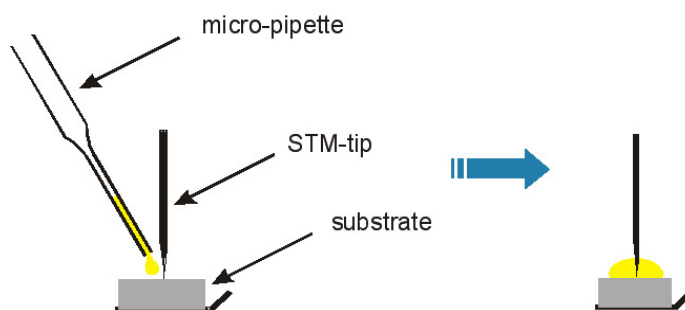
Figure 3: Schematic drawing of STM at the liquid solid interface.

For sample preparation a small droplet (2 … 10 µl) of solution is deposited onto the basal plane of a freshly cleaved HOPG (highly oriented pyrolytic graphite) crystal (cf. chapter 3.3). Normally, saturated solutions of adsorbate molecules (chapter 3.5) dissolved in a proper solvent (chapter 3.4) are used.

3.1.2. STM Systems

Two different STM instruments were used for the experiments:
The majority of the experiments was carried out using a a home built 'Pocket Size' STM with an analog control electronic SPM-100 from RHK. The system is equipped

with a horizontal sample stage for the liquid-solid experiments and is characterized by a very compact setup and a reasonable compensation of thermal drift. .

The experiments for M3: Fabrication and in situ Modulation of Multicomponent Hydrogen-bond driven Two-dimensional Networks (cf. chapter 4.3) were carried out at Columbia University with a Nanoscope IIIa Scanning Tunneling Microscope from Digital Instruments. This system's big advantage is the easy handling including the automatic approach.


(a)   (b)
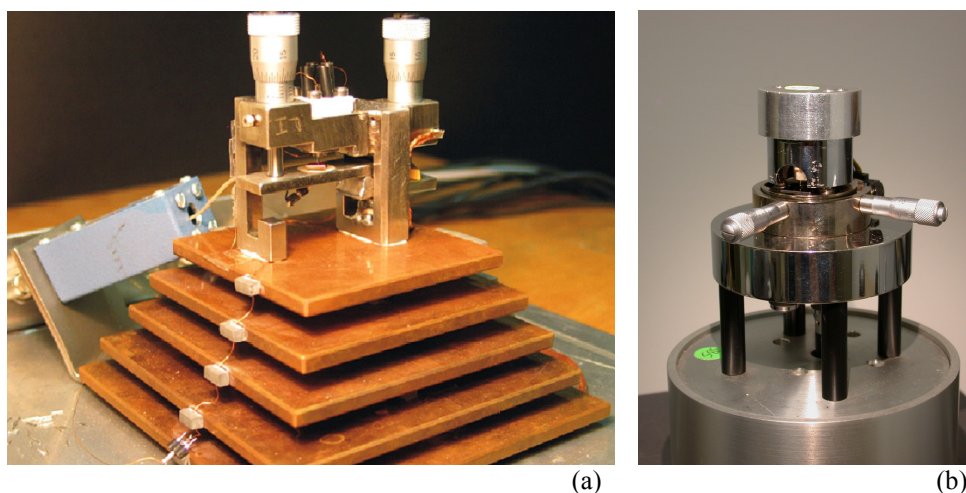
Figure 4: Different STM instruments: (a) home built 'Pocket Size' STM, (b) Nanoscope STM from Digital Instruments

To investigate dynamic processes of the adsorbate layer (see chapters 4.4 and 4.5) the samples were observed by means of video-STM: A series of still images is taken at a rate of 10 ... 20 s per frame and subsequently merged into a movie. In order to image the same sample area despite large drifts (mostly thermal drift) a drift-correction algorithm was essential during the measurements. For this purpose a feature of the RHK control software was used, stabilizing the position of a randomly chosen, unambiguously recognizable feature in subsequent scanning frames. Furthermore cross correlation provides the necessary offsets, needed to align all images before merging them into a movie. The maximum of the cross-correlation with a master image gives coordinates for the necessary lateral displacement. The duration of the observation period was mainly limited by the stability of the STM tip, or by solvent evaporation.

Mechanically cut tunneling tips from either Platinum/Iridium (90/10) or Platinum/Rhodium (87/13) wire were used for all experiments. The wire diameter was 0.25 mm, and no insulation of the tips was needed. If necessary the tips were conditioned in situ by short voltage pulses (20 … 150 ms, 2 … 5 V)

3.1.3. Calibration of STM Images

A calibration of the STM images is necessary to determine the exact size of the molecular adsorbate layers. For this purpose so called split images are used, displaying the adsorbate layer in one part of the picture and the underlying graphite layer in the other part. These images are produced by changing the tunneling parameters form adsorbate conditions (high voltage, low current) to graphite conditions (low voltage,

high current) during the scan of the image frame[68]. A typical split image is shown in Figure 5. Since the unit cell parameters of graphite are known very precisely (a = 2.46 Å, b = 2.46 Å, α = 120°) the STM image can be calibrated with these values and the unit cell of the adsorbate layer can be determined.

(a)   (b)
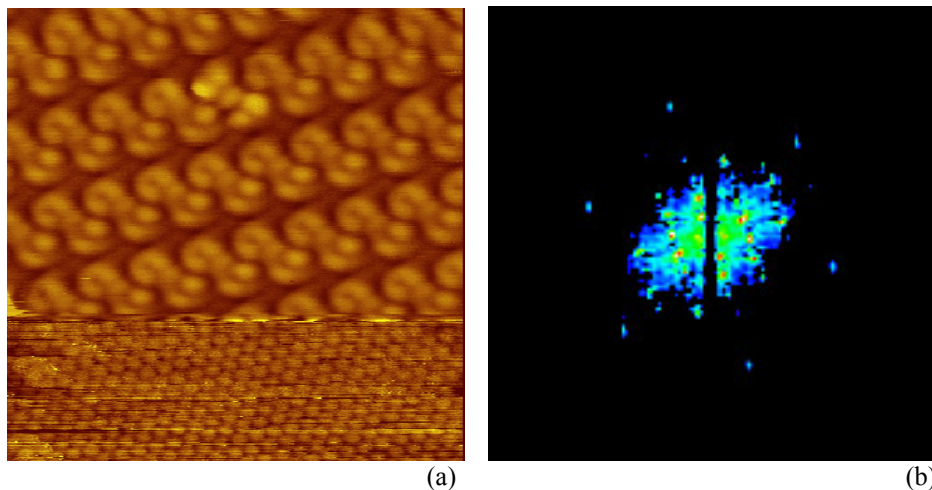
Figure 5: (a) Split image: the upper part shows the adsorbate layer (SDA), the lower part shows the underlying substrate (graphite), image size 12.1 × 12.1 nm. (b) Fourier transformation of the split image: the outer 6 spots originate from the hexagonal graphite lattice, the inner spots represent the adsorbate layer.

To accomplish these calibrations the two dimensional discrete Fourier transformation is used. The periodicities contained in the STM image appear as discrete frequency peaks in the Fourier image. The periodicity of the graphite lattice appears as a hexagonal peak pattern in the reciprocal space (cf. Figure 5(b)). To remove drift induced distortion and incorrect scaling the image is corrected with the known lattice parameters of graphite. A linear transformation is calculated to project the peaks on the correct position. After this transformation the image is retransformed to the real space. The Fourier image is further used to easily measure the unit cell parameters of the adsorbate structure.

3.2. Simulation

For the molecular mechanical simulations supporting this study two different software packages were used, both are based on a Dreiding II Force Field model[69]. Generally speaking Force Field calculations are based on various assumptions and simplifications depending on the size of the system under investigation to reduce the number of variable parameters and thus the computational cost. Therefore, the results are not as trust worthy as those from ab-initio methods, nevertheless offer meaningful comparison and estimates. Furthermore large system and unit cells respectively can be studied. Although the accuracy of the absolute values of binding energies as determined by force field calculations is somewhat questionable – for example, the liquid phase is totally neglected and important interactions like mirror charges in the semimetal graphite are not included – they are suited for a direct comparison of related systems since the molecules used have similar size, shape, properties, and are adsorbed on the same substrate. Furthermore the Dreiding II Force Field model includes a specific term for

hydrogen bonding, the main driving force in the molecular monolayer systems studied here .

For quick verfication of proposed structural models by 'trail-and-error' simulations the DS Viewer Pro 5.0 complemented by the Dreiding conformer package from Accelrys[i] was used. More sophisticated calculations were conducted with a Cerius2 software package (as well from Accelrys) including periodic boundary conditions.

3.3. Substrate Material

Graphite is a chemically inert layered crystal. The individual layers of the crystal are kept together by van der Waals forces. The carbon atoms in the layers are covalently bound and sp2 hybridized. They form a hexagonal lattice with a nearest neighbor distance of 1.42 Å. The ABAB stacking of the layers however, reduces the symmetry to trigonal. (cf. Figure 6(a)).

(a)   (b)   (c)
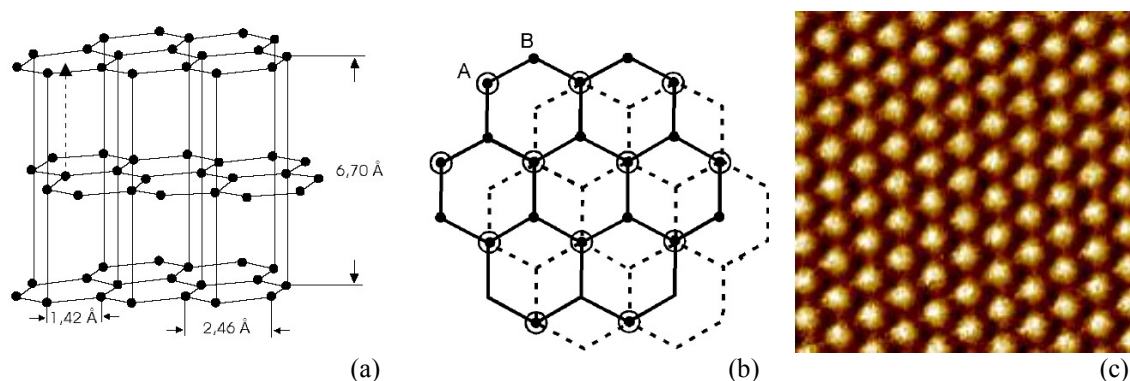
Figure 6: Graphite: (a) layered structure of a Graphite crystal; (b) top view of the (0001) plane: atoms at the positions marked A (large circles) have a nearest neighbor in the layer directly underneath, whereas atomic positions marked B (black dots) do not have a nearest next neighbor in the layer underneath. (c) STM image of a 0001 surface: the bright spots arise from atoms in position B (size: 2.25 × 2.25 nm, V_T = 0.217 V, I_T = 2.46 nA, distortion corrected, no filtering).

The difference between neighboring atoms due to AB stacking is apparent in STM images of the (0001) surface: Figure 6(c) depicts an STM image of a pristine graphite surface, the periodicity between bright spots amounts to 2.46 Å. The intensity maxima indicate spots with enhanced tunneling probability, which are usually assigned to Carbon atoms in position B (cf. Figure 6(b)) since their LDOS at the Fermi level is significantly larger[70,71].

Since interlayer van der Waals forces are comparatively weak, the crystal can easily be cleaved along the (0001) plane using adhesive tape. The resulting surfaces are almost defect free and exhibit atomically flat terraces with widths in the range of several hundred nanometers.

For all experiments shown here Highly Oriented Pyrolytic Graphite (HOPG) of ZYH grade was used. This is a synthetically produced graphite with domain sizes in the range of several microns (vs. millimeters for natural graphite). Since STM being a local technique, the domain size of the substrate does not impose any experimental limitations to the systems investigated in this study.

3.4. Solvents

The proper choice of solvent is crucial for STM experiments at the liquid-solid interface. Since the tip is totally immersed into the solution it is important to either use solvents with a low dielectric constant and polarizability (e.g. $\varepsilon < 12$ at room temperature) or to use coated tips. Another important property of the solvent is a sufficiently low vapor pressure. When the solvent is evaporating too fast, experimental time spans are greatly reduced, and on the other hand resolution is reduced through thermal drift induced by the evaporation. Moreover the solvent must be able to sufficiently dissolve the targeted adsorbate molecules, and exhibit a lower affinity and adsorption energy respectively for the substrate than the solute. Otherwise the preferred adsorption of solvent molecules, which normally outnumber solute molecules, would be manifested in the self-assembly of a solvent monolayer.

For the interfacial self-assembly of molecular monolayers the solvent can also have great influence on the structure formation[51]. For example two different polymorphs of the adsorbate layers were found for Trimesic acid depending on the chain length of the applied fatty acid solvents[1]. A similar effect was found for 1,3,5-Benzenetribenzoic acid and is detailed in chapter 4.2.

Table 1 summarizes the solvents used in this study and denotes their most relevant properties.
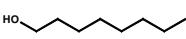
|	
	1-Octanol, $C_8H_{18}O$ Molecular weight: 130.23; CAS Registry Number: 111-87-5 Dielectric constant ε (temp. [K]): 10.30 (293.2)[72] Vapor pressure (295K): 0.08 mbar
	1-Nonanol, $C_9H_{20}O$ Molecular weight: 144.25; CAS Registry Number: 143-08-8 Dielectric constant ε (temp. [K]): 8.83 (293.2)[72] Vapor pressure (295K): < 0.1 mbar
	1-Decanol, $C_{10}H_{22}O$ Molecular weight: 158.28; CAS Registry Number: 112-30-1 Dielectric constant ε (temp. [K]): 7.93 (293.2)[72] Vapor pressure (295K): < 0.1 mbar
	Butanoic acid, $C_4H_8O_2$ Molecular weight: 88.11; CAS Registry Number: 107-92-6 Dielectric constant ε (temp. [K]): 3.02 (303.2)[73] Vapor pressure (295K): 1.2 mbar
	Pentanoic acid, $C_5H_{10}O_2$ Molecular weight: 102.13; CAS Registry Number: 109-52-4 Dielectric constant ε (temp. [K]): 2.93 (303.2)[73] Vapor pressure (295K): < 0.1 mbar
	Hexanoic acid, $C_6H_{12}O_2$ Molecular weight: 116.16; CAS Registry Number: 142-62-1 Dielectric constant ε (temp. [K]): 2.61 (303.2)[73] Vapor pressure (295K): < 0.1 mbar
	Heptanoic acid, $C_7H_{14}O_2$ Molecular weight: 130.18; CAS Registry Number: 111-14-8 Dielectric constant ε (temp. [K]): 3.04 (303.2)[73] Vapor pressure (295K): < 0.1 mbar
	Octanoic acid, $C_8H_{16}O_2$ Molecular weight: 144.21; CAS Registry Number: 124-07-2 Dielectric constant ε (temp. [K]): 2.82 (303.2)[73] Vapor pressure (295K): < 0.1 mbar
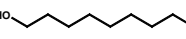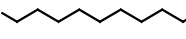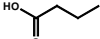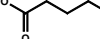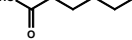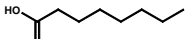
|	
	Nonanoic acid, $C_9H_{18}O_2$ Molecular weight: 158.24; CAS Registry Number: 112-05-0 Dielectric constant ε (temp. [K]): 2.50 (302.8)[73] Vapor pressure (295K): < 0.1 mbar
	1-Phenyloctane, $C_{14}H_{22}$ Molecular weight: 190.32; CAS Registry Number: 2189-60-8 Dielectric constant ε (temp. [K]): 2.26 (293.2)[72] Vapor pressure:
	Dodecane, $C_{12}H_{26}$ Molecular weight: 170.33; CAS Registry Number: 112-40-3 Dielectric constant ε (temp. [K]): 2.01 (293.2)[72] Vapor pressure (295K): < 0.1 mbar
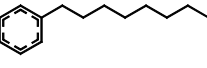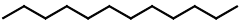
Table 1: Solvents used in this study (source of data if not indicated otherwise: NIST Chemistry WebBook, National Institute of Standards and Technology, www.nist.gov)

3.5. *Adsorbate Molecules*

Since the focus of this study is the fabrication of two-dimensional hydrogen bonded monolayers and the comparative investigation of different adsorbate molecules building those, the molecules have some properties in common: First, all the molecules are relatively small, the dimensions are in the range of 5 … 20 Å, and their weight is between 166 amu and 438 amu. Secondly, all of them are planar or nearly planar molecules, thereby maximizing the molecule-substrate interaction and providing sufficiently stable adsorption. Some of the molecules (e.g. TPT and BTB) are slightly non planar according to molecular mechanics calculations of their gas phase minimum energy structure, but get planarized while adsorbing on the surface. Thirdly, and maybe most important, all molecules have the ability to form hydrogen bonds. Almost all molecules are equipped with carboxylic groups which are ideal functional groups for the formation of hydrogen-bond networks since they can act as both H-bond donor and acceptor at the same time, and therefore can bind to themselves in any conformation. Most of the networks exhibit a bonding angle of 180° between two carboxylic groups, being the binding configuration with the lowest energy. TPT is one exception to the rule: lacking carboxylic or other groups being able to act as a hydrogen bond donor, it cannot form homo-molecular H-bond bridged networks. But the molecule has the ability to accept H-bonds through the three outer nitrogens making coadsorbed networks possible together with a linker molecule (cf. chapter 4.1).
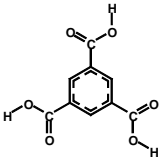
|	
	TMA, $C_9H_6O_6$ 1,3,5-Benzenetricarboxylic acid, Trimesic acid Molecular weight: 210.14 g/mol CAS Registry Number: 554-95-0
	TPA, $C_8H_6O_4$ 1,4-Benzenedicarboxylic acid, Terephthalic acid Molecular weight: 166.13 g/mol CAS Registry Number: 100-21-0
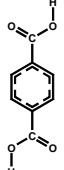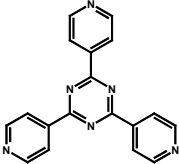
|	
	TPT, $C_{18}H_{12}N_6$ 1,3,5-Tris(4-pyridyl)-2,4,6-triazine Molecular weight: 312.33 g/mol (Synchem OHG, Felsberg) CAS Registry Number: 42333-78-8
	BTB, $C_{27}H_{18}O_6$ 1,3,5-Benzenetribenzoic acid Molecular weight: 438 g/mol
	NDA, $C_{12}H_8O_4$ 2,6-Naphthalenedicarboxylic acid Molecular weight: 216.19 g/mol CAS Registry Number: 1141-38-4
	BPDA, $C_{14}H_{10}O_4$ 4,4'-Biphenyldicarboxylic acid Molecular weight: 242.23 g/mol (Sigma Aldrich Inc.) CAS Registry Number: 787-70-2
	SDA, $C_{16}H_{12}O_4$ 4,4'-Stilbenedicarboxylic acid Molecular weight: 268.27 g/mol (ABCR GmbH, Karlsruhe) CAS Registry Number: 100-31-2
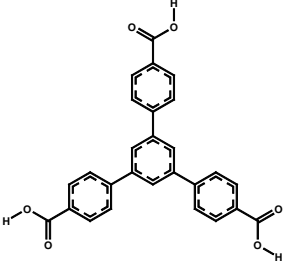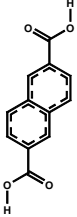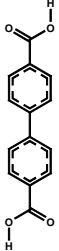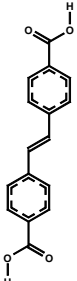
Table 2: List of adsorbate molecules investigated in this study (source of data if not indicated otherwise: NIST Chemistry WebBook, National Institute of Standards and Technology, www.nist.gov)

4. Results

In chapter 4.1 to 4.4 the results already published are briefly described, chapter 4.5 shows more recent results not yet published in peer reviewed journals. The complete manuscripts are attached in appendix 1, page 47 et sqq.

4.1. M1: Mediated Coadsorption at the Liquid-Solid Interface: Stabilization through Hydrogen Bonds

(Manuscript see page 47)

The adsorption behavior of 1,3,5-tris(4-pyridyl)-2,4,6-triazine (TPT) molecules from the liquid phase in binary solutions, i.e. in the presence of a second (adsorptive) species was investigated. Adsorption with the molecular plane parallel to the substrate is observed for comparable aromatic molecules, thereby optimizing the interaction with the substrate. However, despite many attempts, the adsorption of TPT from heptanoic acid solution only containing this species has never been observed. In an equilibrated system, TPT molecules remain dissolved and do not form an interfacial monolayer. Stronger interacting substrates, for example, metal surfaces, might possibly shift the equilibrium toward adsorption. However, simultaneously performed ultrahigh vacuum (UHV) experiments revealed, that densely packed structures evolve when a monolayer of TPT is evaporated onto graphite at room temperature (cf. Figure 7(c)).
The process of mediated coadsorption of the TPT molecules at the liquid-solid interface was accomplished through complexation of TPT with a second type of molecule acting as a 'molecular glue'. H-bonds are utilized to create non-covalently bound complexes of TPT and the second type of molecule. Because stable adsorption of TPT itself from the liquid phase has never been observed, these complexes facilitate the adsorption through an increased adsorption energy. Trimesic acid (TMA) and terephthalic acid (TPA) – both benzene rings with disposed carboxylic acid groups – were appropriate to precipitate the stable adsorption of TPT. According to the different symmetry and number of carboxylic acid groups, various networks were observed.

<p>(a)</p> <p>(b)</p> <p>(c)</p>
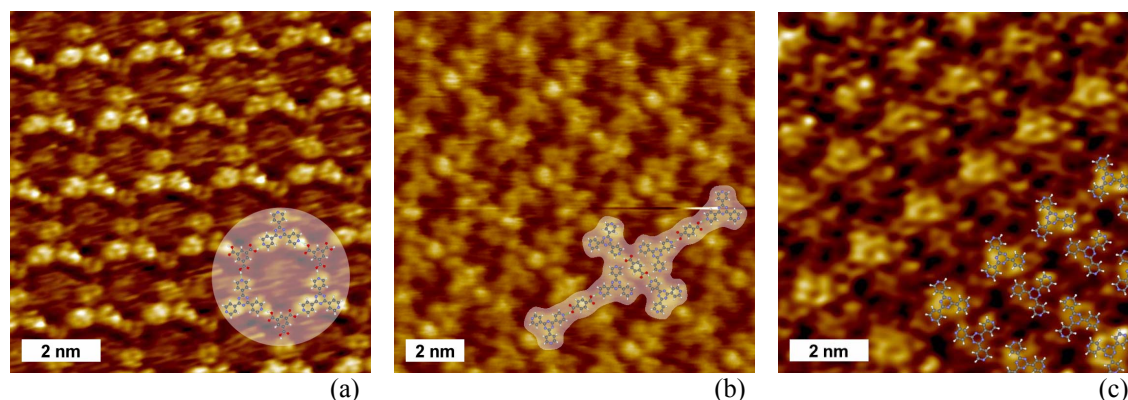
Figure 7: STM images of the emerging structures: (a) liquid-solid STM topograph of the hexagonal 2D TPT-TMA co-crystal on HOPG (0001), the position of the individual molecules can be seen in the overlay. (b) liquid-solid STM image of the TPT-TPA co-crystal, TPT molecules appear as several bright, triangularly arranged features, whereas TPA appears as a single round feature. Three bone shaped building blocks consisting of two TPT and one TPA molecules each are overlaid. (c) UHV STM image of an in-situ prepared TPT monolayer at room temperature, the molecules are densely packed on the surface.

The binary solution of TPT and TMA leads to a coadsorbed monolayer with a 6-fold symmetry, as seen in the STM image presented in Figure 7(a). The cavities have a diameter of roughly 1.6 nm. The coadsorption of TPT and TPA molecules on HOPG(0001) leads to a comparatively close-packed structure with a bone shaped packing motif, as seen in the STM image in Figure 7(b). The TPT-TPA network is built of small hydrogen-bond units, comprised of two TPT molecules interconnected by a TPA molecule. In each case the carboxylic hydrogen atoms are bound to the outer nitrogen atoms of TPT via N⋯H-O H-bonds.

4.2. M2: Solvent Induced Polymorphism in Supramolecular 1,3,5-Benzenetribenzoic Acid Monolayers

(Manuscript see page 53)

In this work two-dimensional supramolecular host structures were realized by the adsorption of 1,3,5-Benzenetribenzoic acid (BTB) molecules on graphite(0001) surfaces from the liquid phase. The emerging monolayers were investigated by in situ STM. Depending on the solvent used, two crystallographically different BTB structures were found – both hydrogen bonded networks. The two structures substantially differ in their hydrogen bonding pattern, but have the dimer motif as basic building block in common. One of them, the so-called chicken-wire polymorph (cf. Figure 8(a)), has a hexagonal building scheme and exhibits fairly large circular cavities with a diameter of 2.8 nm, which are suitable for the incorporation of other nanoscopic objects. The large cavity size of the chicken-wire structure was made possible through comparatively strong 2-fold hydrogen bonds between carboxylic groups. In addition, the low conformational flexibility of BTB was supportive to combat the tendency for dense packing. The second structure (cf. Figure 8(b)) exhibits an oblique unit cell and a different hydrogen bonding pattern. Since the resolution of the STM images does not allow a apodictic statement about the hydrogen bonding scheme, two different bonding patterns for this structure are suggested.
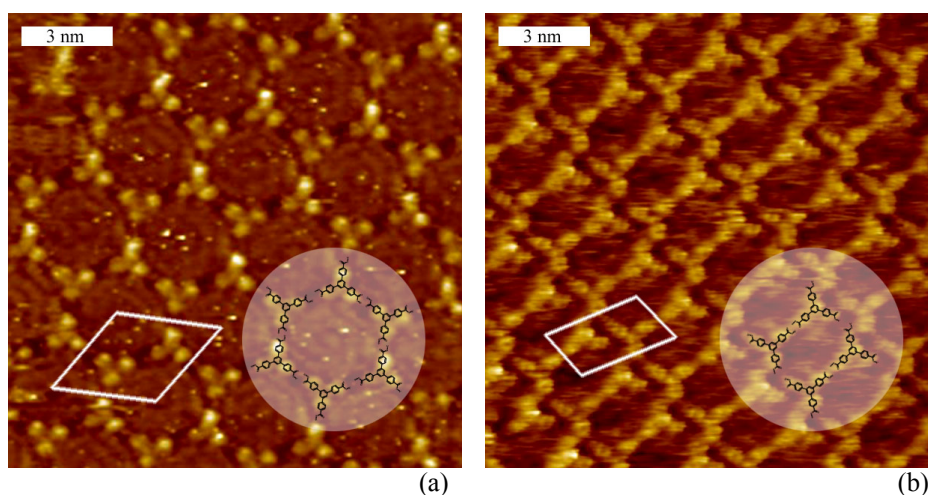
Figure 8: STM topographs of the BTB monolayers, self-assembled on a HOPG(0001) surface. The positions of individual BTB molecules are indicated. Image (a) shows the hexagonal chicken-wire modification as obtained in nonanoic acid and 1-phenyloctane, image (b) shows the modification with the oblique unit cell as obtained in butanoic through heptanoic acid, 1-octanol, 1-nonanol, and 1-decanol. For octanoic acid and dodecane both modifications were observed. The unit cell parameters are (a): $a = 3.2$ nm, $b = 3.2$ nm, $\alpha = 60°$, and (b): $a = 1.7$ nm, $b = 3.1$ nm, $\alpha = 76°$.

The evolution of different structures for varying solvents is discussed in the light of adsorption rates and of stabilization of polar units during the growth. As solvents six different acids, three different alcohols, as well as 1-phenyloctane and dodecane were investigated. For the solvents with functional groups (OH or COOH) being able to hydrogen bond to the solute, a general, i.e. not strict dependence of the structure formation on the dielectric constant was found. The more dense and more polar oblique BTB structure was only observed for solvents with a dielectric constant $\varepsilon > 3$. Experiments with the other classes of solvents, however, have pointed out that further parameters can be decisive for the structure formation as well.

4.3. M3: Fabrication and in situ Modulation of Multicomponent Hydrogen-bond driven Two-dimensional Networks

(Manuscript see page 62)

In this study the co-adsorption of two different molecules, BTB (1,3,5-Benzenetribenzoic acid) and TMA (Trimesic acid) in open (loosely packed) networks was studied at the liquid-solid interface in two different solvents (Heptanoic and Nonanoic acid). A phase diagram of the binary solute system was probed by means of in-situ STM. Depending on the concentrations of the two solutes, TMA and BTB, six different hydrogen bonded monolayer structures were discovered with Heptanoic acid as the solvent (cf. Figure 9), three of them being mixed TMA/BTB phases. Although both species are always present in solution, the different molecular arrangements observed on the surface range from pure TMA networks to different hexagonal and rectangular mixed networks (containing BTB and TMA) to arrangements built up from BTB molecules only. All of these structures are stabilized by twofold intermolecular

hydrogen bonding between the carboxylic acid head groups and exhibit a periodic arrangement of large internal cavities of various sizes (1.1 nm – 2.8 nm) and shapes.
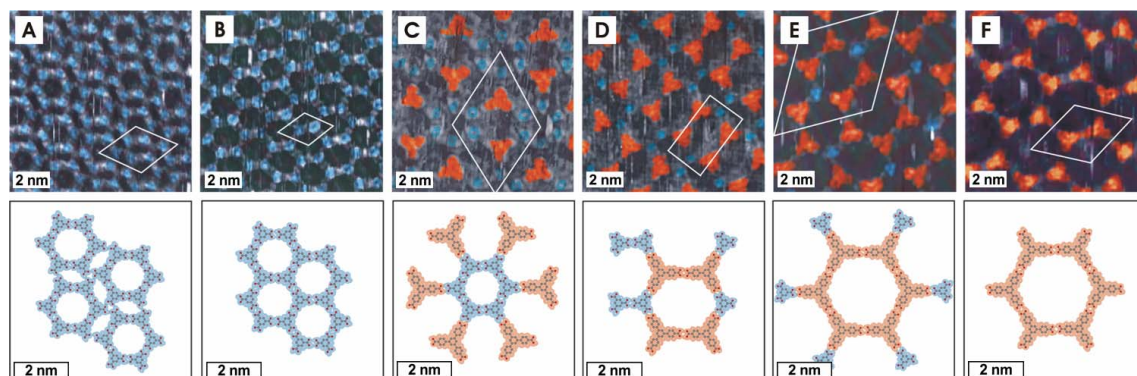

Figure 9: Observed two-dimensional structures of the BTB-TMA system: STM-images (top) and molecular mechanics simulations (bottom) of the six different structures (A-F), TMA molecules are colored blue, the larger triangular shaped BTB molecules are colored orange.
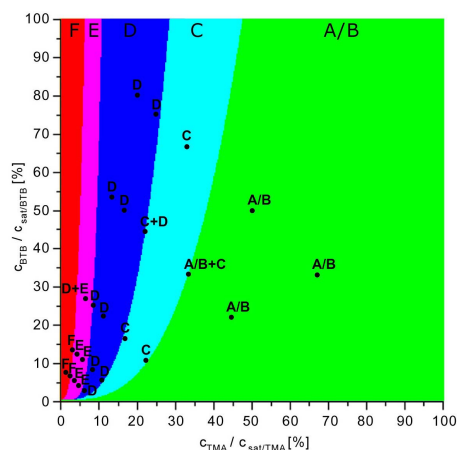

Figure 10: Phase diagram of the bimolecular system in Heptanoic acid. The abscissa depicts the relative TMA-concentration, whereas the ordinate depicts the relative BTB-concentration, both normalized to solubility. Probed points are indicated in the diagram by the respective letter(s) of the structure(s) found. Uniformly colored regions depict the area of thermodynamical stability, i.e. the minimum in free energy of the respective phase, according to the thermodynamic model.

In addition, in-situ dilution of the solutions with pure solvent resulted in phase transitions as anticipated from and consistent with the phase diagram, thereby proofing that the growth of these mixed networks is thermodynamically controlled. This in-situ convertibility of the networks provides an opportunity to construct monolayer host networks that offer a tunable cavity size, lattice constant, and stoichiometry.

The measured phase diagram was reproduced by means of a simple thermodynamic model, based on the concentration dependence of the chemical potential for TMA and BTB in solution (cf. Figure 10). Measured unit cell parameters of the respective structures and the related molecular area densities of the two compounds were employed as experimental input to this model.

Different types of STM image contrasts were observed inside the putative 'empty' cavities of the TMA/BTB networks providing experimental evidence for co-adsorption

of solvent molecules. The different patterns of the solvent structures within the cavities suggest that either upright or parallel adsorption of the alkane solvent backbone can occur. This already suggests the possibility of incorporating other molecules or clusters – metallic or semi conducting – within the cavities of the host network.

4.4. M4: Dynamics of Grain Boundaries in Two-Dimensional Hydrogen-Bonded Molecular Networks

(Manuscript see page 78)

Room-temperature Video-STM at the liquid–solid interface was utilized to compare the temporal evolution of the nanostructure of one-dimensionally (Terephthalic acid, TPA) versus two-dimensionally (Trimesic acid, TMA) H-bonded supramolecular structures. The 1D-networked TPA structure is comprised of densely packed, H-bonded linear chains of molecules. By means of a series of STM images it was possible to show that larger TPA domains grow at the expense of smaller domains on a timescale of minutes. The coarsening of the nanostructure can be considered as an example of the more general concept of Ostwald ripening. Since the TPA lattice exhibits only a twofold symmetry, two vastly different facets exist, with the edge molecules exhibiting a remarkable variation in binding energies. Therefore, the domain boundaries, where edge molecules are bound by two H-bonds only, are the starting points for structural changes and reorganization respectively in the monolayer. Furthermore, adsorption and desorption events within a small hole in the TPA monolayer were tracked on a single-molecule level, until the hole eventually had been entirely closed by adsorption of TPA from the liquid phase.

Figure 11: Selected snapshots of a series of STM images: (a) TMA domain boundaries. Only minor changes happen on the domain edge indicated by the red (upper) frame. At the domain boundary in the lower left corner (blue box) no changes occur during the observation period of ~ 20 min. The picture on the right is the standard deviation of the whole series of 47 STM images. Red areas indicate larger values of the standard deviation, and therefore represent regions that exhibit enhanced molecular dynamics. (b) TPA monolayer on HOPG(0001): The images show a small island surrounded by a domain with different

rotational orientation. Within ~ 4 min the surrounding area is growing at the expense of the small island until only a small hole is left (from left to right). The entire series of subsequent STM images for both systems can be found in the Additional Material section in Appendix 2.

In comparison, due to the six-fold symmetry of the structure, TMA islands have three equivalent domain boundaries where edge molecules have even larger binding energies than in the TPA structure. The main reason is that TMA edge molecules are bound by at least four H-bonds (two per carboxylic group), whereas one facet of the TPA edge molecules exhibits only two H-bonds. Consequently the TMA domain boundaries are relatively stable at room temperature, and the shape and size of islands is mainly preserved, except for very small islands. This is also in accordance with the binding energy of edge molecules as estimated for both systems by molecular mechanics simulations. In summary, by the combination of experimental results from STM measurements with theoretical calculations of edge-molecule binding energies it was possible to consistently demonstrate the relationship between symmetry of the building block, the bonding scheme of the H-bonded supramolecular structure, and the molecular dynamics at grain boundaries.

4.5. Unpublished Results

4.5.1. Another BTB Polymorph: A Close-Packed Structure

Interesting results could be achieved using aged (three months old) solutions of BTB molecules dissolved in Heptanoic or Octanoic acid. Following the experiments of chapter 4.2, using Heptanoic acid as solvent one would expect a structure with an oblique unit cell, or for Octanoic acid both, structures with hexagonal and oblique unit cells respectively. Instead, for saturated solutions, which were mixed more than three months prior to the experiment a very different packing motif of the monolayer could be found. An STM image of the structure is shown in Figure 12(a), along with a molecular mechanics simulation on the right hand side (b). The network is comprised of BTB dimers arranged in rows, resulting in an almost close-packed monolayer. A BTB dimer is hold together by two C···H-O hydrogen bonds. Within the rows the dimers are bonded via two C···H-O hydrogen bonds. The rows itself are interconnected via one O···H-O hydrogen bond per BTB dimer (the latter ones are marked by an asterisk in Figure 12(b)). By means of split images (cf. chapter 3.1.3) the unit cell of the structure could be determined and amounts to a = 3.1 nm, b = 1.3 nm, α = 107°. This effect could be shown for five different samples, all of them were previously used for experiments described in chapter 4.2 and 4.3, and in the beginning exhibited the previously described structures. So where does this new structure come from?

(a)   (b)
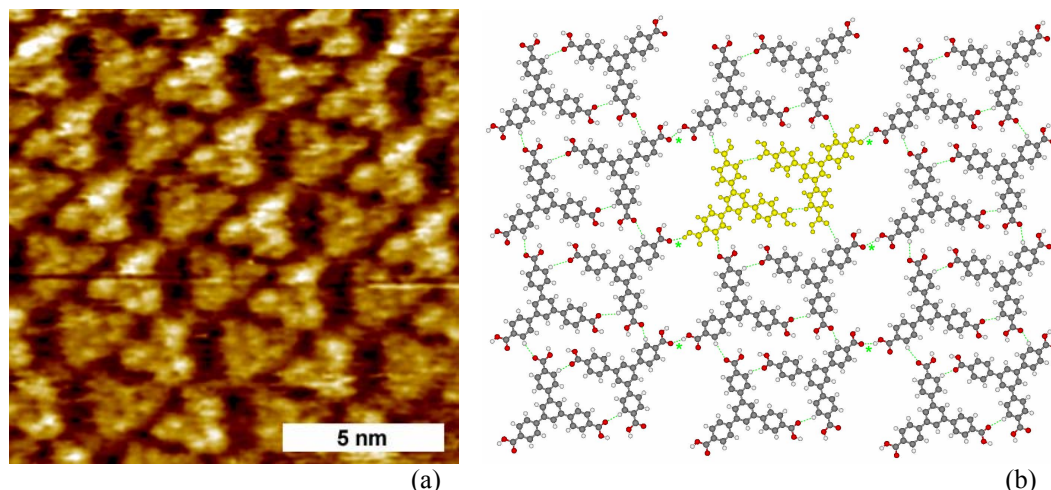
Figure 12: Close-packed BTB structure on HOPG: (a) STM image of the structure (solvent: Octanoic acid, solution aged for ~3 month, U_T = -1.2 V, I_T = 1.5 nA), (b) molecular mechanics simulation of the structure, green dashed lines indicate hydrogen bonds, those marked with an asterisk are O···H-O bonds, all others are energetically weaker C···H-O bonds.

Macroscopically the three months old saturated solutions do not show a significant difference, but upon further aging, (around six months) the solution becomes a little bit blear and somewhat slimy. This might provide some evidence for effects induced by the solvent. An aspect to be considered is an increasing concentration caused by solvent evaporation. Since we are generally working with saturated solutions, containing a sediment of bulk material, an increase of the concentration by evaporation of solvent can be ruled out, because additional material would fall out of the solution. Furthermore, no significant loss of solvent could be observed in the containers. Another fact could be degeneration of the solvent, possibly caused by daylight. Fatty acids are known to degrade when exposed to air for longer periods, usually this leads to acids with shorter chain length or degeneration of the acid group to an OH group. Fatty acids with shorter chain length have a very significant smell, which can be used as a means of detection. However, this could not be observed at any of the samples. Alcohols as well as fatty acids with a short alkyl chain have a much higher vapor pressure than the fatty acids intentionally used. Presuming a mixture of two solvents with different vapor pressure (e.g. Heptanoic acid as main solvent, and Butanol as additional solvent resulting from the degeneration of the main solvent), the solvent with the higher volatility could evaporate when the sample droplet is applied to the surface. This would lead to a super-saturated solution on the sample, eventually resulting in a higher packing density on the surface than for a comparable sample with only the main solvent.

To test this behavior a droplet of a three months old sample of BTB saturated solution in heptanoic acid was applied to an HOPG surface and subsequently diluted with additional solvent (Heptanoic acid) in a stepwise manner. Some of the resulting STM images can be seen below. Figure 13(a) shows the old sample directly after applying the droplet onto the HOPG surface, two domains of the close-packed structure can be seen. Adding 2.5 µl of solvent initiates a conversion on the surface, and some domains with the oblique structure appear Figure 13(b). After adding another 7.5 µl of Heptanoic acid all close-packed domains have disappeared and only oblique structures remain on the surface.

(a)   (b)   (c)
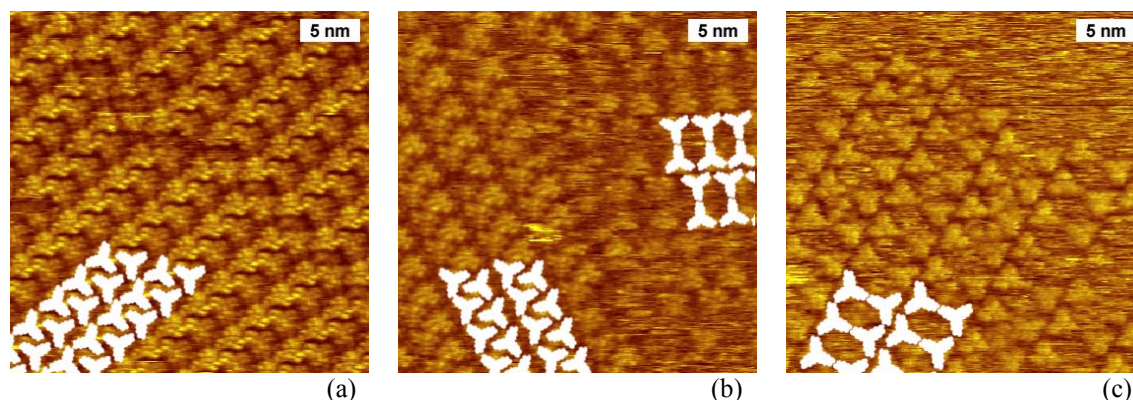
Figure 13: Dilution of a three months old BTB solution (solvent: Heptanoic acid): (a) close-packed structure: initial state with 2.5 µl old saturated solution on the sample; (b) intermediate state after adding 2.5 µl solvent: domains with close-packed and oblique structure appear simultaneously on the surface; (c) state after adding in total 10 µl additional solvent onto the sample: solely the oblique structure is found on the surface ($U_T \sim$ -1.1 V, $I_T \sim$ 1 nA).

Another influence could be material dissolved from the polypropylene (PP) cryo containers by the fatty acids. This can not totally be ruled out, but the same effect occurred for two samples stored in glass containers, therefore this is definitely not the main effect. Two other ideas refer to the dissolution process in general: it is conceivable that dissolution of BTB molecules in fatty acids takes place on a much longer time scale than expected. Generally the samples are prepared by mixing solvent and solute in an ultrasonic bath for 10-15 minutes and subsequently allowing the sample to settle. Then one waits until larger agglomerates sediment and the supernatant solution is totally clear. This process usually takes several days, depending on the adsorbate molecules and the solvent used. Subsequently the solutions are used for the experiments. It is possible but rather unlikely that the total solution of BTB molecules takes place on a timescale of month. Additionally there is a huge reservoir of BTB molecules in the droplet on the sample, so if this was an energetically favorable structure there should be enough molecules available to build it. Another aspect deals with the aggregates BTB molecules may form in the solution. Lackinger et al. suggest, that TMA molecules are basically present as dimers or trimers in solution[1]. This could also be the case for BTB, since the symmetry and binding conditions are almost identical. The ratio of dimers to single molecules in solution might develop towards more single molecules over time, induced by slow since energetically not very significant dissolution of dimers. This theory is supported by the fact, that both structures found for freshly prepared samples consist of dimers as basic building blocks, whereas the close-packed structure could not be build from dimers. This argumentation shows that there are several possibilities influencing the structure growths, to proof these different approaches and to rise a definite statement additional experiments are required.

4.5.2. *Comparing Three Similar One-Dimensional H-bonded Molecules*

The monolayer formation and the dynamic behavior of various related dicarboxylic acid molecules were investigated by comparison of structurally related compounds. The three compounds have two interconnected benzoic acid groups in a 180° conformation in common, however the spacing between the groups varies. The experiments were conducted at the liquid-solid interface using HOPG as crystalline substrate. Saturated

solutions of the respective compound dissolved in Nonanoic acid were used for all experiments.

2,6-Naphthalenedicarboxylic acid (NDA)

2,6-Naphthalenedicarboxylic acid (NDA) has two directly connected benzene rings between the carboxylic groups and is therefore the smallest molecule among the three compounds (cf. Figure 14(a)).

(a)   (b)
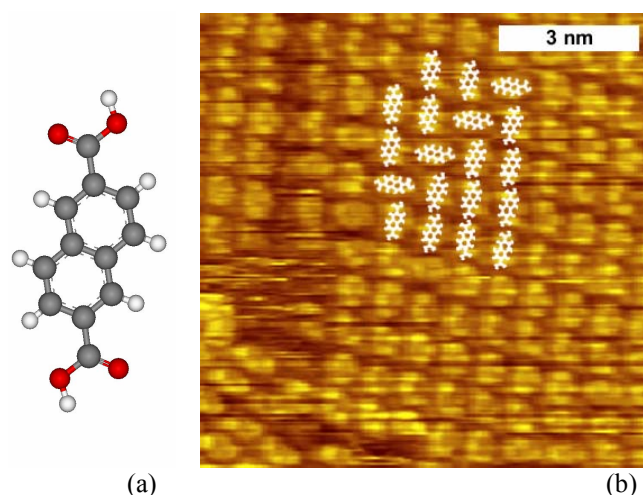
Figure 14: (a) 'Ball and Stick' model of 2,6-Naphthalenedicarboxylic acid (NDA), (b) STM image of the monolayer structure of NDA ($U_T = 1.4$ V, $I_T = 348$ pA).

NDA networks form immediately after applying the solution to the sample. The monolayers exhibit relatively small domains with average area distribution ranging from ~150 … 350 nm². Almost all molecules are aligned in chains, bonded together via two hydrogen bonds originating form the carboxylic groups. The spacing between the single rows is relatively large, the unit cell parameters of the structure amount to a = 1.1 nm, b = 0.8 nm, α = 93°. The domains itself are not highly ordered, as can be seen in the STM image in Figure 14(b): most of the molecules in the large domain on the right hand side are oriented with their long axis roughly vertical, but the two domains are separated by a row of molecules rotated ~90°, inducing almost no distortions in the network due to the large spacing between the rows.

4,4'-Biphenyldicarboxylic acid (BPDA)

The core of 4,4'-Biphenyldicarboxylic acid (BPDA) is comprised of two benzene rings separated by a single C-C sigma bond located diametral to the carboxylic group.


<div align="center">(a)   (b)</div>
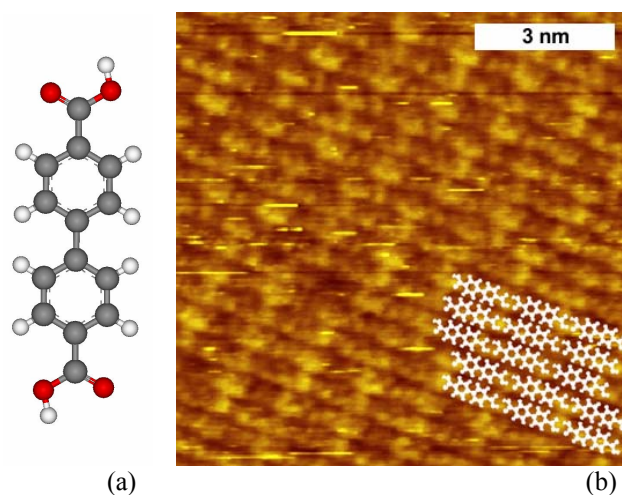
Figure 15: (a) 'Ball and Stick' model of 4,4'-Biphenyldicarboxylic acid (BPDA), (b) STM image of the monolayer structure of BPDA (U_T = 1.33 V, I_T = 1.2 nA).

Compared to NDA, BPDA takes a much higher preparation effort to achieve monolayer growth. While for most molecules investigated, simply applying a droplet of saturated solution onto the substrate is sufficient to initiate the growth of self-assembled monolayers, for BPDA the affinity of the molecules to the surface is lower than the affinity of the solvent. Thus no ordered structures of solute molecules can be found. This can be evaded by heating the sample with the droplet applied to 55°C for 10 min and a subsequent fast cool down on a heat sink (copper block) for another few minutes. After this processing fairly large (10.000 … 25.000 nm²), well ordered domains were found on the surface.

There are two possible reasons for the heat induced monolayer growth: One possibility is that even for saturated solutions the concentration is not high enough to precipitate monolayer growth. By heating the sample solvent is evaporating and the concentration increases until the critical point for structure formation is reached. Another possibility is, that the additional heat leads to higher mobility of the adsorbate molecules (possibly also by reducing the viscosity of the solvent), thereby providing thermal energy to overcame barriers for formation of the molecular network.

The molecules assemble in one-dimensional hydrogen bonded chains, which are associated mainly through comparatively weak van der Waals forces. Neighboring chains have two possible conformations: either the molecules are right next to each other, or they are shifted by half a molecule length (cf. inset in Figure 15(b)). Obviously the registry with the substrate perpendicular to the chains is unfavorable, resulting in a stress relaxation through buckling visible in the apparent height modulation of the molecules. This is hardly noticeable in Figure 15(b), but it gets more obvious by calculating a cross-correlation of a larger STM image. Figure 16 shows the cross-correlation for a small quadratic block (about 3 molecules) for a 20 x 20 nm STM image. It can be seen that every third or fifth row is slightly elevated (indicated by red spots in the image, and red bars on the left side of the image), whereas the rows in between exhibit normal contrast (green spots, white bars).
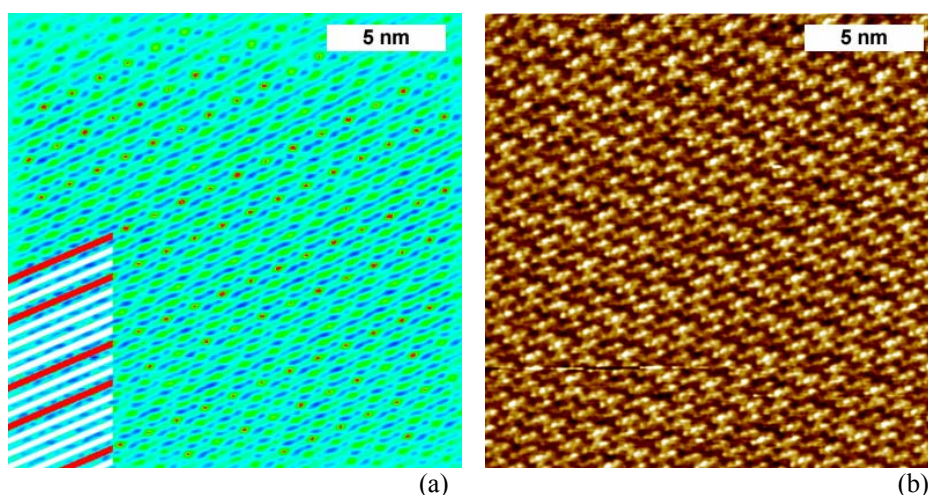
Figure 16: (a) Cross-correlation of a 20 x 20 nm^2 STM image (b) of a BPDA monolayer. Every third or fifth row is slightly elevated (see red dots of higher cross-correlation agreement), the rows in between show normal contrast. The bars on the left image side indicate the rows, red bars mark elevated chains, white bars chains with normal contrast respectively). Tunneling parameters for (b): $U_T \sim 1.23$ V, $I_T \sim 0.8$ nA).

The BPDA monolayers prepared by heating the sample are not very stable. The stress induced by the scanning process, i.e. forces exerted by the tip, leads to rapid decomposition of the network structures, usually starting at defects, like vacancies or unidentified dirt particles (cf. section 'Dynamic Behavior of the Monolayers' below for details).

4,4'-Stilbenedicarboxylic acid (SDA)

4,4'-Stilbenedicarboxylic acid (SDA) consists of two benzoic acid molecules, interconnected via a -C=C- bond.
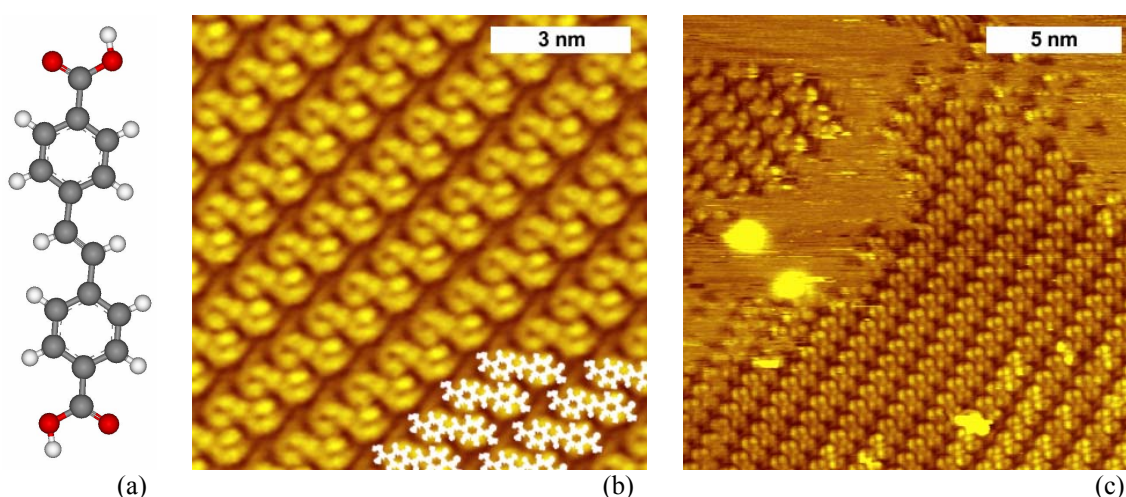

Figure 17: (a) 'Ball and Stick' model of 4,4'-Stilbenedicarboxylic acid (SDA), (b) STM image of the monolayer structure of SDA ($U_T = 0.5$ V, $I_T = 1.4$ nA), (c) STM image at an early stage of the structure formation, between the domains large blurry areas can be seen ($U_T = 0.9$ V, $I_T = 1.1$ nA).

The growth of SDA monolayers is significantly slower than that of NDA. After applying a droplet of saturated solution onto the sample crystal at room temperature, it takes ~1h until the monolayer can be observed with STM. In the first images the process of structure formation can clearly be observed, starting with some smaller domains with large areas of blurry features in between (cf. Figure 17(c)). Eventually SDA forms large domains, which cover the whole surface and the blurry areas disappear totally. Similarly, after recording split images for calibration purposes (and therefore damaging the adsorbate layer, cf. chapter 3.1.3), the reorganization takes some time (40 … 80 sec). In the first scans taken subsequently to a split image the monolayers are not totally reassembled. All SDA domains consist of chains of molecules lengthwise attached to each other via hydrogen bonds between the carboxylic groups at their ends, see inset in Figure 17(b). The unit cell parameters of the structure are: a = 1.37 nm, b = 0.75 nm, α = 95°.

Another interesting feature of the self-assembled SDA monolayers can be seen in the lower right corner of the image depicted in Figure 17(c): Some of the molecules appear brighter than most of the rest of the domain. Figure 18(a) shows a specially color coded image where 'normal' molecules are colored blue, and brighter ones are colored yellow. They also differ in the apparent shape: While 'normal' molecules appear in the shape of a number eight, the brighter ones have a significantly different shape. One half looks like the upper lobe of a number eight, whereas the bar in the middle of the molecule appears higher, and the other lobe of the eight shape is deformed. Although the contrast is different, the size of the molecules within the network is very similar, so no distortions of the overall network occur. A plausible explanation can be provided by enantiomeric point defects, i.e. single enantiomers of pseudo-chiral molecules are embedded in a matrix of the other enantiomer. Molecular mechanics calculations of the structure suggest, that single molecules which are the mirror image of the majority molecules, embedded in a domain of 'normal' molecules, stick out of the otherwise planar monolayer, whereas lateral distortions remain minor. (cf. Figure 18(c)). The molecules which form these chiral point defects are geometrically elevated, thus result in a brighter contrast and a different shape in the STM images.

(a)   (b)   (c)
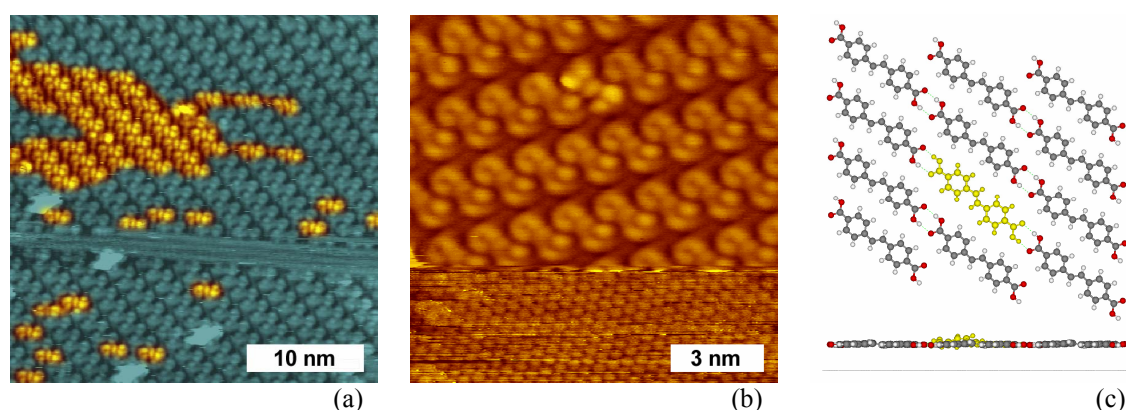
Figure 18: Chiral molecules in an SDA monolayer: (a) Most of the molecules in the monolayer appear in the shape of a number eight (blue colored areas), some appear brighter and with a slightly different shape (colored yellow) (U_T = 0.91 V, I_T = 1.04 nA); (b) close up of one differently shaped molecule within the layer (top in the middle), the lower part of this image shows the underlying graphite layer (U_T = 0.5 V, I_T = 1.01 nA). (c) shows a molecular mechanics simulation of a chiral point defect, i.e. a different enantiomer (yellow) surrounded by 'normal' molecules.

As shown above the self-assembly of SDA monolayers takes some time to start, and some additional time to grow into larger domains. Scanning a new area far away (μm … mm) from the previously imaged areas reveals two interesting effects: Firstly, the substrate is covered with large domains as well in these areas, indicating that the process of domain growths is not induced or perturbed by the scanning process. Secondly it shows that the domains have a high density of defects in the first scan, which are rapidly diminishing in the following scans. The process is illustrated by a series of subsequent STM images depicted in Figure 19.
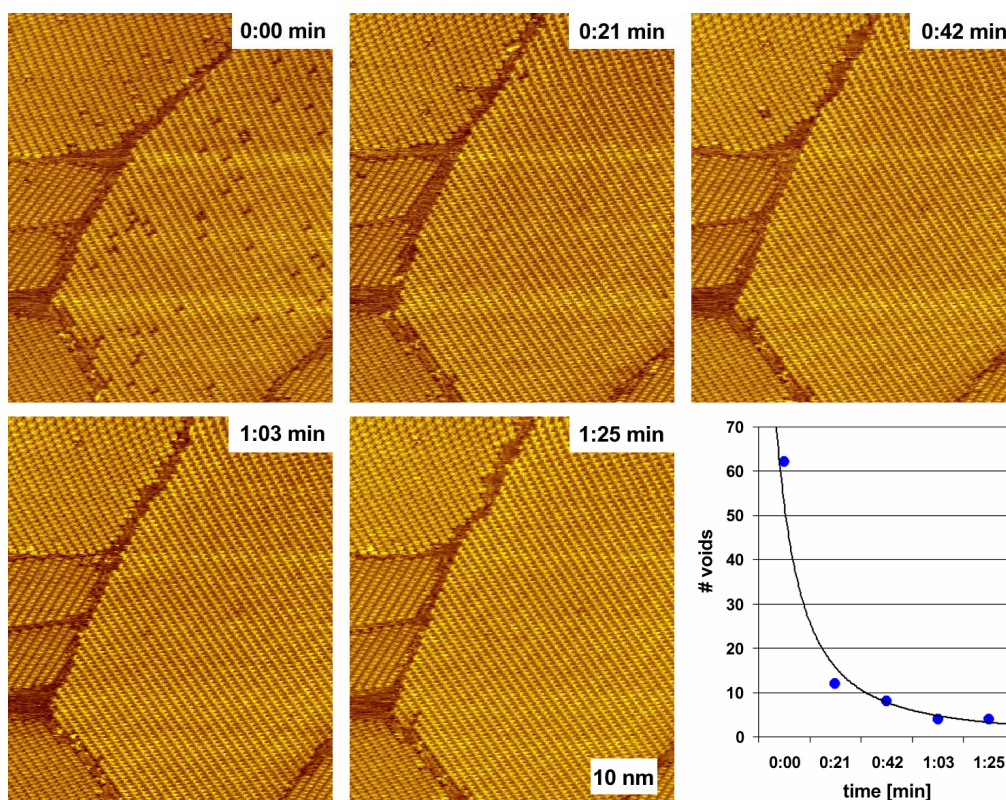

Figure 19: Assisted self-healing effect of an SDA monolayer, induced by successive scanning with STM. The sample was investigated with the STM for ~ 2.5 h, but the area shown has not been scanned prior to the first image. Each scanning of the area reduces the number of voids until it stabilizes around 4 voids.

This in turn indicates that there is an influence of the scanning with an STM tip, leading to a assisted self-healing of the surface defects. This leads to the conclusion, that the basic domain growth in SDA monolayers is not influenced by the scanning process, but the structural quality, i.e. the defect density of the domains is.

Dynamic Behavior of the Monolayers

Although the three molecules NDA, BPDA, and SDA are very similar in their molecular structure and their intermolecular binding, they behave highly different as far as their microstructure is concerned. For instance the growth rate, the size of the domains, the total area of the surface covered by molecules, the stability of the domains, and related to that the demeanor over time, and the behavior of the single domains with respect to each other were found to be very different for the three compounds.

NDA domain growth starts instantly after solution has been applied to the crystal surface. The NDA monolayer initially is comprised of several smaller domains scattered over the surface, growing slowly until the whole surface is covered. The number of domains remains more or less constant while the area covered by each domain is growing. Thus after initial nucleation only domain growth and not the emergence of new domains is observed This is illustrated by the series of STM images depicted in Figure 20 and in the diagram Figure 21.
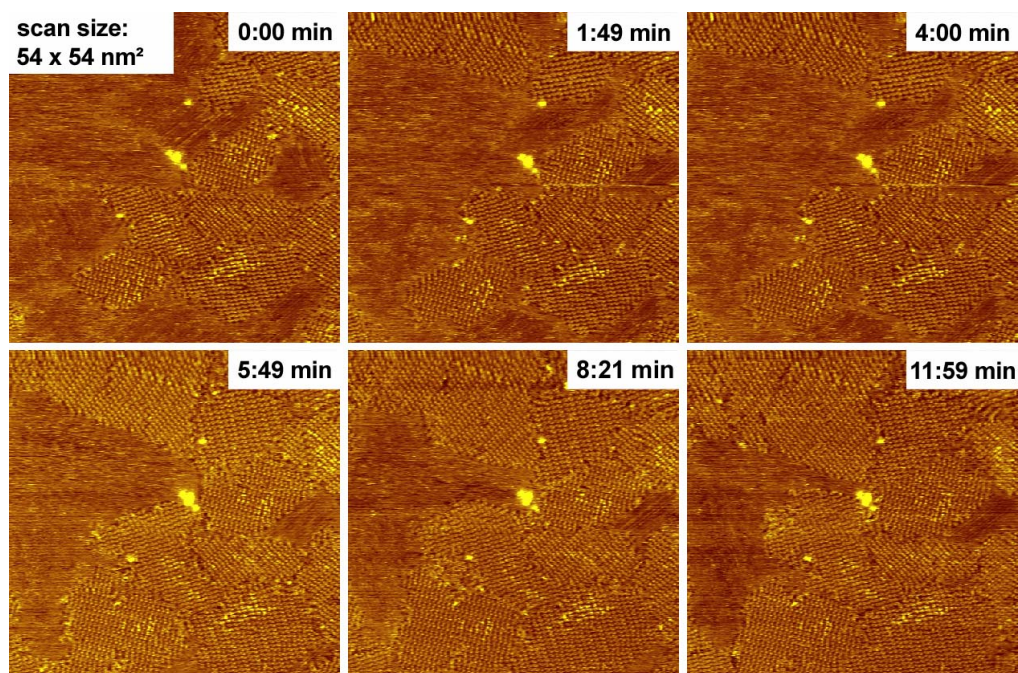

Figure 20: Domain growth of an NDA monolayer. Selected examples of a series of STM images demonstrating the slow domain growth during a time interval of about 12 minutes. The whole series of images is put together to a movie (*movie5_NDA.avi*, cf. appendix, section 2 Additional Material).
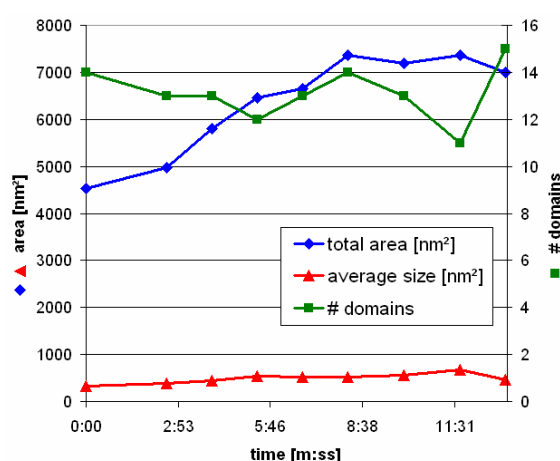
Figure 21: Domain growth of the NDA monolayer: represented are the number of domains within the image frame (green), the average size of the domains (red), and the total area covered by the NDA molecules (blue), source is the movie *movie5_NDA.avi* (cf. appendix, section 2 Additional Material).

A quite different behaviour was found for BPDA monolayers. As discussed above, for the growth of BPDA structures on a HOPG surface it is necessary to heat up the whole

system (i.e. substrate covered with solution) to 55°C for several minutes. Since it is technically not possible to image during the temper process with our current STM setup, monolayer growth can not be investigated. Due to the weakly bond network structure the BPDA layers disassemble easily. A small dirt particle on the surface (first image of Figure 22, lower left corner), or even single point defects in the structure (first image of Figure 22, vacancies which appear as several dark spots in the middle) act as starting points for the decomposition of the network. This process evolves rather fast, the time frame of the whole series of STM images covers about 5 minutes. It is noteworthy that the decomposition process is most likely induced by scanning with the STM tip. When moving to a new area, first the monolayer structure is intact but will decompose upon scanning.
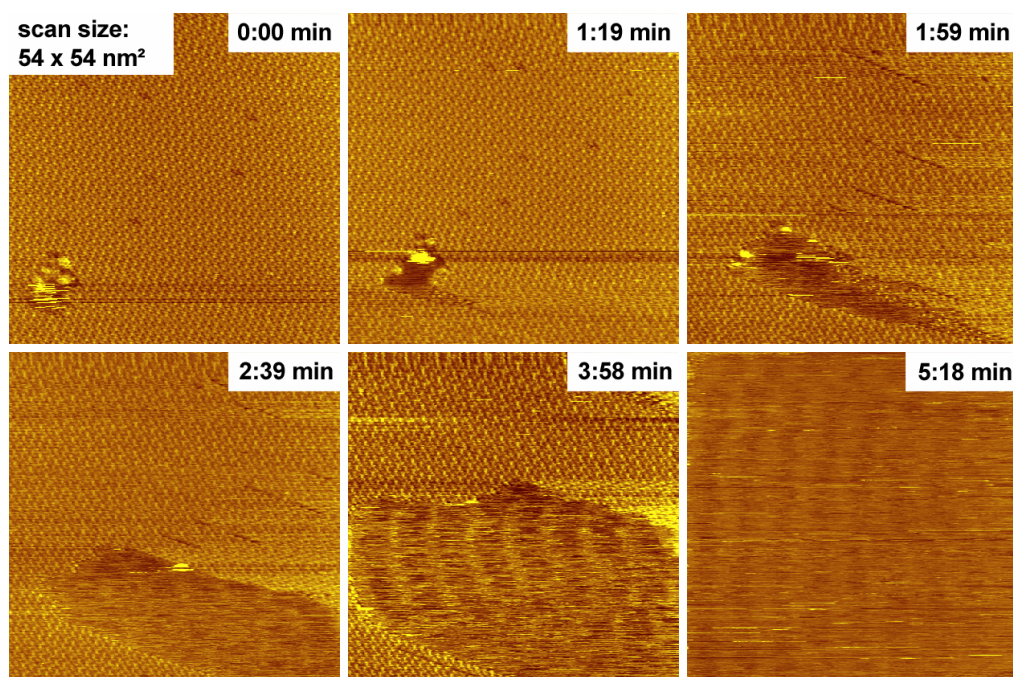
Figure 22: Temporal evolution of the domain structure in a BPDA monolayer. Starting from an impurity on the bottom left corner, and several point defects in the middle of the image, the whole monolayer is disintegrating in roughly 5 minutes. The whole series of images of this experiment can be found in the movie *movie6_BPDA.avi* (cf. appendix, section 2 Additional Material).

SDA monolayers are growing rather slow, but were found to be highly stable. Nevertheless some dynamics occur at the liquid solid interface, mainly reorganization of domains. The series of Figure 23 illustrates, how a domain is first changing its orientation and then is totally overgrown by a neighboring one. The upper half of the domain marked with an asterisk is subsequently incorporated into the domain right next to it (see images 1-5), which has the same orientation but is translated with respect to the neighboring domain. The lower half of the asterisk marked domain is first incorporated into a domain with an orientation rotated about 60° to the initial one (see images 1-4). In the following, that new domain rapidly merges with the large neighboring domain. The new domain, then covers the whole area previously occupied by the asterisk marked domain.

Here a process called Ostwald ripening is taking place, e.g. larger domains grow at the expanse of smaller ones. Driving force is the minimization of total edge-energy, the 2D

equivalent of surface tension. This behavior is similar to the one observed for TPA monolayers (cf. chapter 4.4).
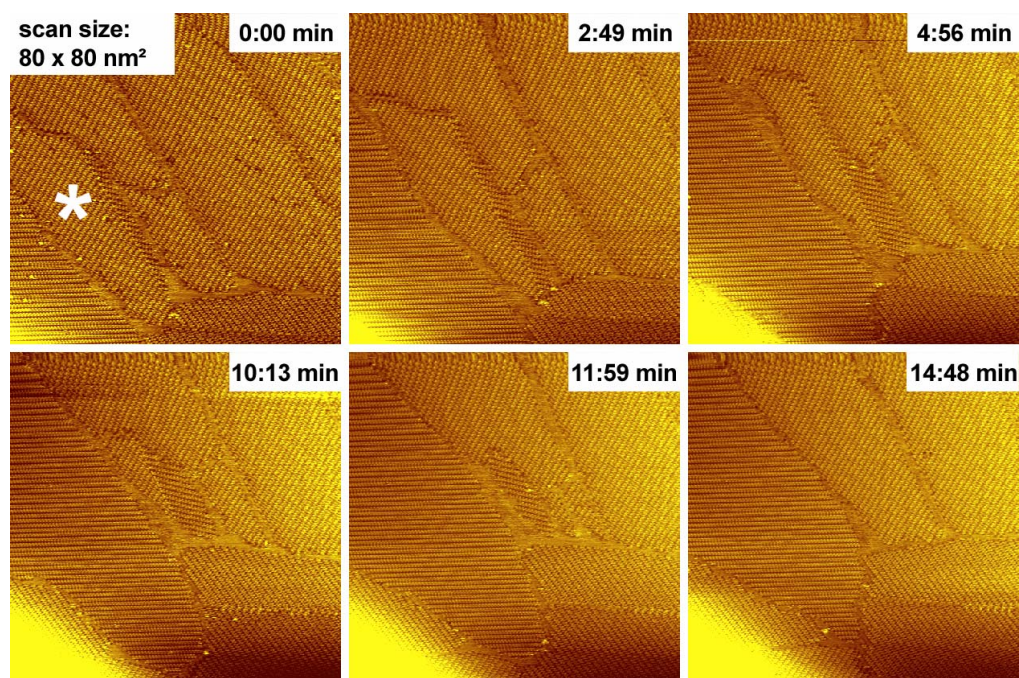

Figure 23: Dynamics of an SDA monolayer: Domains reorganize and grow at the expanse of smaller domains (Ostwald ripening). The white asterisk marks the domain, which disintegrates and is overgrown by neighboring domains (see text for details). The whole series of images of this experiment can be found in the movie *movie7_SDA.avi* (cf. appendix, section 2 Additional Material).

Molecular mechanics simulations were carried out for the three different molecular monolayers. Using a Dreiding II Force Field model (cf. chapter 3.2) several binding properties of the monolayers were calculated, using the experimentally determined unit cell parameters as a constraint. Although the absolute values of this calculation are highly questionable due to the above mentioned inaccuracies of the applied model, especially with layered crystals like HOPG, it is definitely appropriate for a comparison of the three molecules. As shown by the diagram in Figure 24 four different properties were calculated: The binding energy between one molecule and the substrate, indicated by green triangles. The lateral binding energy of one molecule within the structure, i.e. the interaction between one molecule and all its neighbors (without the interaction with the surface), indicated by purple diamonds. Third, the total binding energy of one molecule, which accounts for the sum of surface interaction and lateral interaction (blue circles). Last, the total energy of a singly crystalline monolayer of the respective network per 100 nm², i.e. multiplying the total binding energy per molecule times the number of molecules as derived from the unit cells.
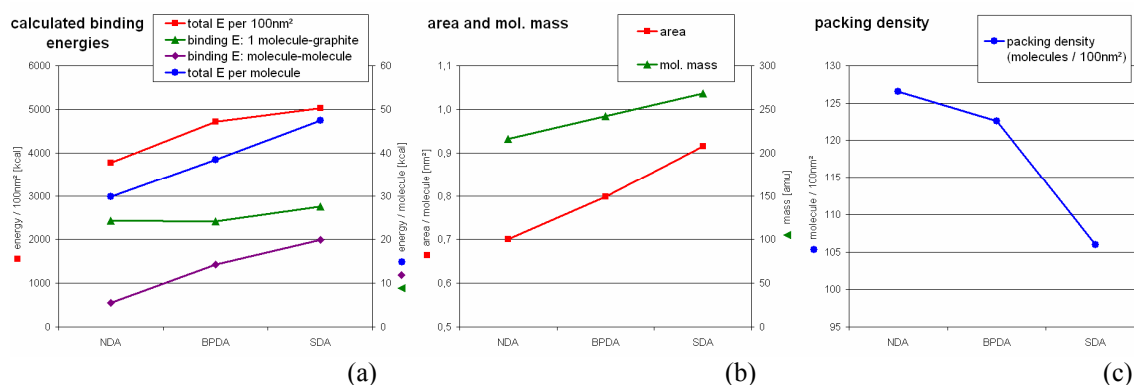
Figure 24: (a) Calculated binding energies of the three different molecules using a Dreiding II Force Field and unit cell parameters as obtained from the experiment; (b) area covered by one molecule and molar mass of the three molecules; (c) packing density of the molecular monolayer (molecules per 100 nm²)

Basically, the results of this calculation show a dependence of the total energy on the area per molecule, i.e. the size of the respective compound. On one hand, the adsorbate-graphite interaction scales with the size of the molecule, mainly due to the larger number of atoms available for van der Waals attraction. On the other hand, also the molecule-molecule interaction grows stronger, which can mainly be attributed to an increasing packing density. Nevertheless, all simulation results indicate that NDA forms the network with the lowest binding energy, i.e. stability. Whereas SDA networks exhibit the highest binding energy, and BPDA lays in between. However, the experimental results contradict to the simulations. This leads to the conclusion, that for the systems investigated here the differences in binding energy of the monolayers is not dominated by molecule-molecule and molecule substrate interactions, but must be significantly influenced by the local environment, namely the surrounding solution.

5. Conclusion

The focus of this work is on the investigation and the understanding of the adsorption processes of molecules at the liquid-solid interface. All molecules investigated here are physisorbed on a layered crystalline substrate, namely highly oriented pyrolytic graphite (HOPG). For the lateral interconnection between the molecules hydrogen bonds are accountable. Compared to covalent bonds, H-bonds are relatively weak and bonds can easily be formed, broken, and reformed again. This gives rise for the occurrence of dynamic behavior at room temperature, as domain growth.

First of all, a coadsorbed molecular system was investigated. Since 1,3,5-Tris(4-pyridyl)-2,4,6-triazine (TPT) has only the ability to accept hydrogen bonds through the outer three nitrogens, but lacks an H-bond donor, self-assembly was not observed with solutions containing only TPT. However when a second molecule, which acts as a kind of 'molecular glue' was added, ordered monolayers could be observed. Through the assisted adsorption of this second species hexagonal networks (with Trimesic acid (TMA) as linker molecule) or dense packed structures (with Terephthalic acid (TPA) as linker molecule) could be observed.

1,3,5-Benzenetribenzoic acid (BTB) molecules are slightly larger than TPT, and have carboxylic groups at the outer ends rendering monomolecular network structures possible. Thus this specific compound is predestinated for the growth of networks with large cavities. By applying various solvents, two different network structures were revealed experimentally. One is hexagonal with cavities of 2.8 nm in size, whereas the other one is oblique with significantly smaller cavities. A third BTB polymorph with close-packed structure was found later on, when aged solutions (~3 month old) were used. This is discussed in the light of solvent degradation, resulting in enhanced evaporation of part of the solvent after the liquid was applied to the crystal surface.

Subsequently, BTB was used to build bimolecular networks, i.e. structures comprised of two different molecular species. Referring to the previously observed TPT-TMA coadsorbed networks, Trimesic acid was used as secondary species. Probing a series of points in a 2D concentration space, revealed six different network structures, three of them being bimolecular. This information was condensed in a phase diagram of the binary TMA-BTB system. Furthermore it could be shown, that in-situ dilution leads to structural transitions in accordance with the phase diagram. Coadsorption of solvent molecules inside the cavities formed by the network structures was observed. Various reproducibly found contrasts indicated three different ways of solvent adsorption.

The dynamic behavior of monolayers of two different molecules, namely Trimesic acid (TMA) and Terephthalic acid (TPA), was investigated at the liquid-solid interface. Thereby a significant difference was found between three-fold TMA molecules (two dimensionally interconnected by H-bonds) and two-fold TPA molecules (only one dimensionally interconnected by H-bonds). The first one forms highly stable domains where only slight fluctuations of the domain boundaries occur, while the latter one exhibits a much higher mobility, and larger domains grow quickly at the expanse of smaller ones.

Furthermore, the dynamical behavior of various dicarboxylic acid molecules was investigated at the liquid solid interface by comparison of structurally related compounds. The three molecules have two interconnected benzoic acid groups in

common, however the spacing varies. It could be shown, that the dynamic behavior, e.g. island growth and ripening, of the monolayer structures is not dominated by the size, shape and binding properties of the molecules, but by the environment, namely the surrounding solution.

Much is to be learned about the self-assembly processes at the liquid-solid interface. A better understanding of the processes taking place during the growth of monolayer structures will help to promote the versatility and applicability of these highly potential systems for future use. This thesis shines some light on a few different aspects in the much more ample phenomenon of two-dimensional self-assembly, putting together some pieces of a great puzzle.

References

(1)   Lackinger, M.; Griessl, S.; Heckl, W. A.; Hietschold, M.; Flynn, G. W. *Langmuir* **2005**, *21*, 4984.

(2)   Hong, S. H.; Zhu, J.; Mirkin, C. A. *Science* **1999**, *286*, 523.

(3)   Ginger, D. S.; Zhang, H.; Mirkin, C. A. *Angew Chem Int Edit* **2004**, *43*, 30.

(4)   Auletta, T.; Dordi, B.; Mulder, A.; Sartori, A.; Onclin, S.; Bruinink, C. M.; Peter, M.; Nijhuis, C. A.; Beijleveld, H.; Schonherr, H.; Vancso, G. J.; Casnati, A.; Ungaro, R.; Ravoo, B. J.; Huskens, J.; Reinhoudt, D. N. *Angew Chem Int Edit* **2004**, *43*, 369.

(5)   Avouris, P.; Hertel, T.; Martel, R. *Appl Phys Lett* **1997**, *71*, 285.

(6)   Irmer, B.; Kehrle, M.; Lorenz, H.; Kotthaus, J. P. *Appl Phys Lett* **1997**, *71*, 1733.

(7)   Keyser, U. F.; Schumacher, H. W.; Zeitler, U.; Haug, R. J.; Eberl, K. *Appl Phys Lett* **2000**, *76*, 457.

(8)   Eigler, D. M.; Schweizer, E. K. *Nature* **1990**, *344*, 524.

(9)   Eigler, D. M.; Lutz, C. P.; Rudge, W. E. *Nature* **1991**, *352*, 600.

(10)   Manoharan, H. C.; Lutz, C. P.; Eigler, D. M. *Nature* **2000**, *403*, 512.

(11)   Mamin, H. J.; Guethner, P. H.; Rugar, D. *Phys Rev Lett* **1990**, *65*, 2418.

(12)   Jung, T. A.; Schlittler, R. R.; Gimzewski, J. K.; Tang, H.; Joachim, C. *Science* **1996**, *271*, 181.

(13)   Gimzewski, J. K.; Joachim, C. *Science* **1999**, *283*, 1683.

(14)   Joachim, C.; Gimzewski, J. K.; Aviram, A. *Nature* **2000**, *408*, 541.

(15)   Springholz, G.; Holy, V.; Mayer, P.; Pinczolits, M.; Raab, A.; Lechner, R. T.; Bauer, G.; Kang, H.; Salamanca-Riba, L. *Mat Sci Eng B-Solid* **2002**, *88*, 143.

(16)   Raab, A.; Lechner, R. T.; Springholz, G. *Appl Phys Lett* **2002**, *80*, 1273.

(17)   Kiravittaya, S.; Songmuang, R.; Rastelli, A.; Heidemeyer, H.; Schmidt, O. G. *Nanoscale Res Lett* **2006**, *Online Date: July 26, 2006*.

(18)   Heidemeyer, H.; Muller, C.; Schmidt, O. G. *Journal of Crystal Growth* **2004**, *261*, 444.

(19)   Andres, R. P.; Bielefeld, J. D.; Henderson, J. I.; Janes, D. B.; Kolagunta, V. R.; Kubiak, C. P.; Mahoney, W. J.; Osifchin, R. G. *Science* **1996**, *273*, 1690.

(20)   Liu, J.; Lee, T.; Janes, D. B.; Walsh, B. L.; Melloch, M. R.; Woodall, J. M.; Reifenberger, R.; Andres, R. P. *Appl Phys Lett* **2000**, *77*, 373.

(21)   Theobald, J. A.; Oxtoby, N. S.; Phillips, M. A.; Champness, N. R.; Beton, P. H. *Nature* **2003**, *424*, 1029.

(22)   Perdigao, L. M. A.; Champness, N. R.; Beton, P. H. *Chem Commun* **2006**, 538.

(23)   Griessl, S. J. H.; Lackinger, M.; Jamitzky, F.; Markert, T.; Hietschold, M.; Heckl, W. A. *Langmuir* **2004**, *20*, 9403.

(24)   Florio, G. M.; Werblowsky, T. L.; Muller, T.; Berne, B. J.; Flynn, G. W. *J Phys Chem B* **2005**, *109*, 4520.

(25)   Gyarfas, B. J.; Wiggins, B.; Zosel, M.; Hipps, K. W. *Langmuir* **2005**, *21*, 919.

(26)   Ball, P. *Nature* **2001**, *413*, 667.

(27) Hecht, S. *Angew Chem Int Edit* **2003**, *42*, 24.
(28) Sowerby, S. J.; Heckl, W. M. *Origins Life Evol B* **1998**, *28*, 283.
(29) Smith, R. K.; Lewis, P. A.; Weiss, P. S. *Prog Surf Sci* **2004**, *75*, 1.
(30) Jeffrey, G. A. *An introduction to hydrogen bonding*; Oxford University Press: New York ; Oxford, 1997.
(31) Lackinger, M.; Griessl, S.; Markert, T.; Jamitzky, F.; Heckl, W. M. *J Phys Chem B* **2004**, *108*, 13652.
(32) Stepanow, S.; Strunskus, T.; Lingenfelder, M.; Dmitriev, A.; Spillmann, H.; Lin, N.; Barth, J. V.; Woll, C.; Kern, K. *J Phys Chem B* **2004**, *108*, 19392.
(33) Yokoyama, T.; Yokoyama, S.; Kamikado, T.; Okuno, Y.; Mashiko, S. *Nature* **2001**, *413*, 619.
(34) Rosei, F.; Schunack, M.; Jiang, P.; Gourdon, A.; Laegsgaard, E.; Stensgaard, I.; Joachim, C.; Besenbacher, F. *Science* **2002**, *296*, 328.
(35) Schunack, M.; Petersen, L.; Kuhnle, A.; Laegsgaard, E.; Stensgaard, I.; Johannsen, I.; Besenbacher, F. *Phys Rev Lett* **2001**, *86*, 456.
(36) Glass, R.; Moller, M.; Spatz, J. P. *Nanotechnology* **2003**, *14*, 1153.
(37) Shchukin, V. A.; Ledentsov, N. N.; Bimberg, D. *Physica E* **2001**, *9*, 140.
(38) Gerardot, B. D.; Subramanian, G.; Minvielle, S.; Lee, H.; Johnson, J. A.; Schoenfeld, W. V.; Pine, D.; Speck, J. S.; Petroff, P. M. *J Cryst Growth* **2002**, *236*, 647.
(39) Gimzewski, J. K.; Joachim, C.; Schlittler, R. R.; Langlais, V.; Tang, H.; Johannsen, I. *Science* **1998**, *281*, 531.
(40) Mayor, M.; Buschel, M.; Fromm, K. M.; Lehn, J. M.; Daub, J. *Chem-Eur J* **2001**, *7*, 1266.
(41) Griessl, S.; Lackinger, M.; Edelwirth, M.; Hietschold, M.; Heckl, W. M. *Single Mol* **2002**, *3*, 25.
(42) Dmitriev, A.; Lin, N.; Weckesser, J.; Barth, J. V.; Kern, K. *J Phys Chem B* **2002**, *106*, 6907.
(43) Ishikawa, Y.; Ohira, A.; Sakata, M.; Hirayama, C.; Kunitake, M. *Chem Commun* **2002**, 2652.
(44) Su, G. J.; Zhang, H. M.; Wan, L. J.; Bai, C. L.; Wandlowski, T. *J Phys Chem B* **2004**, *108*, 1931.
(45) Han, B.; Li, Z.; Pronkin, S.; Wandlowski, T. *Can J Chem* **2004**, *82*, 1481.
(46) Lu, J.; Zeng, Q. D.; Wang, C.; Zheng, Q. Y.; Wan, L. J.; Bai, C. L. *J Mater Chem* **2002**, *12*, 2856.
(47) Pawin, G.; Wong, K. L.; Kwon, K. Y.; Bartels, L. *Science* **2006**, *313*, 961.
(48) Otero, R.; Schock, M.; Molina, L. M.; Laegsgaard, E.; Stensgaard, I.; Hammer, B.; Besenbacher, F. *Angew Chem Int Edit* **2005**, *44*, 2270.
(49) Bohringer, M.; Morgenstern, K.; Schneider, W. D.; Berndt, R.; Mauri, F.; De Vita, A.; Car, R. *Phys Rev Lett* **1999**, *83*, 324.
(50) Weckesser, J.; De Vita, A.; Barth, J. V.; Cai, C.; Kern, K. *Phys Rev Lett* **2001**, *8709*, art. no.
(51) Mamdouh, W.; Uji-i, H.; Ladislaw, J. S.; Dulcey, A. E.; Percec, V.; De Schryver, F. C.; De Feyter, S. *J Am Chem Soc* **2006**, *128*, 317.
(52) Giancarlo, L. C.; Flynn, G. W. *Annu Rev Phys Chem* **1998**, *49*, 297.
(53) De Feyter, S.; De Schryver, F. C. *J Phys Chem B* **2005**, *109*, 4290.
(54) Heckl, W. M.; Smith, D. P. E.; Binnig, G.; Klagges, H.; Hansch, T. W.; Maddocks, J. *P Natl Acad Sci USA* **1991**, *88*, 8003.

(55)   Reiter, M. M.; Jamitzky, F.; Trixler, F.; Heckl, W. M. *Phys Status Solidi A* **2001**, *187*, 171.

(56)   Binnig, G.; Rohrer, H.; Gerber, C.; Weibel, E. *Appl Phys Lett* **1982**, *40*, 178.

(57)   Binning, G.; Rohrer, H.; Gerber, C.; Weibel, E. *Phys Rev Lett* **1982**, *49*, 57.

(58)   Drobek, T.; Reiter, M.; Heckl, W. M. *Appl Surf Sci* **2004**, *238*, 3.

(59)   Safarowsky, C.; Merz, L.; Rang, A.; Broekmann, P.; Hermann, B. A.; Schalley, C. A. *Angew Chem Int Edit* **2004**, *43*, 1291.

(60)   He, Y.; Ye, T.; Borguet, E. *J Am Chem Soc* **2002**, *124*, 11964.

(61)   Yoshimoto, S.; Higa, N.; Itaya, K. *J Am Chem Soc* **2004**, *126*, 8540.

(62)   Binnig, G.; Rohrer, H.; Gerber, C.; Weibel, E. *Phys Rev Lett* **1983**, *50*, 120.

(63)   Oura, K.; Lifshits, V. G.; Saranin, A. A.; Zotov, A. V.; Katayama, M. *Surface Science - An Introduction*; Springer-Verlag: Berlin, Heidelberg, New York, 2003.

(64)   Tersoff, J.; Hamann, D. R. *Phys Rev Lett* **1983**, *50*, 1998.

(65)   Tersoff, J.; Hamann, D. R. *Phys Rev B* **1985**, *31*, 805.

(66)   Bardeen, J. *Phys Rev Lett* **1961**, *6*, 57.

(67)   Chen, C. J. *Introduction to Scanning Tunneling Microscopy*; Oxford University Press, Inc.: New York, 1993.

(68)   Mizutani, W.; Shigeno, M.; Ono, M.; Kajimura, K. *Appl Phys Lett* **1990**, *56*, 1974.

(69)   Mayo, S. L.; Olafson, B. D.; Goddard, W. A. *J Phys Chem-Us* **1990**, *94*, 8897.

(70)   Batra, I. P.; Garcia, N.; Rohrer, H.; Salemink, H.; Stoll, E.; Ciraci, S. *Surf Sci* **1987**, *181*, 126.

(71)   Tomanek, D.; Louie, S. G. *Phys Rev B* **1988**, *37*, 8327.

(72)   Wohlfarth, C. Static Dielectric Constants of Pure Liquids and Binary Liquid Mixtures. In *Landolt-Börnstein*; Macroscopic and Technical Properties of Matter ed.; Madelung, O., Ed.; Springer-Verlag: Berlin, Heidelberg, New York, 1991; Vol. 6 Numerical Data and Functional Relationships in Science and Technology.

(73)   Landolt-Börnstein. **1991**, *Vol. 6.*

Appendix

1. Manuscripts

Mediated Coadsorption at the Liquid-Solid Interface:
Stabilization through Hydrogen Bonds

Lorenz Kampschulte, Stefan Griessl, Wolfgang M. Heckl, and Markus Lackinger

Mediated Coadsorption at the Liquid−Solid Interface: Stabilization through Hydrogen Bonds

Lorenz Kampschulte,[†] Stefan Griessl,[†] Wolfgang M. Heckl,[†,‡] and Markus Lackinger*,[†]

Ludwig-Maximilians-University Munich, Department for Earth- and Environmental Sciences, and Center for Nanoscience (CeNS), Theresienstr. 41, 80333 München, Germany, and Deutsches Museum, Museumsinsel 1, 80538 München, Germany

Received: February 15, 2005; In Final Form: March 31, 2005

Stable adsorption of 1,3,5-tris(4-pyridyl)-2,4,6-triazine (TPT) molecules from the liquid phase was only observed in binary solutions, that is, in the presence of a second (adsorptive) species. The process of mediated coadsorption of a molecular species at the liquid−solid interface was accomplished through complexation of TPT with a second type of molecule acting as a "molecular glue" via hydrogen bonds. Scanning tunneling microscopy (STM) was utilized to investigate the structure of the coadsorbed monolayers at the liquid−solid interface. Trimesic acid (TMA) and terephthalic acid (TPA)—both benzene rings with disposed carboxylic acid groups—were appropriate to precipitate the stable adsorption of TPT. According to the different symmetry and number of carboxylic acid groups, various networks were observed.

Introduction

Self-assembled monolayers (SAMs) are an important stepping off point for novel applications of long range ordered organic films in molecular electronics, catalysis, or sensor development. Hence, it is of general interest to understand the parameters determining growth and stability. Generally, the self-assembly process of two-dimensional networks on surfaces is governed by a crucial balance between adsorbate−substrate and adsorbate−adsorbate (either direct or mediated by the substrate) interactions. For weak interacting substrates such as layered materials, the molecule−molecule interactions can become predominant, particularly if hydrogen bonds come into play. However, even for inferior substrate influence, normally there is a distinct relation between adsorbate and substrate lattice, for example, commensurability or point on line structures.[1,2] Hydrogen bonds are of particular interest in 2D self-assembled networks because they are highly selective and directional, though moderately strong.[3−6]

Scanning tunneling microscopy (STM) has proven to be an ideal in situ probe for the structural and electronic properties of the coupled adsorbate−substrate system at the interface between solution and solid.[7,8] In contrast to vacuum deposition experiments, stable adsorption at the liquid−solid interface only occurs if it leads to a minimum in free energy (equilibrium); thus, the molecules have an additional degree of freedom to remain dissolved. For these kinds of experiments, the size of the molecular adsorbates always represents a tradeoff: the larger a molecule is, the larger is its adsorption energy. However, the solubility of the compound normally decreases with increasing size. A common strategy to enhance the adsorption energy of compounds is to append alkyl chains, acting as anchor groups on a graphite surface.[9−11] Since there is an almost perfect registry between the graphite(0001) surface and the alkane

backbone, the additional contribution to the adsorption energy increases nearly linearly with chain length, as verified by thermal desorption spectroscopy experiments.[12−14] However, the covalently attached alkane chains alter the molecular structure and can also be used to tailor the monolayer structure, for example, the spacing between lamellae of a porphyrin core.[11] In this work, we implement a different strategy: H-bonds are utilized to create noncovalently bound complexes of 1,3,5-tris(4-pyridyl)-2,4,6-triazine (TPT) and a second type of molecule, which acts as a linker. Because stable adsorption of TPT itself from the liquid phase has never been observed, these complexes facilitate the adsorption through an increased adsorption energy.

Experimental Section

All experiments were conducted at the liquid−solid interface under ambient conditions with a home-built pocket size scanning tunneling microscope driven by a commercial RHK SPM-100 control system. As probes, mechanically cut Pt/Ir tips were used, which were conditioned by short voltage pulses if necessary. Since the solvents used here are electrically nonconducting, it was not necessary to insulate tips.

Samples were prepared by depositing a small droplet (~5 μL) of solution on the basal plane of freshly cleaved, highly oriented pyrolytic graphite (HOPG). It is noteworthy that the influence of the solvent on the equilibrium between molecules in solution and on the surface can be crucial. By means of the homologous series of fatty acids, it has been shown that a particular modification of a polymorphic adsorption system can be selected by solvent identity.[15] A suitable solvent in this case is heptanoic acid ($CH_3(CH_2)_5COOH$), because the carboxylic group is responsible for dissolving the molecules used herein. Also, the vapor pressure of heptanoic acid is low enough for room temperature STM experiments to be performed for up to 1 h after deposition. Elevated temperatures favor solvent evaporation, significantly shortening the sample's lifetime.

Tunneling voltages between +0.3 and +1.6 V, with respect to the tip, and reference currents around 100 pA were used. All STM images shown were recorded in the constant current mode

---

* Corresponding author. Phone: +49 89 2180 4188. Fax: +49 89 2180 4334. E-mail: markus@lackinger.org.
† Ludwig-Maximilians-University Munich and Center for Nanoscience (CeNS).
‡ Deutsches Museum.

Mediated Coadsorption at the Liquid−Solid Interface

*J. Phys. Chem. B, Vol. 109, No. 29, 2005* **14075**
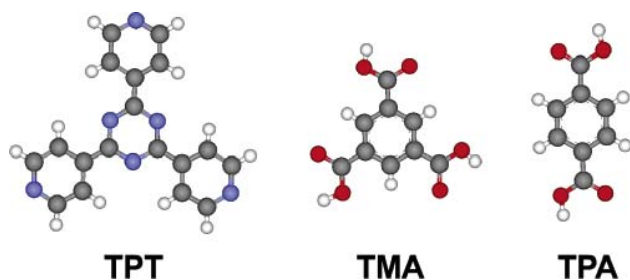
Figure 1. Structures of the adsorbate molecules: 1,3,5-tris(4-pyridyl)-2,4,6-triazine (TPT), trimesic acid (TMA), and terephthalic acid (TPA). In the structures, gray corresponds to carbon atoms, white to hydrogen atoms, red to oxygen atoms, and blue to nitrogen atoms, respectively.

of operation. For noise reduction, the STM images were processed by leveling and 3×3 G filtering.

Results and Discussion

We investigate the adsorption behavior of TPT at the liquid−solid interface in the presence of either trimesic acid (TMA) or terephthalic acid (TPA). TPT consists of a triazine ring in the center with three symmetrically disposed pyridyl rings. Similar to TMA and TPA, TPT is a planar molecule (cf. Figure 1). Adsorption with the molecular plane parallel to the substrate is observed for comparable aromatic molecules, thereby optimizing the interaction with the substrate.[16−18] However, despite many attempts, adsorption of TPT from heptanoic acid solution only containing this species has never been observed. In an equilibrated system, TPT molecules remain dissolved and do not form an interfacial monolayer. Stronger interacting substrates, for example, metal surfaces, might possibly shift the equilibrium toward adsorption. Densely packed structures evolve when a monolayer of TPT is evaporated on graphite at room temperature in an ultrahigh vacuum (UHV) environment.[19]

TMA consists of a benzene ring with three carboxylic acid groups symmetrically attached in the 1, 3, and 5 positions. Because of the carboxylic acid groups, TMA and TPA respectively have the ability to form homomolecular H-bonds. Since carboxyl groups are both proton donors and acceptors, they can hydrogen bond with themselves without the necessity of any other functional group.[20] Consequently, both TMA and TPA form H-bond structures at the liquid−solid interface through spontaneous self-assembly.[15,21] In contrast to TPA, TMA assembles on graphite in a loosely packed structure, with ∼1.0 nm wide cavities appropriate for the incorporation of molecular guests.[22,23] A comparable TMA host structure was also observed in an electrochemical STM study on Au(111) under suitable potential conditions[24] and in UHV experiments with TMA submonolayers evaporated on Cu(100).[25] However, another electrochemical STM study of TMA on Au(111) revealed also potential driven phase transitions and various phases with upright molecules.[26] Similarly, TPA monolayers were investigated on Au(111)[27] and Cu(100)[28] by STM under UHV conditions.

Usually, stable adsorption of molecular monolayers at the liquid−solid interface only takes place in an equilibrium situation when the system minimizes free energy. There are at least four significant contributions to the free energy: adsorption energy, solvation energy, intermolecular interaction, and entropy. In many cases, the adsorption energy of just a monomer is not sufficient for the evolution of stable monolayers, particularly for small molecules on weakly interacting substrates such as layered crystals (e.g., graphite). Therefore, strong intermolecular interactions such as H-bonds enhance the stabilization energy for molecules on the surface and can eventually lead to self-

assembly of stable monolayers at the interface. In this case, coadsorption of TPT as a proton acceptor together with either TMA or TPA molecules as proton donor leads to stable adsorption of TPT through N···H−O H-bonds. Although the self-assembled networks formed by the two systems are quite different, the same driving force, namely, H-bonds, is evident.

For the systems under investigation, the concentration ratio of both adsorbates can be crucial. Because of the possibility of forming two H-bonds per carboxylic group, TMA and TPA molecules have a high affinity to building networks with themselves rather than mixed networks with TPT molecules. For that reason, we used for the system TPT + TMA a volume ratio of (6 parts of TPT solution):(1 part of TMA solution):(8 parts of solvent), where TPT and TMA solution represent a saturated solution in heptanoic acid. Dilution with pure solvent became necessary because more concentrated solutions lead to the precipitation of presumably bulk cocrystals of TPT and TMA all over the surface, as identified with an optical microscope. In the case of TPT and TPA, preparation was straightforward, since a saturated binary solution of TPT and TPA in heptanoic acid with a sediment of both TPT and TPA worked. The sediment should also contain a phase with the TPT−TPA bulk cocrystal in equilibrium with the liquid phase.

TPT and TMA

The binary solution of TPT and TMA leads to a coadsorbed monolayer with a 6-fold symmetry, as seen in the STM image presented in Figure 2a. Assuming parallel adsorption of both molecules, each can be clearly distinguished by means of their apparent size in the STM image. Single TPT molecules appear as a triangle of elevated circular features with a central depression. This 3-fold symmetry of TPT in the STM contrast agrees with the symmetry of the molecular structure. In addition, the spacing between intramolecular intensity minima of TPT (marked by white arrows in Figure 2a and assigned to the center of pyridyl groups) is ∼0.7 nm and matches the distance predicted by a molecular mechanics simulation of the TPT structure. Similar distances were found for the features assigned to the TPT molecule in the TPT−TPA cocrystal as discussed below. Also, the three grouped features identified as the TPT molecule exhibit similar apparent heights, whereas the single circular protrusion assigned to the TMA molecule (marked by a white circle in Figure 2a) appears remarkably darker. This similarity in intensity provides some evidence that the three grouped features can be assigned to the same molecule, namely, TPT. Furthermore, in the STM contrast appears an undefined structure inside the cavities. This might stem from a transient adsorption of guests (either TMA, TPT, or heptanoic acid molecules). However, their adsorption energy is not large enough to allow for a clear imaging process. Possible explanations comprise that the molecules are either pushed away by the tip or desorb again on a rapid time scale. A model of the assembly structure indicating the H-bonding scheme is depicted in Figure 2b. The honeycomb packing motif of TPT−TMA is already known from X-ray diffraction experiments on bulk cocrystals.[29] In this study a dense packing was inhibited by pyrene guests within the cavities of aligned TPT−TMA honeycomb planes, thereby forming pyrene "nanorods". However, the 2D cocrystal is loosely packed and exhibits a periodic arrangement of voids, which might by suited for the guided coadsorption of a guest within this host network. As mentioned previously, TMA by itself also forms a host system on graphite[20] and molecular guests were already incorporated at the liquid−solid interface.[22,23] The lattice constant of the mixed system is
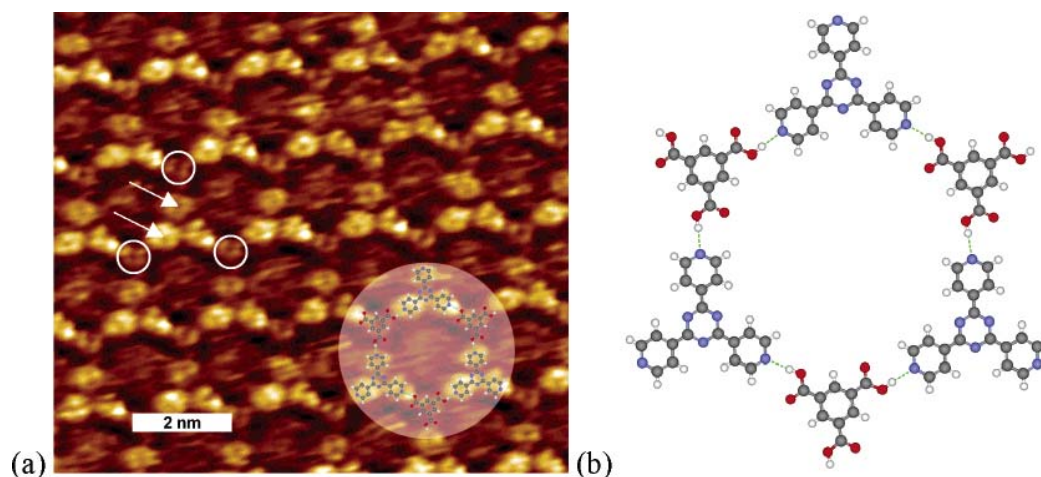
Figure 2. (a) STM topograph of the 2D TPT–TMA cocrystal on HOPG (0001). The white circles indicate TMA molecules, and the arrows mark the center-to-center distance (∼0.7 nm) between two pyridyl groups of one TPT molecule. (b) Molecular model of the structure, where one TMA coordinates three TPT molecules via H-bonds. The cutout shows three TPT molecules and three TMA molecules bordering one cavity of the host network. The dashed lines indicate N· · ·H–O H-bonds.
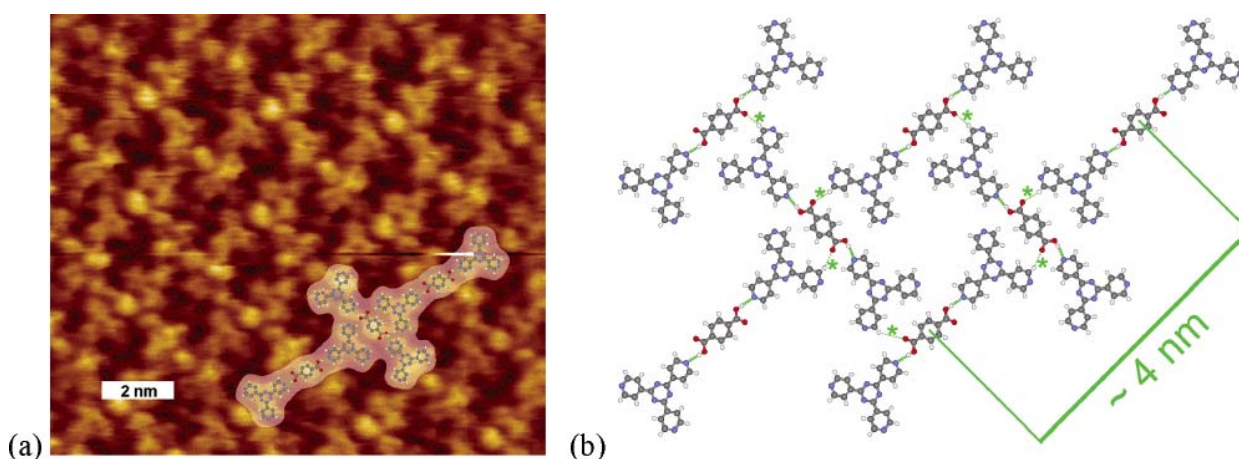

Figure 3. (a) STM topograph of the 80° TPT–TPA cocrystal on HOPG (0001). TPT molecules appear as several bright, triangularly arranged features, whereas TPA appears as a single round feature. (b) Molecular model of the 90° TPT–TPA structure (the bold dashed green lines indicate the N· · ·H–O H-bonds of the TPT–TPA–TPT basic units, and the fine green lines (additionally marked with asterisks) indicate weaker C–H···O H-bonds between these building blocks).

larger than that for pure TMA layers (∼2.0 nm vs ∼1.6 nm), because the TPT molecule is much larger than TMA. Even larger cavities (diameter ∼2.8 nm) could be achieved with benzenetribenzoic acid (BTB) as a building block.[30] The structure of BTB is rather similar to that of TPT but with carboxylic acid groups as linkers at the periphery. Another characteristic of the TPT–TMA system is the free carbonyls of the acid groups of TMA protruding into the cavity. They might serve as sites for H-bonds between the cavity wall and potential guest molecules.

To obtain the crystallographic relation between substrate and adsorbate, that is, the superstructure matrix, the adsorbate and substrate lattices were recorded within one scanning frame, as shown previously for dicarboxylic acids.[21] Fast Fourier transformation (FFT) of those split images allows for a precise determination of the superstructure matrix. By using the graphite lattice as an intrinsic ruler, it was possible to determine the unit cell of the monolayer, thereby excluding external falsifications such as drift or scanner calibration.

$$\begin{pmatrix} \vec{A} \\ \vec{B} \end{pmatrix} = \begin{pmatrix} 7 & 9 \\ -2 & 7 \end{pmatrix} \begin{pmatrix} \vec{a} \\ \vec{b} \end{pmatrix} \text{ or alternatively } \begin{pmatrix} \vec{A} \\ \vec{B} \end{pmatrix} = \begin{pmatrix} 9 & 7 \\ 2 & 9 \end{pmatrix} \begin{pmatrix} \vec{a} \\ \vec{b} \end{pmatrix}$$

The experimental error of the coefficients is in the range ±0.5. This and all following matrices refer to substrate base vectors with an angle of 120°. As the unit cells are rather large, the relative error of the adsorbate vector is still below 7%. According to the commensurate matrix, the length of the adsorbate vectors amounts to 2.01 nm. The angle between the vectors is exactly 60° and thus is consistent with the anticipated 6-fold symmetry of the structure. Both adsorbate vectors are rotated by approximately +12.2° with respect to the graphite lattice. The second matrix was measured as well and describes a symmetry equivalent adsorbate lattice (mirrored on a graphite axis) with an angle of approximately −12.2° to the graphite lattice.

TPT and TPA

The coadsorption of TPT and TPA molecules on HOPG(0001) leads to a comparatively densely packed structure with a bone-shaped packing motif, as seen in the STM image in Figure 3a.

The TPT–TPA network is built up of small hydrogen-bond units, comprised of two TPT molecules interconnected by a TPA molecule (cf. Figure 3b). In this packing motif, the carboxylic hydrogen atoms are bound to the outer nitrogen atoms of TPT
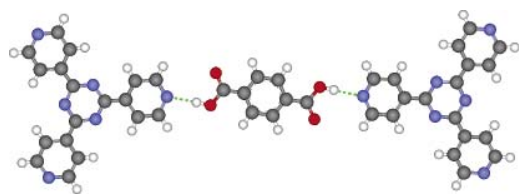
Figure 4. Model of the basic unit of the 2D TPT−TPA crystal consisting of two TPT molecules and one TPA molecule connected via H-bonds. The dashed lines indicate N···H−O H-bonds, and the TPT center-to-center distance amounts to ∼2.5 nm.

via N···H−O H-bonds. This defines the basic unit of the bone-shaped structure, as depicted in Figure 4. The neighboring units are located perpendicular with their axis in the middle of the long axis of the first one, as indicated in Figure 3b. This results in a more or less quadratic weaving pattern of molecules laying length- and crosswise. Referring to the angle between neighboring basic units, two different structures were observed: One structure is quadratic within the experimental error with an angle of 90° between the units, as shown in the model of Figure 3b. The second structure is slightly tilted which results in an angle of ∼80° between the two axes of neighboring basic units. The distance between two equally oriented units is about 4 nm in each direction, as indicated in Figure 3b.

To precisely measure the superstructure matrices, split images with substrate and adsorbate in one frame were recorded. Using FFT and the graphite layer as a reference, the commensurate superstructure matrices of the two TPT−TPA polymorphs were determined:

$$\begin{pmatrix}\vec{A}\\\vec{B}\end{pmatrix}=\begin{pmatrix}8 & 0\\5 & 10\end{pmatrix}\begin{pmatrix}\vec{a}\\\vec{b}\end{pmatrix}\text{ (90° structure) and}$$

$$\begin{pmatrix}\vec{A}\\\vec{B}\end{pmatrix}=\begin{pmatrix}10 & 5\\1 & 9\end{pmatrix}\begin{pmatrix}\vec{a}\\\vec{b}\end{pmatrix}\text{ (80° structure)}$$

It is reasonable to assume that both structures do not exhibit a significant difference in total free energy, an observation which is generally made for polymorphic modifications. For a comprehensive study of the binding energy, calculations, which use the measured unit cell parameters as a constraint, are highly desirable. However, the accuracy of molecular mechanics simulations might not be sufficient to unambiguously reveal small differences (in comparison to the thermal energy) in total energy.

Both the TPT−TMA and the TPT−TPA cocrystals are stabilized by N···H−O H-bonds, and all carboxylic acid groups of either TMA or TPA participate in the H-bonding. The main difference between TPT−TMA and TPT−TPA coadsorption structures is the H-bond networking. In the TPT−TMA structure, all outer nitrogens of TPT are involved in H-bonds, resulting in an actual network. However, for TPT−TPA, only the basic unit—comprised of two TPT molecules and one TPA molecule—is strongly H-bonded. These units interact and assemble through comparatively weak van der Waals bonds. However, additional C−H···O H-bonds between the hydrogen atoms of TPT and the carboxylic oxygen atoms of TPA, as indicated in Figure 3b, might additionally stabilize that structure. The distance between the corresponding carbon and oxygen atoms (∼0.4 nm) as evaluated from the scaled models matches the range for C−H···O bonds (0.3−0.4 nm in a straight configuration).[31] Although this kind of H-bond is comparatively weak, its stabilizing influence exceeds exclusive van der Waals bonding. In all structures, both TPA and TMA coordinate as

many TPT molecules as there are carboxylic acid groups available.

The binding energy for TMA is presumably larger than that for TPA, since it forms three H-bonds versus two for TPA, while both molecules have an aromatic system of equal size. The binding energy of a single N···H−O bond was determined in molecular mechanics simulations, with a Dreiding II force field[32] containing a specific term for H-bonds. It was calculated as the difference in binding energies of a TMA molecule bound to a TPT molecule on graphite and a TMA molecule and a TPT molecule bound to the substrate only without intermolecular interaction (H-bond energy = [TMA···TPT]$_{\text{HOPG}}$ − [TMA-]$_{\text{HOPG}}$ − [TPT]$_{\text{HOPG}}$). It amounts to 0.17 eV versus ∼0.30 eV for a 2-fold H-bond among two carboxylic acid groups. Thus, it is a weaker H-bond but nevertheless still sufficient to mediate the stable adsorption of TPT at the liquid−solid interface.

Conclusion

The possibility of precipitating stable adsorption of TPT from the liquid phase through H-bond linker molecules, namely, TMA or TPA, was demonstrated. In the absence of coadsorbates, the stabilization energy of TPT on a graphite surface is not sufficient to observe adsorption from heptanoic acid solution in situ by STM. However, in binary solutions with either TMA or TPA, the second species enables self-assembly of mixed networks on the surface. Intermolecular N···H−O H-bonds are the predominant interaction and thus the driving force for the self-assembly process. When using the 3-fold symmetric TMA as "molecular glue", a hexagonal structure was observed. However, with the 2-fold symmetric TPA molecule, two slightly different structures were revealed, one of them being quadratic.

The TPT−TMA system can be considered a 2D molecular host system with chemically reactive walls. These walls offer free carbonyls of TMA that protrude into the cavity, as binding sites for potential guests. This system might be suitable for immobilizing further species, enabling spectroscopic measurements without requiring low temperatures or strongly interacting substrates, which may interfere with the object under investigation. By combining two different entities in tailored supramolecular structures, a greater variety of properties can be achieved, which increases the benefits and chances for future applications. For that reason, it is an interesting and challenging goal to investigate the conditions for 2D self-assembly of mixed networks.

References and Notes

(1) Cyr, D. M.; Venkataraman, B.; Flynn, G. W. *Chem. Mater.* **1996**, *8*, 1600.

(2) Jonkheijm, P.; Hoeben, F. J. M.; Kleppinger, R.; van Herrikhuyzen, J.; Schenning, A. P. H. J.; Meijer, E. W. *J. Am. Chem. Soc.* **2003**, *125*, 15941.

(3) Jeffrey, G. A. *An introduction to hydrogen bonding*; Oxford University Press: New York, Oxford, U.K., 1997.

(4) De Feyter, S.; De Schryver, F. C. *Chem. Soc. Rev.* **2003**, *32*, 139.

(5) Yokoyama, T.; Yokoyama, S.; Kamikado, T.; Okuno, Y.; Mashiko, S. *Nature* **2001**, *413*, 619.

(6) Theobald, J. A.; Oxtoby, N. S.; Phillips, M. A.; Champness, N. R.; Beton, P. H. *Nature* **2003**, *424*, 1029.

(7) Claypool, C. L.; Faglioni, F.; Goddard, W. A.; Gray, H. B.; Lewis, N. S.; Marcus, R. A. *J. Phys. Chem. B* **1997**, *101*, 5978.

(8) Giancarlo, L. C.; Flynn, G. W. *Acc. Chem. Res.* **2000**, *33*, 491.

(9) De Feyter, S.; Gesquiere, A.; Abdel-Mottaleb, M. M.; Grim, P. C. M.; De Schryver, F. C.; Meiners, C.; Sieffert, M.; Valiyaveettil, S.; Mullen, K. *Acc. Chem. Res.* **2000**, *33*, 520.

(10) Eichhorst-Gerner, K.; Stabel, A.; Moessner, G.; Declerq, D.; Valiyaveettil, S.; Enkelmann, V.; Müllen, K.; Rabe, J. P. *Angew. Chem., Int. Ed.* **1996**, *35*, 1492.

(11) Wang, H. N.; Wang, C.; Zeng, Q. D.; Xu, S. D.; Yin, S. X.; Xu, B.; Bai, C. L. *Surf. Interface Anal.* **2001**, *32*, 266.

(12) Paserba, K. R.; Gellman, A. J. *J. Chem. Phys.* **2001**, *115*, 6737.

(13) Paserba, K. R.; Gellman, A. J. *Phys. Rev. Lett.* **2001**, *86*, 4338.

(14) Müller, T.; Flynn, G. W.; Mathauser, A. T.; Teplyakov, A. V. *Langmuir* **2003**, *19*, 2812.

(15) Lackinger, M.; Griessl, S.; Heckl, W. M.; Hietschold, M.; Flynn, G. W. *Langmuir* **2005**, *21*, 4984−4988.

(16) Lu, X.; Hipps, K. W. *J. Phys. Chem. B* **1997**, *101*, 5391.

(17) Lackinger, M.; Müller, T.; Gopakumar, T. G.; Müller, F.; Hietschold, M.; Flynn, G. W. *J. Phys. Chem. B* **2004**, *108*, 2279.

(18) Toerker, M.; Fritz, T.; Proehl, H.; Sellam, F.; Leo, K. *Surf. Sci.* **2001**, *491*, 1.

(19) Kampschulte, L. Unpublished observation, 2005.

(20) Griessl, S.; Lackinger, M.; Edelwirth, M.; Hietschold, M.; Heckl, W. M. *Single Mol.* **2002**, *3*, 25.

(21) Lackinger, M.; Griessl, S.; Markert, T.; Jamitzky, F.; Heckl, W. M. *J. Phys. Chem. B* **2004**, *108*, 13652.

(22) Griessl, S.; Lackinger, M.; Jamitzky, F.; Markert, T.; Hietschold, M.; Heckl, W. M. *Langmuir* **2004**, *20*, 9403.

(23) Griessl, S. J. H.; Lackinger, M.; Jamitzky, F.; Markert, T.; Hietschold, M.; Heckl, W. M. *J. Phys. Chem. B* **2004**, *108*, 11556.

(24) Ishikawa, Y.; Ohira, A.; Sakata, M.; Hirayama, C.; Kunitake, M. *Chem. Commun.* **2002**, 2652.

(25) Dmitriev, A.; Lin, N.; Weckesser, J.; Barth, J. V.; Kern, K. *J. Phys. Chem. B* **2002**, *106*, 6907.

(26) Su, G. J.; Zhang, H. M.; Wan, L. J.; Bai, C. L.; Wandlowski, T. *J. Phys. Chem. B* **2004**, *108*, 1931.

(27) Clair, S.; Pons, S.; Seitsonen, A. P.; Brune, H.; Kern, K.; Barth, J. V. *J. Phys. Chem. B* **2004**, *108*, 14585.

(28) Stepanow, S.; Strunskus, T.; Lingenfelder, M.; Dmitriev, A.; Spillmann, H.; Lin, N.; Barth, J. V.; Woll, C.; Kern, K. *J. Phys. Chem. B* **2004**, *108*, 19392.

(29) Ma, B. Q.; Coppens, P. *Chem. Commun.* **2003**, 2290.

(30) Griessl, S.; Lackinger, M.; Maier, A.-K.; Kishore, R. S. K.; Kampschulte, L.; Schmittel, M.; Heckl, W. M. *Chem.—Eur. J.*, submitted for publication, 2005.

(31) Desiraju, G. R. *Acc. Chem. Res.* **1996**, *29*, 441.

(32) Mayo, S. L.; Olafson, B. D.; Goddard, W. A., III. *J. Phys. Chem.* **1990**, *94*, 8897.

Solvent Induced Polymorphism
in Supramolecular 1,3,5-Benzenetribenzoic Acid Monolayers

Lorenz Kampschulte, Markus Lackinger, Anne-Kathrin Maier, Ravuri S. K. Kishore,
Stefan Griessl, Michael Schmittel, and Wolfgang M. Heckl

Solvent Induced Polymorphism in Supramolecular 1,3,5-Benzenetribenzoic Acid Monolayers

Lorenz Kampschulte,[†] **Markus Lackinger,**[*,†,‡] **Anne-Kathrin Maier,**[†] **Ravuri S. K. Kishore,**[§] **Stefan Griessl,**[†] **Michael Schmittel,**[§] **and Wolfgang M. Heckl**[†,#]

Department für Geo- und Umweltwissenschaften, Ludwig Maximilians Universität München and Center for Nanoscience (CeNS), Theresienstrasse 41, D-80333 München, Germany, Department of Physics and Astronomy, University of California Irvine, Frederick Reines Hall, Irvine, California 92697-4575, Center of Micro and Nanochemistry and Engineering, Organische Chemie I, Universität Siegen, Adolf-Reichwein-Strasse 2, D-57068 Siegen, Germany, and Deutsches Museum, Museumsinsel 1, D-80538 München, Germany

Received: December 28, 2005; In Final Form: March 18, 2006

This work presents a scanning tunneling microscopy (STM) based study of benzenetribenzoic acid (BTB) monolayer structures at the liquid−solid interface. On graphite(0001) the tailored molecules self-assemble into 2D supramolecular host systems, suitable for the incorporation of other nanoscopic objects. Two crystallographically different BTB structures were found−both hydrogen bonded networks. A specific structure was deliberately selected by solvent identity. One of the BTB polymorphs is a 6-fold chicken-wire structure with circular, approximately 2.8 nm wide cavities. The other structure exhibits an oblique unit cell and a different hydrogen bonding pattern. The large cavity size of the chicken-wire structure was made possible through comparatively strong 2-fold hydrogen bonds between carboxylic groups. In addition, the low conformational flexibility of BTB was supportive to combat the tendency for dense packing.

Introduction

Due to their high directionality, hydrogen bonds play a key role in molecular recognition processes, in solution, in the solid state and for surface patterning. Two-dimensional hydrogen bonded networks on surfaces demonstrate the unique potential of tailoring supramolecular assemblies for nanotechnology applications. Among others, the carboxylic acid functionality typically exhibits robust hydrogen bonds with itself, with the hydroxyl group acting as a donor and the carbonyl oxygen as an acceptor. In a symmetrical, polyfunctional disposition, the interplay of multiple hydrogen-bonding leads to well organized structures on surfaces and in bulk crystals. For instance, the para-position of the carboxylic groups in terephthalic acid (TPA) results in formation of hydrogen bonded linear chains on a surface.[1,2] Also, the relative position of functional groups in substituted porphyrin molecules can be exploited to steer the self-assembly process.[3] Among hydrogen bonded supramolecular structures, two-dimensional template structures enable ordering[4,5] and addressing of nanometer sized objects such as clusters[6−8] or functional molecules[9,10] on surfaces with subnanometer precision. These template structures exhibit a periodic arrangement of cavities of various size and shape, where the guest species can be confined. As has been shown recently, the archetypical supramolecular model system trimesic acid (TMA, cf. Figure 1a) is well suited for this purpose. TMA can be considered a smaller analogue of BTB (cf. Figure 1b), with similar symmetry and the same functional groups for forming hydrogen bonds. Scanning tunneling microscopy (STM) experi-
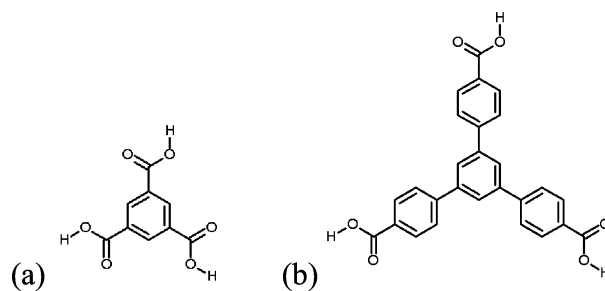

Figure 1. Chemical structures of (a) trimesic acid (TMA, $C_9H_6O_6$) and its larger analogue (b) 1,3,5-benzenetribenzoic acid (BTB, $C_{27}H_{18}O_6$)

ments in an UHV environment with evaporated TMA monolayers on graphite(0001) revealed two different polymorphs: chicken-wire and flower structure.[11] Both structures are governed by intermolecular hydrogen bonding and exhibit a periodic arrangement of approximately 1.0 nm wide circular cavities. Similarly, a TMA chicken-wire structure was found on Cu(100).[12] However, due to stronger interaction with the metal substrate, the TMA lattice was slightly distorted and no large domains could be grown. Among others, a TMA chicken-wire structure was realized on Au(111) in an electrochemical STM study for suitable potential conditions.[13] Another EC-STM study of TMA, equally on Au(111) found various densely packed phases with upright molecules and potential driven phase transitions, revealing the influence of a stronger adsorbate−substrate interaction.[14] In addition, a more comprehensive EC-STM study of TMA on Au(111) complemented by ATR SEIRAS (attenuated total reflection surface enhanced infra red adsorption spectroscopy) found phases with upright TMA molecules and coadsorbed interfacial water molecules inhibiting intermolecular hydrogen bonds between TMA molecules.[15] Bai et al. succeeded in growing and characterizing a hexagonal two-dimensional host system, likewise on HOPG (highly oriented pyrolytic graphite)

* Corresponding author. Phone: +49 89 2180 4185. Fax: +49 89 2180 4334. E-mail: markus@lackinger.org.
† Ludwig Maximilians Universität München and Center for Nanoscience (CeNS).
‡ University of California Irvine.
§ Universität Siegen.
# Deutsches Museum.

with an enlarged cavity diameter of 1.9 nm.[16] This study applied a molecule related to TMA, but with additional C−O−C spacers between the aromatic core and the three carboxylic groups, respectively. In UHV co-deposition experiments, Theobald and co-workers combined PTCDI (*perylene tetracarboxylic diimide*) and melamine to form a hexagonal hetero-molecular host network with a fairly large lattice constant of 3.46 nm.[17] In this case 3-fold intermolecular hydrogen bonds were the driving force for the self-assembly process and the symmetry of the adlayer was governed by the 3-fold symmetry of melamine. As has been shown in this work, the cavities are large enough to incorporate up to seven C_{60} fullerene molecules within a single cell. Equally, it was possible to prepare a mixed-network at the liquid−solid interface composed of TMA and TPT (1,3,5-tris-(4-pyridyl)-2,4,6-triazine) through adsorption from binary solutions.[18] Furthermore, it has been demonstrated that in equilibrium with the liquid phase TPT only adsorbs in the presence of a second species, which acts as a linker. Thereby, larger noncovalently bonded aggregates with sufficiently large adsorption energy are generated. The necessity for a linking species arises because TPT by itself provides only a functional group acting as a hydrogen bond acceptor, thereby rendering intermolecular TPT-TPT hydrogen bonds impossible. However, adding TMA or TPA as a linker molecule provided mixed networks bonded over N···H−O hydrogen bonds. Because the size and geometric structure of TPT is comparable to BTB, these results already indicate the crucial role of the carboxylic groups for the stabilization of the discussed interfacial monolayers. Various studies demonstrated that the increased binding strength of metal−organic coordination complexes can be exploited to grow various host-systems.[19] However, up to now this approach seems to be limited to UHV based preparation techniques.

Moreover, it was demonstrated at the liquid−solid interface that a supramolecular TMA host structure, as its primary purpose, can be used for the storage and manipulation of single molecules approximately one nanometer in size.[20,21] Similarly, it has been shown that copper phthalocyanine as well as coronene are suitable guests in a host network composed of 1,3,5-tris(10-carboxydecyloxy)benzene on HOPG.[22] In the latter study a volatile solvent (toluene) was used and in contrast to the results presented herein, the structures were not investigated in equilibrium with the liquid phase above.

Because functional molecules, such as amino acids and small proteins in biology or metal clusters in solid-state physics and molecular electronics, vary in size and shape, deliberate tuning of the cavity dimensions of the host structure is a basic requirement for incorporation of these guests. To generate a two-dimensional homomeric (i.e., composed of one kind of molecule only) host network on a graphite surface with large cavities, we turned our attention to 1,3,5-benzenetribenzoic acid (BTB), a D_{3h} symmetric molecular building block (cf. Figure 1b) equipped with three 4-carboxyphenyl arms. BTB is also a popular ingredient for highly porous bulk crystals with large specific surfaces, which often take advantage of metal−organic bonds.[23]

A major challenge in the design of host systems is tuning the cavity size and shape in a controlled manner. It is necessary to combat the tendency of the molecular building blocks toward dense packing, instead of crystallization in a structure with large, energetically unfavorable cavities. The principle of closest packing as enunciated by Kitaigorodskii[24,25] holds for weak interacting building blocks. Thus, increasing the interaction through hydrogen bonds offers a way to circumvent the tendency for close packing.

In STM studies of Bai et al.,[26] comparable C_3 symmetric molecules with a benzene ring as a core and three attached alkoxycarbonyl acid groups as hydrogen bonding sites were used. However, due to the use of flexible aliphatic spacers of variable length, these molecules preferred dense packing on the surface. In contrast, any conformational changes in 1,3,5-benzenetribenzoic acid (BTB), i.e., rotation around the C_{ph}−C_{ph} and the C_{ph}−C_{COOH} bonds, will not change the main directionality of the hydrogen bonding units, i.e., the carboxylic groups. In this work we show that the rigidity of the BTB molecules and the strong intermolecular interaction introduced by hydrogen bonds in combination with a proper solvent result in a periodic adsorbate structure with fairly large cavities. In addition, with various other solvents a more densely packed structure was observed.

Experimental Section

BTB [1,3,5-tris(4-carboxyphenyl)benzene (1,3,5-benzene-tribenzoic acid)] was synthesized according to a known literature procedure[27] by a triscarboxylation of 1,3,5-tris(*p*-bromophenyl)-benzene. BTB: ^{1}H NMR (400 MHz, DMSO-d_6) δ 8.00 (d, J = 8 Hz, 6 H, m-H), 8.29 (d, J = 8.03 Hz, 6 H, o-H), 8.05 (s, 3 H, H); ^{13}C NMR (100.6 MHz, DMSO-d_6) δ 125.6, 127.5, 130.0, 130.1, 140.8, 143.9, 167.3; EI mass (*m/z*) 438 (M^+); IR (KBr) 3600−2400 (OH), 1680 (C=O), 1600, 1560, 1420 (C=C), 1290 (C−O), 850, 765, 700 (CH) cm^{-1}.

STM measurements at the liquid−solid interface were carried out at room temperature with a home-built STM, driven by a commercial SPM-100 control system from RHK. Submolecularly resolved images were obtained in the constant current mode of operation. Typically, bias voltages of +0.3, ..., +1.5 V with respect to the tip, and current set points of about 0.1, ..., 0.9 nA were applied. For noise reduction, all STM images were processed by leveling and a 3 × 3 G filtering. The following solvents were used for the experiments: butanoic acid (∼99%, Fluka), pentanoic acid (>98%, Fluka), hexanoic acid (>98%, Fluka), heptanoic acid (>99%, Sigma Aldrich), octanoic acid (>99%, Sigma Aldrich), nonanoic acid (>97%, Fluka), 1-octanol (>99%, Merck), 1-nonanol (>98%, Merck Schuchardt), 1-decanol (>97%, Merck Schuchardt), 1-phenyl-octane (>98%, Merck Schuchardt), dodecane (>98%, Fluka). These solvents are electrically nonconductive and their vapor pressure at room temperature is sufficiently low to allow for stable tunneling experiments in the order of 1 h. Mechanically cut tunneling tips from a Pt/Ir wire (90/10) without any insulation were used.

All samples were prepared by applying a droplet of the respective BTB solution on a freshly cleaved HOPG(0001) surface. The self-assembled interfacial monolayer was characterized by in-situ STM with the tip being immersed in the solution. To precisely measure lattice parameters and determine the superstructure matrices, the graphite lattice and the self-assembled monolayer were imaged within the same frame. In the first part the adsorbate layer was imaged; in the second part the substrate lattice was imaged by decreasing the tunneling voltage and increasing the tunneling current set point. The experimental error in the coefficients of the superstructure matrix is in the range of ±0.5. Although the accuracy does not allow the assignment of a truly commensurate adsorbate lattice, the matrices have been assumed to be commensurate. Even on weak interacting substrates, like layered materials, normally a certain relation between adsorbate und substrate lattice like commensurability or point-on-line structures exist.

Polymorphism in 1,3,5-Benzenetribenzoic Acid

J. Phys. Chem. B, Vol. 110, No. 22, 2006 **10831**
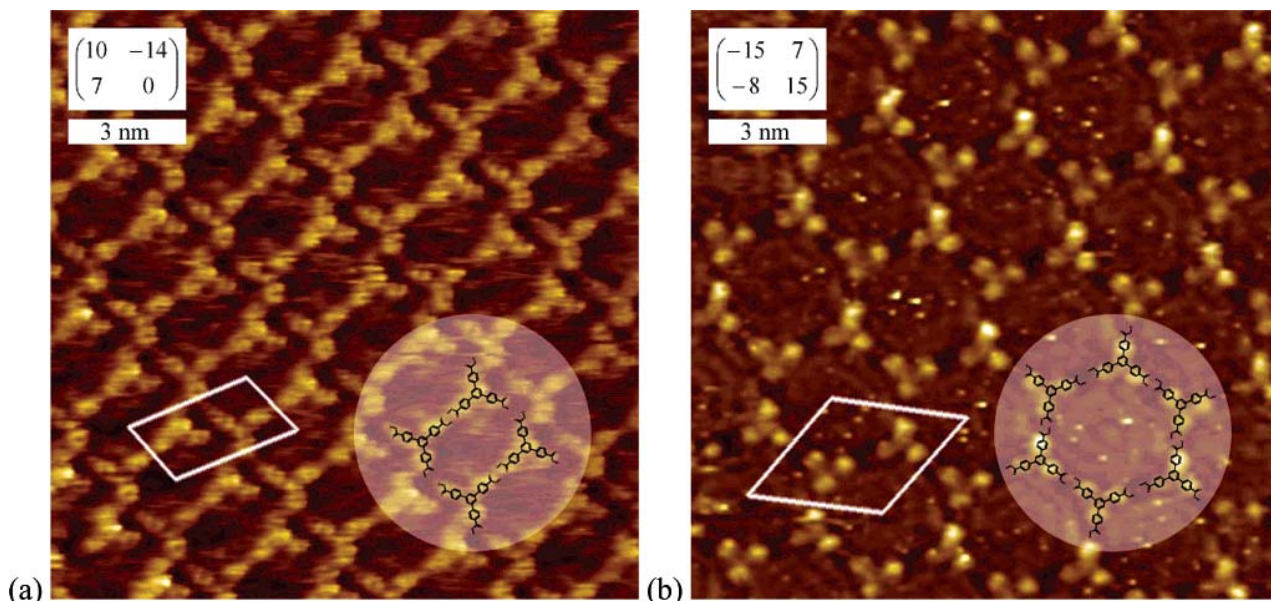
Figure 2. STM topographs of the BTB monolayers, self-assembled on a HOPG(0001) surface. The superstructure matrices (referred to the hexagonal lattice of every second graphite atom—lattice constant 0.246 nm and 60°—as visible in atomically resolved STM images) are given in the insets and the positions of individual BTB molecules are indicated. (a) shows the modification with the oblique unit cell as obtained in butanoic through heptanoic acid, 1-octanol, 1-nonanol, and 1-decanol, and (b) shows the hexagonal chicken-wire modification as obtained in nonanoic acid and 1-phenyloctane. For octanoic acid and dodecane both modifications were observed.

Results and Discussion

For BTB monolayers at the interface between graphite(0001) and saturated solution two different, non-densely-packed polymorphic modifications were revealed as a function of the applied solvent by means of in-situ STM. These two structures differ in their hydrogen bonding pattern and their particular molecular packing density. Dependent on solvent identity either an oblique or a hexagonal unit cell was observed, with the former structure exhibiting rectangular cavities, and the latter circular cavities. Representative STM topographs of both structures are depicted in Figure 2a,b, respectively. The superstructure matrices of the adsorbate lattices with respect to the graphite substrate are given in the insets.

In both structures, single BTB molecules appear with a 3-fold symmetric shape in the STM topographs and their size is consistent with flat lying molecules. Thus, the STM contrast is dominated by the geometry of the molecule.

It has been shown recently that fatty acid solvent molecules can form mixed monolayers with coronene solute molecules on Au(111).[28] Thus, solvent coadsorption can have a great impact on both the emerging monolayer structure and the STM contrast within the cavities. In this study, upright fatty acid molecules adsorbed with their carboxylic groups directly to the substrate were proposed and clearly resolved in the STM topographs. But the adsorption energy on Au(111) exceeds that on weakly interacting graphite(0001). Furthermore, deprotonation of the bonding carboxylic group might play a crucial role for their bonding to metal surfaces. In our networks, however, we do not clearly observe the incorporation of solvent molecules in the BTB structures. On the other hand, an internal structure was reproducibly found within the cavities of the chicken-wire structure. For reasons of spacing and symmetry, it can be ruled out that just the underlying graphite substrate is atomically resolved within the cavity. It is, however, most likely that either solvent or additional BTB molecules are loosely bound within the cavities.

Butanoic, pentanoic, hexanoic, and heptanoic acid, 1-octanol, 1-nonanol, and 1-decanol as solvents lead to a BTB surface structure with an oblique unit cell (indicated in Figure 2a), where four molecules border rectangular cavities. The positions of the molecules within the unit cell as well as the superstructure matrix are given in Figure 2a. The size of the unit cell amounts to (1.7×3.1) nm^2 with an angle of 76° between the adsorbate lattice vectors and contains two BTB molecules. Evidently, the basic unit of this structure is a BTB dimer motif, where the BTB molecules are rotated 180° with respect to each other and bonded by a 2-fold hydrogen bond between two carboxylic groups. These dimers are aligned along rows with their axis almost perpendicular to the row. However, it is difficult to assign the bonding scheme among those dimers. A tentative model, which is based on the relative position as deduced from the STM images, is depicted in Figure 3a. The bonding pattern proposes four O···H−O hydrogen bonds per BTB dimer within the rows and additional four weaker O···H−C hydrogen bonds per BTB dimer among neighboring rows. According to the scaled model, the distance between the free carbonyls of the acid groups and the H atoms amounts to ∼0.29 nm and thus lies well within the range of O···H−C hydrogen bonds.[29] Furthermore, an ab initio calculation concludes that the supposedly weak O···H−C bonds can have a major impact on the structure formation, rather than being a mere consequence of the crystal packing.[30] According to this packing, the rows of dimers are shifted with respect to each other.

In general, the packing of BTB or analogous compounds in bulk crystals should give an indication of the nature of the hydrogen bonding that such systems might show affinity for on the graphite−liquid interface. Although there has been no report on the X-ray crystal structure of BTB, systems containing multiple carboxylic acid moieties have been studied.[31,32] Of specific interest is the hydrogen-bonding behavior in TMA bulk crystals. The most common polymorph of TMA in crystals is the infinite chicken-wire motif arising from the dimer motif, which is observed commonly in 90% of the carboxy containing crystal structures in the Cambridge Structural Database (CSD) analysis.[33] This behavior is consistently carried on to the liquid−solid interface, as has been reported recently.[34]
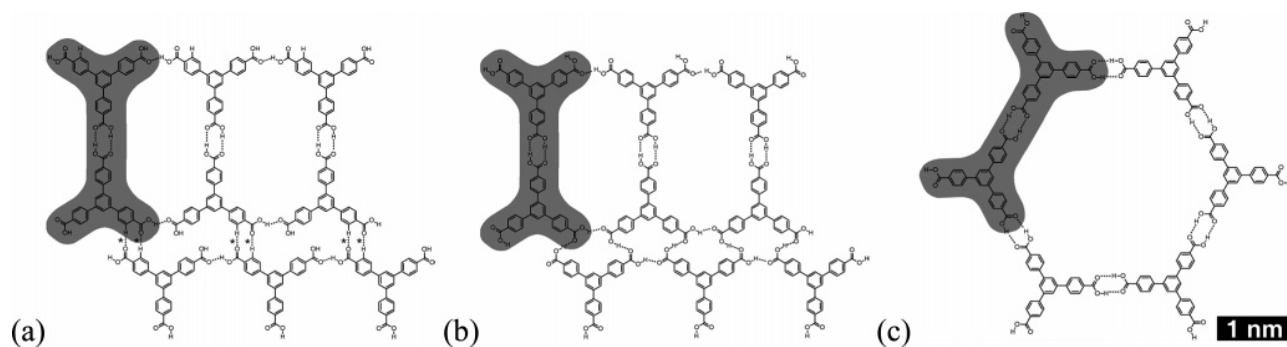
Figure 3. (a) Proposed hydrogen bonding pattern for the oblique BTB polymorph. Dimers in the same row are bonded by a total of four O···H−O hydrogen bonds to their neighboring dimers. Between the rows the BTB dimers are bonded by weak O···H−C hydrogen bonds only (marked by asterisks). To establish those bonds, the rows are shifted with respect to each other by approximately half the dimer−dimer distance. (b) An alternative model for the oblique BTB polymorph based on syn−anti−syn catemer hydrogen bonding between the dimer rows. Similar to (a), the dimer rows are shifted with respect to each other. (c) Proposed hydrogen bonding pattern of the BTB chicken-wire polymorph solely based on the dimer motif. Every carboxylic group forms a 2-fold straight hydrogen bond with an adjacent carboxylic group, resulting in a total of six hydrogen bonds per BTB molecule.
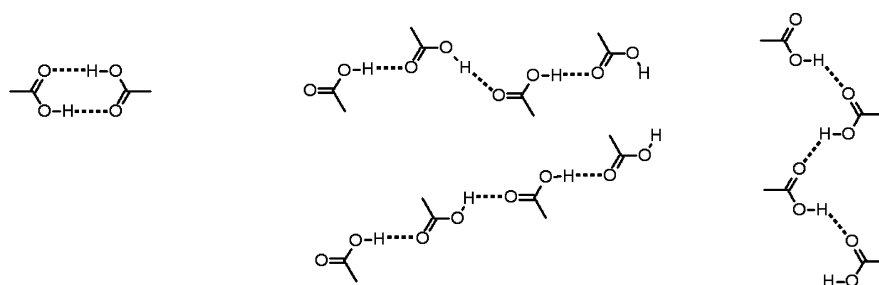
Figure 4. Observed hydrogen bonding patterns in organic crystals of carboxy containing compounds: left-hand side, dimer motif with a 2-fold hydrogen bond; center and right-hand side, various catemer motifs depending on the syn and anti conformation of the constituent carboxylic acid.

However, there exist other hydrogen bonding patterns in carboxylic acid crystal structures apart from the dimer, namely the catemer motifs, which account for the remaining 10% of the crystal structures in the CSD.[33] Three different catemer motifs are known to exist depending on the syn and anti conformation of the constituent carboxylic acid groups.[31] Figure 4 provides an overview about the dimer and the various catemer hydrogen bonding patterns among carboxylic groups.

Based on the catemer hydrogen bonding pattern, an alternative model for the rectangular BTB polymorph is equally conceivable and depicted in Figure 3b. Both the O···H−C hydrogen bond stabilized structure and the syn−anti−syn catemer pattern are in accordance with the 2D crystallographic data as obtained by STM. Based on the 2D pattern only, it is not possible to predict which of the above patterns is followed, yet total energy calculations might provide deeper insight. Nevertheless, the materialization of a lower symmetry structure in the self-assembly process implies the evolution of alternative hydrogen bonding patterns besides the dimer motif. Deviations from the ideal dimer motif in the hydrogen bonded monolayer structures have been observed in various other systems.[34,35]

The second BTB structure as observed in nonanoic acid and 1-phenyloctane, consists of hexagonally arranged and inter-connected six-membered rings. Basically, those rings are composed of three BTB dimers each. Every possible hydrogen bond between the three carboxylic groups of BTB is formed under an energetically ideal bonding angle of 180°. This results in a total of six hydrogen bonds (two for each two adjacent carboxylic groups) per molecule. Each BTB molecule is part of three adjacent rings. A model of the structure is given within the STM image in Figure 2b and in Figure 3c. The circular cavities have diameter of about 2.8 nm. Similar to the oblique structure, the basic unit is a dimer motif.

It is noteworthy that, by using octanoic acid as a solvent—the size and molecular weight of which lies between heptanoic and nonanoic acid—both polymorphic modifications can be found coexisting on the surface. The coexistence of both monolayer structures has also been observed in dodecane. During the experimental time span, which is limited by evaporation of the solvent, no transformations of one phase into the other was observed. Thus, a conclusion of which phase is thermodynamically more stable cannot be drawn.

The effect of solvent induced polymorphism is well-known from organic bulk crystals and of great importance, for example, in the pharmaceutical industry, because different modifications usually differ in their physical properties. Similarly, in a previous study we found different monolayer polymorphs for TMA depending on the solvent at the liquid−solid interface.[34] Both TMA and BTB form a related chicken-wire structure, which is identical in symmetry and the hydrogen bonding pattern but differs by a factor of ~1.9 in lattice constant. However, the respective second polymorphic modification is not related at all. Only the respective chicken-wire polymorph exhibits the energetically ideal, straight 2-fold hydrogen bond between adjacent carboxylic groups, whereas, in the so-called TMA flower structure one-third of all hydrogen bonds participate in a circular scheme with three carboxylic groups of three TMA molecules involved. Another comparable circular arrangement of hydrogen bonds has been proposed by Bai and co-workers for tetrakis(carboxylphenyl)porphyrin monolayers on graphite.[35] For TMA as well as for BTB, the denser structure was found for fatty acids with shorter chain length: In the case of BTB values of 0.39 molecules/nm^2 for the oblique structure vs 0.23 molecules/nm^2 for the chicken-wire polymorph were found; lattice parameters of all respective TMA and BTB structures are listed in Table 2. Of course, the difference in the absolute

TABLE 1: Solvents Applied in This Study and the Resulting BTB Monolayer Structure on the Solvent−HOPG Interface[a]

no.	solvent	chemical structure	functional group	ϵ (temp. (K))	monolayer structure
1	1-octanol		R-OH	10.30 (293.2) [36]	oblique
2	1-nonanol		R-OH	8.83 (293.2) [36]	oblique
3	1-decanol		R-OH	7.93 (293.2) [36]	oblique
4	butanoic acid		R-COOH	3.02 (303.2) [37]	oblique
5	pentanoic acid		R-COOH	2.93 (303.2) [37]	oblique
6	hexanoic acid		R-COOH	2.61 (303.2) [37]	oblique
7	heptanoic acid		R-COOH	3.04 (303.2) [37]	oblique
8	octanoic acid		R-COOH	2.82 (303.2) [37]	oblique + hexagonal
9	nonanoic acid		R-COOH	2.50 (302.8) [37]	hexagonal
10	1-phenyloctane		R-(aromatic)	2.26 (293.2) [36]	hexagonal
11	dodecane		R	2.01 (293.2) [36]	oblique + hexagonal
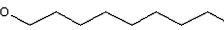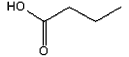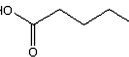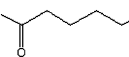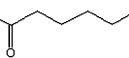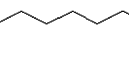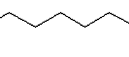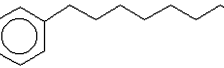
[a] The temperature dependence of the dielectric constants in the range room temperature ±10 K is insignificant.[37]

TABLE 2: Unit Cell Parameters and Molecular Area Densities of the Two BTB and TMA Polymorphic Structures

structure	unit cell parameters			area density ($1/nm^2$)	relative area density (%)	
	a (nm)	b (nm)	α (deg)		molecules	cavity
BTB oblique	1.7	3.1	76	0.39	66	34
BTB chicken-wire	3.2	3.2	60	0.23	38	62
TMA flower	2.5	2.5	60	1.11	84	16
TMA chicken-wire	1.7	1.7	60	0.80	61	39

values in comparison to those for TMA is because of the larger size of BTB. In addition, based on these molecular densities, the relative area of the cavity, where the pristine substrate is exposed to the liquid phase has been calculated for all BTB and TMA structures. The projection of the van der Waals surface perpendicular to the molecular plane was used as molecular area, resulting in 1.69 nm² for a BTB and 0.76 nm² for a TMA molecule.

As stated above, a common feature of the self-assembly of TMA and BTB monolayers at the liquid−solid interface is the chicken-wire polymorph emerges for fatty acid solvents with longer aliphatic tail. The general trend of seeing a higher symmetrical arrangement (chicken-wire) of the TMA and BTB molecules on the substrate by using these solvents can readily be explained by invoking the principle of polarity. The dielectric constant ϵ (cf. Table 1) decreases along the homologous series from butanoic acid (3.02) to nonanoic acid (2.50) and is known to play a strong role in dictating the properties of alkanoic acids.[38,39] For example, the association constants of aliphatic monocarboxylic acids are known to be inversely linear to the dielectric constants.[40] Even more important is the fact that lower

analogues of linear alkyl acids tend to exist as multimers, e.g., formic acid trimers[41] and pentamers[42] were found to be stable according to ab inito calculations. As the alkyl chain length increases, the enhanced hydrophobic effects drive the polar carboxylic acid groups to assemble or aggregate in a less polar fashion so as to minimize electrostatic effects in solution. Indeed, those with longer chain lengths tend to form dimers having zero dipole moment, thus allowing for a stabilization of the carboxylic acid groups in a hydrophobic environment with low dielectric constant.[43,44]

The general trend of alkanoic acid aggregation in solution may also play a role in the 2D assembly of TMA and BTB on a graphite surface. In the case of BTB, a polarity effect can be applied to rationalize the 2-D structures. In contradiction to TMA, where the flower structure is built up by trimers and the chicken-wire structure by dimers, respectively, the basic unit is now a dimer for both BTB polymorphs. Despite having the dimer dictating the seeding in both cases, the polarity of the solution orchestrates the arrangement of the larger BTB aggregates on the surface, as illustrated by Figure 6. The less polar and less dense chicken-wire structure is generated in the case of the more hydrophobic nonanoic acid, whereas the more polar and denser oblique structure is materialized with the more polar heptanoic acid, as shown in Figure 6. Because the chicken-wire structure exposes a lower number of polar groups, per unit area as well as per number of participating molecules, during the growth, this structure is clearly preferred in a solvent of low dielectric constant and vice versa.

Comparing the different solvents described in Table 1, it seems reasonable to assume a disparate mechanism for the formation of the interfacial monolayer structures depending on whether the solvent can or cannot exert strong hydrogen bonds,

solubility
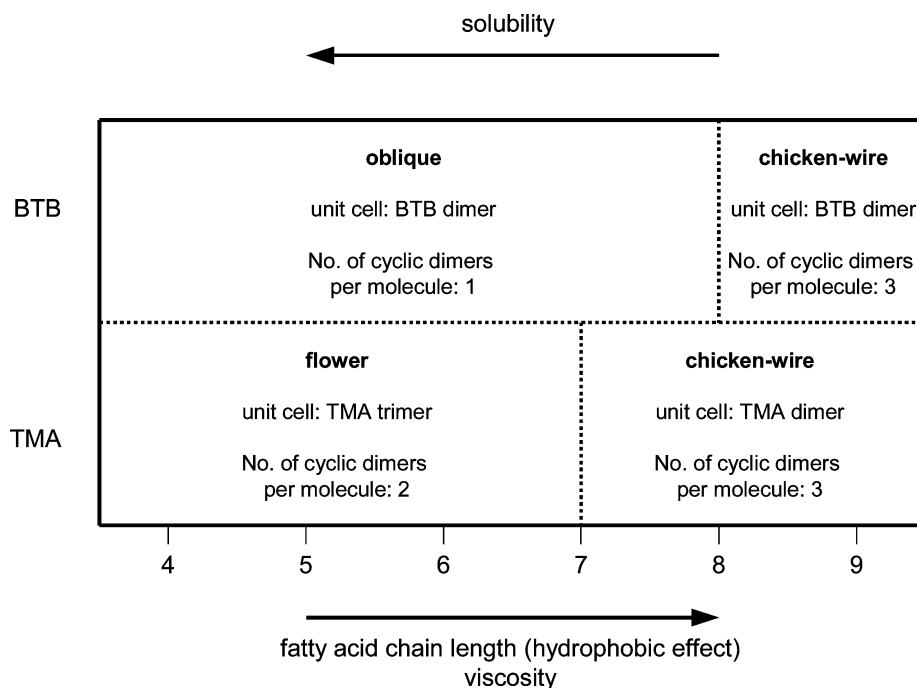
Figure 5. Schematic representation of the properties observed along the homologous series of alkanoic acids from butanoic to nonanoic acid and the respective interfacial monolayer structure.

because the latter is a highly directional intermolecular interaction. In contrast, sizable hydrophobic interactions through van der Waals interactions will require a sufficiently long alkyl chain of the solvent. Thus, it is to be expected that in alkanols and alkanoic acids the interfacial structure will be controlled through hydrogen bonding as long as it is the dominating contribution as compared to hydrophobic contributions, i.e., for shorter and more polar solvents. Indeed, experiments with different hydrogen bonding solvents, altogether three aliphatic alcohols and six fatty acids (see Table 1), reveal a rough dependence of the BTB interfacial monolayer structure on the dielectric constant of the solvent. For $\epsilon = 3, ..., 10$ the oblique BTB structure is observed exclusively, whereas for $\epsilon \leq 2.5$ the hexagonal BTB structure is preferred. In the intermediate range of $\epsilon = 2.5, ..., 3$ addressed by testing the homologous series of alkanoic acids, the oblique structure is preferred for $CH_3(CH_2)_nCOOH$ with $n = 2, ..., 5$, whereas coexistence of oblique and hexagonal domains was found in the case of octanoic acid ($n = 6$). With nonanoic acid ($n = 7$) only the hexagonal structure is detected. Unfortunately, there is not a monotonic decrease of ϵ when varying n from $2-7$, indicating that in this intermediate range subtle differences in the dielectric constants may be overridden by other effects. Despite these irregularities in the range $3 < \epsilon \leq 2.5$, it seems, however, that there is an overall polarity dependence on the surface structuring for the alkanols and alkanoic acids.

For alkanes and arylalkanes, solvent deviations from the predictions based on the dielectric constant are attributed to the lack of any polar anchor group to induce orientation by hydrogen bonding. For 1-phenyloctane ($\epsilon = 2.26$) the BTB monolayer structure was found to be hexagonal, whereas a mixture of oblique and hexagonal structures was obtained in dodecane ($\epsilon = 2.01$). As stated above, the absence of specific interactions between solvent and solute molecules is expected to lead to a different orienting mechanism as compared to fatty acids and alkanols.

Besides the plausible stabilization of polar units by polar solvents during growth, kinetic effects offer an alternative explanation for the observed polymorphism. It is reasonable to assume that the adsorption rate (i.e., the number of molecules adsorbing from the liquid on the surface per unit of area and time) of BTB decreases monotonically with increasing solvent chain length. As the length of the aliphatic tail of the solvent molecules increases, the interaction strength between molecules and thus the viscosity of the respective liquid rises. For this reason the diffusion constant of BTB in the respective solvent decreases with increasing chain length of the solvent molecules. Also the solubility of BTB will decrease from heptanoic to nonanoic acid, similar to TMA.[34] In general, the longer the chain length of a fatty acid, the more hydrophobic is the liquid. This is because the weight of the carboxylic acid group, also being the responsible functional group for dissolving BTB, diminishes from heptanoic to nonanoic acid. An indication that the structure formation also might be influenced by the adsorption rate was seen in UHV deposition experiments of TMA, where higher deposition rates lead to a preference of the more dense flower structure.[45] A more dense arrangement would be favored for a higher adsorption rate, because the fast association of the molecules does not allow the system to adopt the structure with the lowest free energy. Also the observed coexistence of both BTB (TMA) polymorphs in octanoic acid and dodecane (heptanoic acid) indicate that kinetics rather than thermodynamics indeed might govern the monolayer structures.

Another explanation is offered by solvent coadsorption; i.e., a particular solvent stabilizes a particular modification by lowering its free energy. Yet, in the STM images a second type of molecule cannot be resolved, we thus exclude incorporation of rather large solvent molecules in neither of the BTB polymorphs. But inclusion of small impurity molecules (e.g., H_2O or other carboxylic acids) cannot be ruled out, especially because the solvents used here exhibit a chemical purity only. In particular, water would be suited for bridging gaps between BTB molecules and might not be resolved in the STM images.
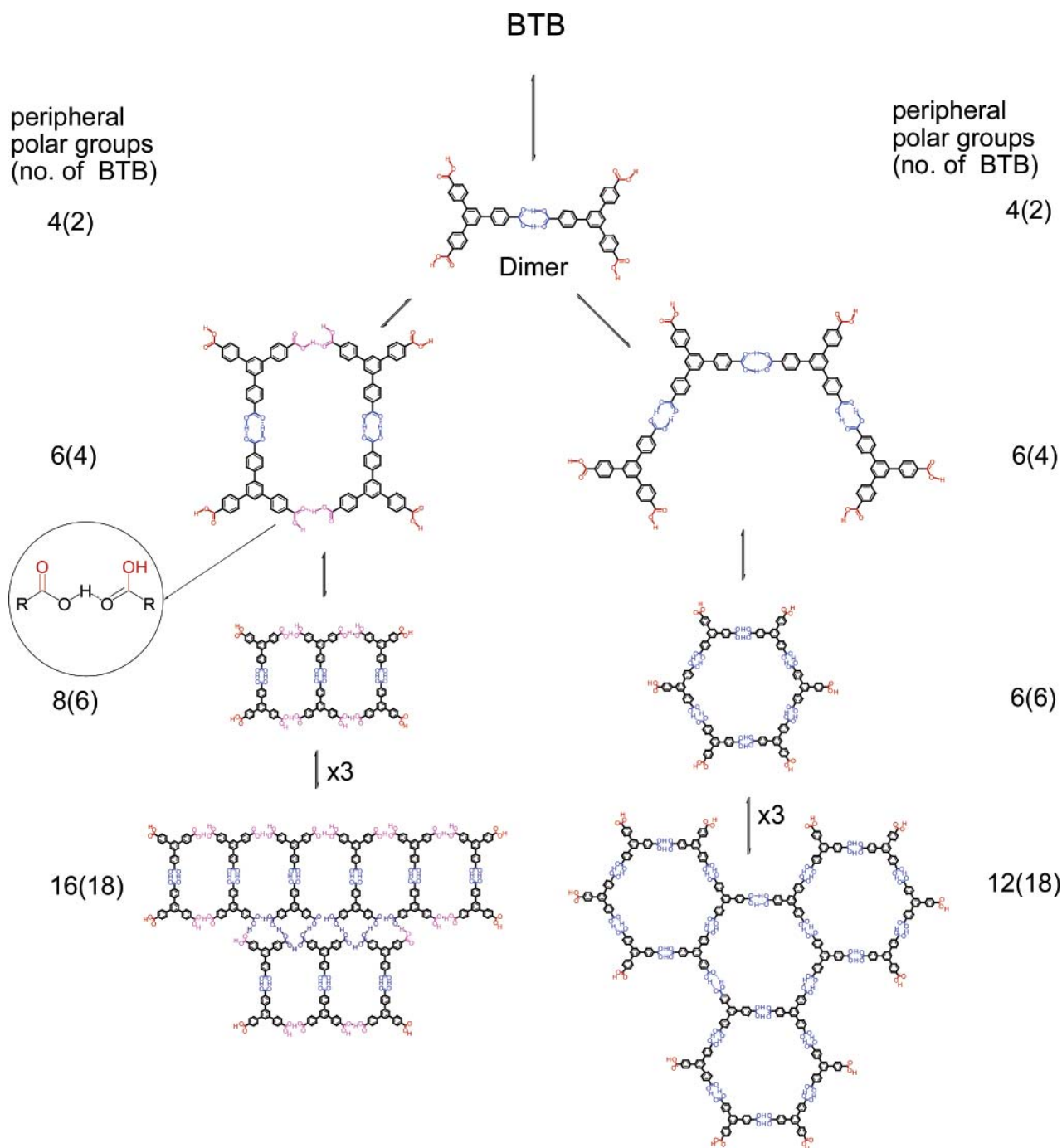
Figure 6. Cartoon of the seeding process on the surface with the BTB dimer as the repeating unit forming the oblique pattern (left) and the chicken wire motif (right). The count represents the number of polar functional groups exposed to the solvent, and those in the brackets represent the number of BTB molecules involved in the assembly. The free polar groups are marked in red and the cyclic dimers of carboxylic acids that have zero dipole effects are marked in blue. The inset circle depicts the catemeric hydrogen-bonding motifs that due to their residual polarity have to be accounted for in the polarity count. Hydrogen bonds interconnecting the dimer rows of the oblique structure are marked violet (saturated bonds) and pink (unsaturated bonds) respectively.

Conclusion

In this work two-dimensional supramolecular host structures were realized by adsorption of BTB molecules on graphite surfaces from the liquid phase. Depending on the solvent used, two different structures with a hexagonal and an oblique unit cell respectively were revealed by means of in situ STM. One of them, the so-called chicken-wire polymorph, exhibits fairly large circular cavities with a diameter of 2.8 nm. Both structures substantially differ in their hydrogen bonding pattern but have

the dimer motif in common. The evolution of different structures for varying solvents is discussed in light of adsorption rates and of stabilization of polar units during the growth. For solvents with functional groups being able to hydrogen bond to the solute, a rough dependence of the structure formation on the dielectric constant was found. The more dense and more polar oblique BTB structure was only observed for solvents with a dielectric constant $\epsilon > 3$. Experiments with other classes of solvents, however, have pointed out that further parameters can be

decisive for the structure formation as well. The subject of ongoing research is the coadsorption of guests such as semi-conducting metal clusters within these cavities, thereby introducing a long-range lateral order of these nanoparticles. Moreover, the spatial fixation of these objects enables further investigations—like scanning tunneling spectroscopy—on isolated objects without the large experimental effort caused by sample cooling.

References and Notes

(1) Lackinger, M.; Griessl, S.; Markert, T.; Jamitzky, F.; Heckl, W. M. *J. Phys. Chem. B* **2004**, *108*, 13652.

(2) Stepanow, S.; Strunskus, T.; Lingenfelder, M.; Dmitriev, A.; Spillmann, H.; Lin, N.; Barth, J. V.; Woll, C.; Kern, K. *J. Phys. Chem. B* **2004**, *108*, 19392.

(3) Yokoyama, T.; Yokoyama, S.; Kamikado, T.; Okuno, Y.; Mashiko, S. *Nature* **2001**, *413*, 619.

(4) Rosei, F.; Schunack, M.; Jiang, P.; Gourdon, A.; Laegsgaard, E.; Stensgaard, I.; Joachim, C.; Besenbacher, F. *Science* **2002**, *296*, 328.

(5) Schunack, M.; Petersen, L.; Kuhnle, A.; Laegsgaard, E.; Stensgaard, I.; Johannsen, I.; Besenbacher, F. *Phys. Rev. Lett.* **2001**, *86*, 456.

(6) Glass, R.; Moller, M.; Spatz, J. P. *Nanotechnology* **2003**, *14*, 1153.

(7) Shchukin, V. A.; Ledentsov, N. N.; Bimberg, D. *Physica E* **2001**, *9*, 140.

(8) Gerardot, B. D.; Subramanian, G.; Minvielle, S.; Lee, H.; Johnson, J. A.; Schoenfeld, W. V.; Pine, D.; Speck, J. S.; Petroff, P. M. *J. Cryst. Growth* **2002**, *236*, 647.

(9) Gimzewski, J. K.; Joachim, C.; Schlittler, R. R.; Langlais, V.; Tang, H.; Johannsen, I. *Science* **1998**, *281*, 531.

(10) Mayor, M.; Buschel, M.; Fromm, K. M.; Lehn, J. M.; Daub, J. *Chem. Eur. J.* **2001**, *7*, 1266.

(11) Griessl, S.; Lackinger, M.; Edelwirth, M.; Hietschold, M.; Heckl, W. M. *Single Mol.* **2002**, *3*, 25.

(12) Dmitriev, A.; Lin, N.; Weckesser, J.; Barth, J. V.; Kern, K. *J. Phys. Chem. B* **2002**, *106*, 6907.

(13) Ishikawa, Y.; Ohira, A.; Sakata, M.; Hirayama, C.; Kunitake, M. *Chem. Commun.* **2002**, 2652.

(14) Su, G. J.; Zhang, H. M.; Wan, L. J.; Bai, C. L.; Wandlowski, T. *J. Phys. Chem. B* **2004**, *108*, 1931.

(15) Han, B.; Li, Z.; Pronkin, S.; Wandlowski, T. *Can. J. Chem.* **2004**, *82*, 1481.

(16) Lu, J.; Zeng, Q. D.; Wang, C.; Zheng, Q. Y.; Wan, L. J.; Bai, C. L. *J. Mater. Chem.* **2002**, *12*, 2856.

(17) Theobald, J. A.; Oxtoby, N. S.; Phillips, M. A.; Champness, N. R.; Beton, P. H. *Nature* **2003**, *424*, 1029.

(18) Kampschulte, L.; Griessl, S.; Heckl, W. M.; Lackinger, M. *J. Phys. Chem. B* **2005**, *109*, 14074.

(19) Stepanow, S.; Lingenfelder, M.; Dmitriev, A.; Spillmann, H.; Delvigne, E.; Lin, N.; Deng, X. B.; Cai, C. Z.; Barth, J. V.; Kern, K. *Nat. Mater.* **2004**, *3*, 229.

(20) Griessl, S. J. H.; Lackinger, M.; Jamitzky, F.; Markert, T.; Hietschold, M.; Heckl, W. M. *J. Phys. Chem. B* **2004**, *108*, 11556.

(21) Griessl, S. J. H.; Lackinger, M.; Jamitzky, F.; Markert, T.; Hietschold, M.; Heckl, W. A. *Langmuir* **2004**, *20*, 9403.

(22) Lu, J.; Lei, S. B.; Zeng, Q. D.; Kang, S. Z.; Wang, C.; Wan, L. J.; Bai, C. L. *J. Phys. Chem. B* **2004**, *108*, 5161.

(23) Chae, H. K.; Siberio-Perez, D. Y.; Kim, J.; Go, Y.; Eddaoudi, M.; Matzger, A. J.; O'Keeffe, M.; Yaghi, O. M. *Nature* **2004**, *427*, 523.

(24) Kitaigorodskii, A. I. *Organic Chemical Crystallography*; Consultants Bureau: New York, 1959.

(25) Kitaigorodskii, A. I. *Acta Crystallogr.* **1965**, *18*, 585.

(26) Yan, H. J.; Lu, J.; Wan, L. J.; Bai, C. L. *J. Phys. Chem. B* **2004**, *108*, 11251.

(27) Weber, E.; Hecker, M.; Koepp, E.; Orlia, W.; Czugler, M.; Csoregh, I. *J. Chem. Soc., Perkin Trans. 2* **1988**, 1251.

(28) Gyarfas, B. J.; Wiggins, B.; Zosel, M.; Hipps, K. W. *Langmuir* **2005**, *21*, 919.

(29) Desiraju, G. R. *Acc. Chem. Res.* **1996**, *29*, 441.

(30) Neuheuser, T.; Hess, B. A.; Reutel, C.; Weber, E. *J. Phys. Chem.* **1994**, *98*, 6459.

(31) Kuduva, S. S.; Craig, D. C.; Nangia, A.; Desiraju, G. R. *J. Am. Chem. Soc.* **1999**, *121*, 1936.

(32) Berkovitch-Yellin, Z.; Leiserowitz, L. *J. Am. Chem. Soc.* **1982**, *104*, 4052.

(33) Kolotuchin, S. V.; Thiessen, P. A.; Fenlon, E. E.; Wilson, S. R.; Loweth, C. J.; Zimmerman, S. C. *Chem. Eur. J.* **1999**, *5*, 2537.

(34) Lackinger, M.; Griessl, S.; Heckl, W. A.; Hietschold, M.; Flynn, G. W. *Langmuir* **2005**, *21*, 4984.

(35) Lei, S. B.; Wang, C.; Yin, S. X.; Wang, H. N.; Xi, F.; Liu, H. W.; Xu, B.; Wan, L. J.; Bai, C. L. *J. Phys. Chem. B* **2001**, *105*, 10838.

(36) Wohlfarth, C. *Static Dielectric Constants of Pure Liquids and Binary Liquid Mixtures, Macroscopic and Technical Properties of Matter*; Vol. 6 Numerical Data and FunctionalRelationships in Science and Technology; Springer-Verlag: Berlin, Heidelberg, New York, 1991.

(37) *Landolt-Börnstein*. 1991; Vol. 6.

(38) Fisher, C. H. *J. Am. Oil Chem. Soc.* **1988**, *65*, 1647.

(39) Shanmugasundaram, V.; Thiyagarajan, P. *J. Indian Chem. Soc.* **1986**, *63*, 589.

(40) Conti, F.; Franconi, C. *Ber. Bunsen-Ges. Phys. Chem.* **1967**, *71*, 146.

(41) Roy, A. K.; Thakkar, A. J. *Chem. Phys. Lett.* **2004**, *386*, 162.

(42) Roy, A. K.; Thakkar, A. J. *Chem. Phys.* **2005**, *312*, 119.

(43) Loveluck, G. *J. Phys. Chem.* **1960**, *64*, 385.

(44) Mognaschi, E. R.; Zullino, L.; Chierico, A. *J. Phys. D-Appl. Phys.* **1984**, *17*, 1007.

(45) Griessl, S.; Lackinger, M. Unpublished observation.

Fabrication and in situ Modulation of
Multicomponent Hydrogen-bond driven Two-dimensional Networks

in preparation

L. Kampschulte, M. Lackinger, T. Adlerstein, R.S.K. Kishore, M. Schmittel, W.M. Heckl, B.J. Berne, G.W. Flynn

Fabrication and *in situ* Modulation of Multicomponent Hydrogen-bond driven Two-dimensional Networks

L. Kampschulte 1)2), M. Lackinger 2)3), T. Adlerstein 1), R. S. K. Kishore 4), M. Schmittel 4) W.M. Heckl 2)5), B. J. Berne 1), G.W. Flynn 1)

1) Department of Chemistry, Columbia University, New York, New York 10027, USA; 2) Department for Earth- and Environmental Sciences, Ludwig-Maximilians-University Munich, and Center for Nanoscience (CeNS), Theresienstr. 41, D-80333 Munich, Germany; 3) Department of Physics and Astronomy, University of California - Irvine, Irvine, CA 92697-4575, USA; 4) Universität Siegen, Center of Micro and Nanochemistry and Engineering, Organische Chemie I, Adolf-Reichwein-Str. 2, D-57068 Siegen, Germany; 5) Deutsches Museum, Museumsinsel 1, 80538 Munich, Germany

Abstract:

The co-adsorption of two different molecules, BTB (1,3,5-benzenetribenzoic acid) and TMA (trimesic acid) in open (loosely packed) networks was studied at the liquid-solid interface in two different solvents (heptanoic and nonanoic acid). Altering the absolute and relative concentrations of the two compounds in binary solutions resulted in phases with six different structures, as revealed by means of in-situ Scanning Tunneling Microscopy (STM). All of these structures are stabilized by twofold intermolecular hydrogen bonding between the carboxylic acid head groups. Moreover, in-situ dilution of liquid mixtures induced phase transitions of the monolayer structures, accompanied by an alteration of the size and shape of cavity voids in the 2-dimensional molecular assembly. Reversibly resolved patterns within the cavities of different structures provide evidence for adsorption of solvent molecules inside these voids.

Introduction:

Two-dimensional supramolecular nano-networks of functionalized molecular components fabricated by self-assembly processes represent an interesting class of materials with promising potential for future technological impact.[1] Many applications, such as the arrangement of nano-scale objects (e.g. quantum dots) in regular arrays with a specific distance between them, require highly structured surfaces. Today's lithographic production techniques[2] are far from being able to pattern surfaces with features in the low-nanometer regime. Self-assembly methods provide a promising and reliable alternative approach for the rapid preparation of well-defined structures having nano-scale dimensions over a relatively large area.

Aided by high spatial resolution provided by near-field techniques such as STM, a wide range of 2D ordered assemblies of organic molecules have been investigated utilizing varied non-covalent interactions such as hydrogen bonding,[3-7] dipolar coupling,[8-10] or metal co-ordination[11]. Hydrogen bonding in particular is a widely exploited mechanism for self-assembly of highly ordered monolayers, providing both high selectivity and directionality.[12]

While a large majority of networks are based on self-assembly of a single molecular component,[13-15] there has been growing interest in the design of multi-component 2D assemblies at the surface interface.[16-19] However fabrication of a uniform multi-component

monolayer structure on a surface has been a challenging task. A number of binary mixtures investigated tend to show phase separation or mixed monolayers.[20-25] Recently a few efforts have been successful in obtaining uniform monolayers of nanostructures from multiple components leading to well defined patterns different from those of the individual components.[26,27] It is, however, desirable to have a tunable multi-component 2D nanostructure whose cavity size and overall pattern could be modulated, just by varying parameters such as the concentrations of the components.

In this work a two-dimensional self-assembled supramolecular system composed of two different molecules BTB and TMA is investigated. We present STM data for the different self-assembled structures and determine their area of stability in a phase diagram. Co-adsorption of solvent molecules in the cavities of the open structures formed by adsorption of the solute molecules is also important in determining the geometrical arrangement of the observed interfacial assemblies. The influence of co-adsorbed solvent molecules on the self-assembly is examined as well, and a thermodynamic model is used to explain the emergence of different structures.

Experimental:

All experiments were conducted at the liquid-solid interface with a Nanoscope IIIa Scanning Tunneling Microscope from Digital Instruments. Platinum/Rhodium (87/13) tips were used as probes (wire diameter 0.25 mm, Omega Engineering, Inc.). Since the solvents employed in the present study are electrically non-conducting, insulated tips were not required. The sample temperature range was between 14.2°C and 20.4°C. However, within this range, no influence of temperature on the phase diagram was discernible. All compounds except for BTB (1,3,5-benzenetribenzoic acid) were provided by Sigma-Aldrich, Inc. and used without further purification (purities: TMA > 95%, heptanoic acid > 99%, nonanoic acid > 97%). The BTB was synthesized according to a known literature procedure[28] by a triscarboxylation of 1,3,5-tris(p-bromophenyl)benzene. Binary solutions containing both TMA (trimesic acid) and BTB were prepared by mixing/diluting mono-molecular saturated solutions of BTB and TMA in heptanoic (nonanoic) acid. The solutions were prepared fresh prior to the experiment, since solvent evaporation can have a significant impact on small (~50μl) sample volumes. The saturated solutions and the solvent were deposited in a clean test tube by means of a 50 μl micro-pipette, subsequently mixed in a supersonic bath for 5 minutes and allowed to cool down for ~15 minutes. For sample preparation a small droplet (~10 μl) of solution was deposited onto the basal plane of a freshly cleaved HOPG (highly oriented pyrolytic graphite) crystal. The vapor pressure of the solvents used is sufficiently low to allow experiments to continue with stable conditions for about 30 – 45 minutes. Typical tunneling parameters for the systems under investigation include a bias voltage of ~ +1.7 V referred to the tip, and tunneling currents of 100 pA to 300 pA. Occasionally, short voltage pulses (0.5 V – 3 V) were applied to recondition the tunneling tip. All topographs were taken in the constant current mode of operation. The images were processed by leveling, 3 x 3 Gauss filtering, and in the case of Table 1 (C, E, F), distortion correction using the graphite lattice as a reference.

Results and Discussion:

1) Observation of Multiple Two Dimensional Phases:

To investigate the subtle balance leading to co-adsorption of BTB and TMA, as well as the role of solvent identity, requires a system offering stable adsorption of both molecules, ready identification of the two species in STM images, and the possibility of preparing molecular mixtures in different solvents. Recent in-situ studies of relatively small molecules at the liquid-solid interface have demonstrated the stabilizing influence of hydrogen-bonds and the feasibility of using fatty acids as solvents.[29-33] It has been shown, that carboxylic acid functional groups attached to an aromatic system drive the self-assembly process forming monolayers on a graphite surface.[34]

Generally, predicting whether molecules will form mixed networks on a surface in equilibrium with a liquid phase is quite difficult. In the present study the similarity of the symmetry and functional groups appear to promote the compatibility of BTB/TMA co-adsorption. In previous studies we combined TPT (1,3,5-tris(4-pyridyl)-2,4,6-triazine) with trimesic and terephthalic acid.[35] However TPT does not have carboxylic acid groups (being both a donor and acceptor for hydrogen-bonds) and, therefore, requires a mediator to form stable monolayers at the liquid-solid interface near room temperature. BTB can be considered an enlarged derivative of TMA, with additional phenyl spacers between the carboxylic groups and the central benzene ring (c.f. Figure 1). It has the ability to self-assemble in monolayers in different solvents[36] and is considerably larger than TMA (diameter 1.8 nm vs. 0.9 nm for TMA). Thus, BTB is relatively easily distinguished from TMA even in STM images with only molecular resolution. Since both molecules have carboxylic acid groups attached to a benzene ring, the homo- and hetero-intermolecular hydrogen-bonds are very comparable, which is expected to facilitate network formation.
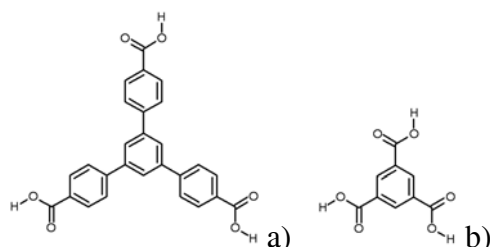

Figure 1: Structure of the adsorbate molecules: (a) BTB (1,3,5-benzenetribenzoic acid) and (b) TMA (1,3,5-tricarboxybenzene, trimesic acid); gray corresponds to carbon, red to oxygen, and white to hydrogen atoms, respectively. Both molecules exhibit the same three-fold symmetry (D_{3h}) and have three carboxylic acid groups as intermolecular linkers attached to benzene rings.

For the investigation of BTB/TMA co-adsorption, three main parameters were changed: the type of solvent, the mixing ratio of the BTB/TMA molecules, and the amount of solvent in the system (dilution). As solvents, two alkanoic acids with different chain lengths were used: heptanoic acid and nonanoic acid. The mixing ratio between the two monomolecular saturated solutions (containing either BTB or TMA molecules) was varied between 2TMA+1BTB (2 parts saturated solution of TMA and 1 part saturated solution of BTB) and 1TMA+4BTB for the system with heptanoic acid as solvent and between 5TMA+1BTB and 1TMA+2BTB for the system with nonanoic acid. Further solutions were prepared by diluting up to 10 parts solvent with 1 part (mixed) saturated solution. From the mixing ratios, the

relative concentrations of TMA (BTB) were calculated as the ratio of the volume portion containing TMA (BTB) to the total volume including the dilution with the other monomolecular BTB (TMA) solution and pure solvent. Note that with this simple but reliable method of mixing saturated monomolecular solutions only binary solutions with $c_{TMA} + c_{BTB} \leq 100\,\%$ are accessible, where c_{TMA}, c_{BTB} are the concentrations relative to a saturated solution ($c_i = 100\%$).

In this parameter space six different self-assembled networks were observed (c.f. Table 1): two networks consisting of only TMA molecules (A, B), one network containing only BTB molecules (F), and three mixed networks (C, D, E).
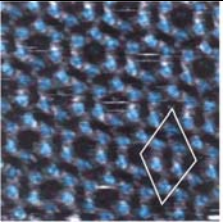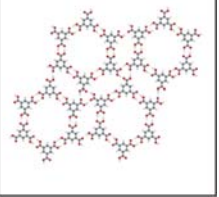
|		unit cell parameters	area density [1/nm²]	relative area density [%]
A		a = 2.5 nm b = 2.5 nm α = 120°	BTB = 0.00 TMA = 1.11	BTB = 0 TMA = 84 cavity = 16
B		a = 1.7 nm b = 1.7 nm α = 120°	BTB = 0.00 TMA = 0.80	BTB = 0 TMA = 61 cavity = 39
C		a = 4.3 nm b = 4.2 nm α = 120°	BTB = 0.13 TMA = 0.39	BTB = 22 TMA = 29 cavity = 49
D		a = 4.3 nm b = 2.5 nm α = 90°	BTB = 0.19 TMA = 0.19	BTB = 32 TMA = 14 cavity = 54
E		a = 5.7 nm b = 5.7 nm α = 60°	BTB = 0.21 TMA = 0.07	BTB = 36 TMA = 5 cavity = 59
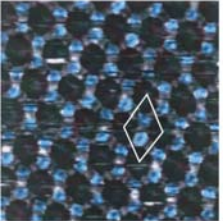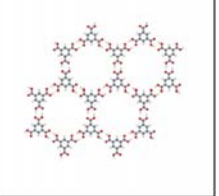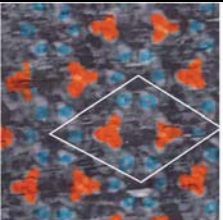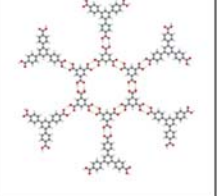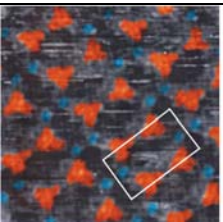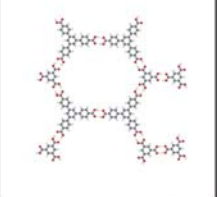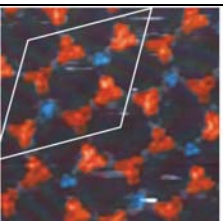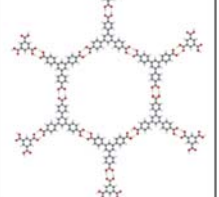
F		a = 3.2 nm b = 3.2 nm α = 60°	BTB = 0.23 TMA = 0.00	BTB = 38 TMA = 0 cavity = 62

Table 1: Observed two-dimensional structures for the BTB-TMA system. On the left hand side the STM-images of the different structures are shown, where TMA molecules are colored blue, and the larger triangular shaped BTB molecules are colored orange (image size 10×10 nm²). Typical tunneling conditions are described in the Experimental Section. Molecular Mechanics simulations using a Dreiding II force field[37] for the different networks (frame size 7.5×7.5 nm²) are depicted right next to the STM-images. Experimentally determined structural parameters for the different observed networks are shown on the right hand side: Unit cell parameters (experimental errors: a, b = ± 0.3 nm, α = ± 3°), area density of the molecules (molecules/area), and the relative proportion of molecules and cavities on the surface (see also Figure 3(a) below) were measured from the STM images.

Table 1 summarizes the experimentally determined lattice parameters for all observed structures. The relative area density of BTB and TMA respectively was estimated by applying the projected area of molecules lying flat on the surface. This results in an area of 1.69 nm² for one BTB and 0.76 nm² for one TMA molecule including the area occupied by intermolecular bonds. The remaining area was taken as the cavity size on the surface. Structures A and B are well known from previous experiments with only TMA on graphite, both in UHV[4] and at the liquid solid interface.[30] By applying a homologous series of fatty acids as solvents, we have shown recently,[30] that the formation of two TMA polymorphs at the liquid solid interface can be controlled by solvent identity. In the case of heptanoic acid the growth of both the so called "flower" (A) or the "chickenwire" (B) TMA structures was revealed, occasionally in coexistence. Solvents with a longer aliphatic tail, e.g. nonanoic acid, precipitate exclusively the "chickenwire" structure (B). The structures C, D, and E are mixed networks, comprised of both BTB and TMA molecules in different stoichiometries. Structure C consists of six membered TMA rings, with three of these rings being interconnected by one BTB molecule. Both TMA-TMA and BTB-TMA bonds are two-fold hydrogen-bonds between adjacent carboxylic acid groups. The directionality of the hydrogen-bonds is clearly an important factor that determines the formation and stability of these structures. All networks – except for the pure TMA "flower structure" (A) – exhibit the energetically most favorable hydrogen-bonding angle of 180° for the carboxylic acid dimer groups. E is the inverse structure to C, i.e. it can be constructed by interchanging TMA and BTB molecules. Thus, structure E is build up of six membered rings of BTB interconnected by TMA molecules. Except for structure D all observed networks can be described by a hexagonal unit cell. The unit cell of structure D is rectangular and contains an equal number of TMA and BTB molecules. Structure F is the corresponding network to B, but with BTB molecules instead of TMA and therefore an enlarged lattice constant and cavity size. This structure was found previously for mono-molecular BTB solutions.[36] However, the BTB chickenwire network was only observed with nonanoic acid as a solvent. For heptanoic acid a rectangular network was found. Apparently, when TMA is present in small concentrations, playing the role of an impurity, it can influence the growth of BTB monolayers.
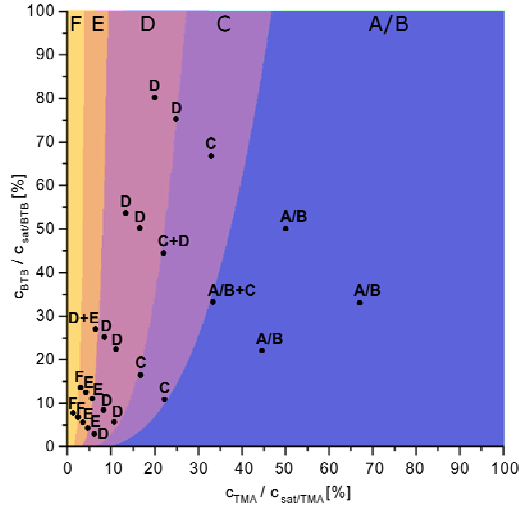
Figure 2: Phase diagram for the bimolecular system TMA+BTB in heptanoic acid. The abscissa depicts the relative TMA-concentration, whereas the ordinate depicts the relative BTB-concentration. Both concentrations are normalized to the concentration of saturated monomolecular solutions, i.e. the solubility of the respective compound. The occurrence of the structures A-F is indicated in the diagram. The uniformly colored region depicts the range of thermodynamic stabilty, i.e. the minimum of free energy of the respective phase, according to a thermodynamic model described in the text body.

Figure 2 shows a phase diagram of the parameter-space probed with heptanoic acid as the solvent. The structures containing predominantly TMA molecules were observed on the right hand side, i.e. for solutions with a high TMA concentration, whereas networks mainly build up of BTB molecules occur on the left hand side, implying a very low TMA concentration.

In the following a model based on a thermodynamic equilibrium is applied in order to explain the structural versatility of the binary TMA-BTB system. This approach is based on the monotonic increase of the chemical potential of the respective compound with concentration. In this model the Gibbs free energy G of each structure is calculated under the assumption of thermodynamic equilibrium, i.e. $\partial G = 0$ or equality of the chemical potentials of TMA and BTB on the surface and in solution. The Gibbs free energy of each structure is then given by:

$$G = \left[\left(\sigma(structure)_{TMA} \cdot \mu_{TMA}(c_{TMA}) \right) + \left(\sigma(structure)_{BTB} \cdot \mu_{BTB}(c_{BTB}) \right) \right] \cdot A \qquad (1)$$

Here $\sigma(structure)$ denotes the area densities (molecules/area) of TMA and BTB for the respective structure as summarized in Table 1. This model assumes that the chemical potential $\mu(c)$ of the adsorbates is dependent on the concentration but does not change during monolayer growth, otherwise equation (1) must be replaced by an integral. Since, the number of molecules needed to form the monolayer is orders of magnitude smaller than the number in the liquid phase, the concentration, and hence the chemical potential of each species in solution can be assumed constant. (The solubility of TMA in heptanoic acid at room temperature is on the order of 1 mmol/l.[30] Taking the sample area and the amount of solvent deposited on the surface into account, the number of TMA molecules in solution is around two orders of magnitude larger than the number in the surface monolayer.)
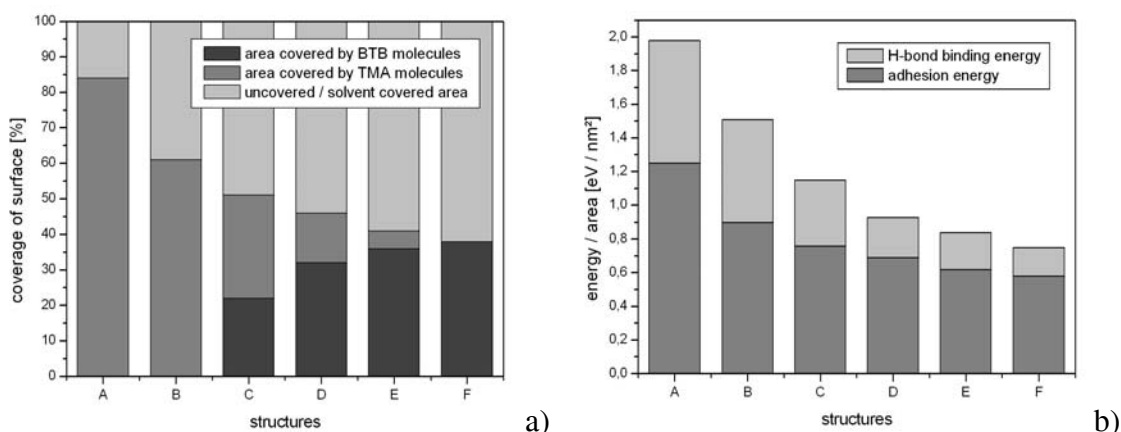
Figure 3: (a) relative coverage of the surface for different network structures (see Table 1); (b) total binding energy of the different observed structures, split into adhesion energy between the molecules and the surface and the intermolecular H-bond binding energy. For better comparison, the respective energies have been normalized to the surface area.

Figure 3(a) displays the relative portions of each molecule and the cavity area for all structures. A Molecular Mechanics simulation was performed to calculate the binding energies of the different structures. For these calculations the unit cell parameters deduced from the STM measurements were employed as a constraint. Figure 3(b) shows the total binding energy for the various structures and the relative fractions resulting from H-bonding and adhesion, respectively, of the aromatic systems TMA and BTB on the graphite surface. As expected, the surface adhesion energy is exactly (regression coefficient $r^2 = 0.98$) proportional to the relative area covered by TMA and BTB, and, thus, to the area of interaction between the aromatic π-systems of the molecules and the electron system of the graphite substrate.

Although Molecular Mechanics simulations neglect and approximate a number of interactions in such a system, which are important for determining the absolute value of the binding energy, they allow a relative comparison to be made among different monolayer surface structures. Since all structures employ the same substrate, have the same bond type, and the same molecules in common, considerable insight can be obtained about the relative energetics even from such simplified model calculations. As can be seen in Figure 3, the cavity area portion increases monotonically going from structures A to F, whereas both the adhesion and H-bonding energies of the molecules decrease monotonically. Normally, in a polymorphic system the total free energy of all phases is comparable within the scale of thermal energy.[38] Here the Molecular Mechanics simulations of the adsorbed monolayer indicate that the adhesion plus H-bonding energies differ by about a factor of 2 over the range of systems studied. However, these calculations neglect the role of co-adsorption by the solvent within the cavities where pristine substrate is exposed to solution. Assuming the additional binding energy contribution from solvent co-adsorption is proportional to the cavity area of the respective structures, the total energy is given by:

$$E_{total} = E_{BTB+TMA} + e_{solvent} \cdot A_{cavity} \tag{2}$$

Here E_{total} denotes the total energy of the monolayer including solvent co-adsorption, $E_{BTB+TMA}$ the contribution from the TMA+BTB lattice (adhesion + H-bonding) as calculated by the Molecular Mechanics simulations, $e_{solvent}$ the energy/unit area for solvent co-adsorption, and A_{cavity} the relative area of the cavities in the respective structures. Assuming E_{total} is roughly constant (within kT^{30}) for all observed structures, a plot of simulated $E_{BTB+TMA}$ versus measured A_{cavity} should result in a straight line. The absolute value of the slope of this line corresponds to the energy/unit area for solvent co-adsorption and the intercept is the total energy. Such a plot is displayed in Figure 4.

$$E_{BTB+TMA} = -e_{solvent} * A_{cavity} + E_{total}$$

$$E_{BTB+TMA} = (-2.77 * A_{cavity} + 2.48) \text{ eV/nm}^2$$

$$r^2 = 0.98$$
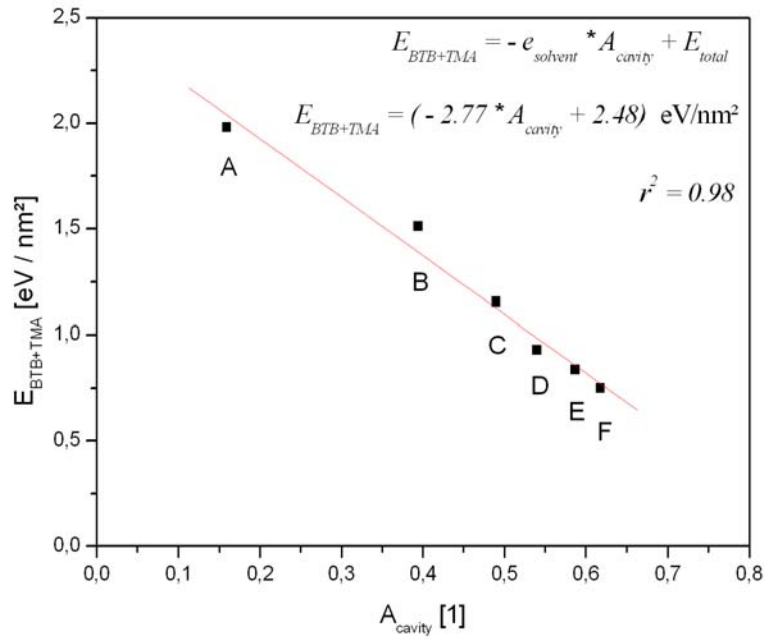
Figure 4: plot of simulated $E_{BTB+TMA}$ versus measured A_{cavity} assuming a constant total energy for all structures. The absolute value of the slope corresponds to the energy/area of solvent co-adsorption ($e_{solvent}$), and the intercept to the total energy. r^2 is the regression coefficient. $E_{BTB+TMA}$ values were taken from the Molecular Mechanics simulations, whereas A_{cavity} was calculated in the way described above from the unit cell parameters as determined from STM measurements.

Since the combination of simulated binding energies and measured cavity area seems to satisfy equation (2), we conclude that there is an additional contribution to the binding energy from solvent co-adsorption. This hypothesis is supported by the observation of various types of image contrast within the cavities as discussed in more detail below. Thus, we add a correction term to equation (1), which considers a contribution to the Free Energy from solvent co-adsorption, which is proportional to the cavity area:

$$G = \left[\left(\sigma(structure)_{TMA} \cdot \mu(c)_{TMA} \right) + \left(\sigma(structure)_{BTB} \cdot \mu(c)_{BTB} \right) + \left(C \cdot A_{cavity}(structure) \right) \right] \cdot A \quad (3)$$

Based on equation (3) the phase diagram for monolayer structures on the surface of the binary system was simulated in the following way. For each point in concentration space (c_{TMA}, c_{BTB}) the chemical potential of each compound was calculated assuming the concentration dependence of an ideal solution (4)[i]:

$$\mu(c) = \mu_0 - akT \cdot \ln(c) \hspace{4cm} (4)$$

μ_0 depicts the standard chemical potential, k, T are the gas constant and temperature respectively, and a is a universal free parameter, i.e. independent of the structure, used to adjust the model to our measurements.

The values for the concentration dependent chemical potentials of TMA and BTB were used to evaluate the total free energy G according to equation (3) for all structures A-F, applying the area densities of BTB, TMA, and the cavity area as determined by the STM measurements. The free parameters ($\mu_{0\ TMA}$, $\mu_{0\ BTB}$, a_{TMA}, a_{BTB}) were adjusted to reproduce the measured phase diagram. (Although different monotonically increasing functions for the chemical potentials reproduce a similar order of the phases with respect to the concentrations, the exact shape of the phase boundaries is dependent on the particular functional form of the chemical potential.) Finally a specific point in the two-dimensional concentration space was assigned to the structures A-F, which corresponds to the minimum in free energy. Iterations of the free parameters were performed for a quadratic grid (spacing 0.1 %) of TMA and BTB concentrations, the result is depicted in Figure 2.

It is noteworthy, that the simulated phase diagram is very sensitive to the value of the energy area density for solvent co-adsorption; whereas the simulated phase diagram is rather robust with respect to changes in the free parameters of the chemical potential. Furthermore, in regions where structures A/B represent the thermodynamical most stable phase (this is the right hand side of the phase diagram), structure (B) leads to the minimum in G due to its larger cavity area and the affiliated solvent co-adsorption. However, the stabilisation of phase (A) might be caused by kinetic effects as elaborately discussed in previous work.[30]

2) Solution Precursors:

One possible explanation for the observation of multiple arrangements of BTB and TMA on the surface is the formation in solution of basic supramolecular units such as [TMA]$_2$, [BTB]$_2$, [BTB-TMA], or [TMA]$_3$. The networks in Table 1 can all be built up from the following basic units: (A) [TMA]$_3$, (B) [TMA]$_2$, (C) [TMA]$_2$ + [BTB-TMA], (D) [TMA]$_2$ + [BTB]$_2$, (E) [BTB-TMA] + [BTB]$_2$, (F) [BTB]$_2$, as depicted in Table 2.

---

[i] the chemical potential of each compound was assumed to be independent of the concentration of the other compound.

structure	[TMA]$_3$	[TMA]$_2$	[TMA-BTB]	[BTB]$_2$
A	100%			
B		100%		
C		50%	50%	
D		50%		50%
E			50%	50%
F				100%

Table 2: Decomposition of the six different network structures shown in Figure 2 into four supramolecular building blocks. The numbers in the table indicate the portion of the respective dimer or trimer in percent found experimentally for each of the 6 observed cases.

Of course, all structures could be seeded by even larger supramolecular units – e.g. for structure (C) from [BTB(TMA)$_3$] tetramers; however, the stability of such structures is likely to be low, and hence the existence of these large aggregates in solution is less likely. In solution encounters of two monomers result in formation of these supramolecular units:

TMA + TMA $\Leftrightarrow$ [TMA]$_2$

TMA + BTB $\Leftrightarrow$ [BTB-TMA]
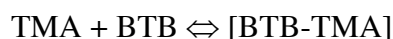
At constant temperature equilibrium is determined by the monomer and dimer concentrations. For example, as the BTB concentration is increased, the formation of mixed [BTB-TMA] structures and eventually [BTB]$_2$ dimers becomes favoured. As the concentration of supramolecular units in solution increases, the possibility that they can seed the different structures A-F on the surface will be enhanced. Since the surface structures are in dynamic equilibrium with the liquid phase, altering the stability of the various basic supramolecular units in solution will change the surface structure as well.

3) Nonanoic acid as a solvent:

For the experiments using nonanoic acid as a solvent, similar network structures were found. The arrangement of the structures in the phase diagram is similar to that for heptanoic acid as a solvent. For saturated solutions containing a high concentration of TMA molecules, networks consisting only of TMA molecules were observed. In accordance with previous results,[30] only structure B and not A was observed using nonanoic acid as solvent. For mixtures with a higher BTB concentration and a higher solvent concentration, structure F, the pure BTB chickenwire network, was found. Mixed structures (E) were found in the regime between these two extreme cases.

4) Reorganization via in-situ changes of concentration:

All experiments described so far were conducted with pre-mixed solutions, but it is of interest to ask how the surface structures of the adsorbed monolayers are altered by changing the identity of the liquid phase through *in-situ* dilution when solvent is added. To test these ideas, a droplet (~5 µl) of pre-mixed solution was applied to the graphite sample, and the emerging monolayer was imaged with the STM. Then the tip was retracted, a small amount of solvent (~1 µl) was added to the sample, the tip was re-approached immediately, and the new system was imaged. Dilution was repeated in this stepwise manner until the desired point in concentration space, indicated by the monolayer surface structure, was reached or until all network structures were dissolved. Although the concentration after dilution is not precisely defined[ii], each phase along the "dilution path" could be imaged. Because adding solvent dilutes both BTB and TMA, the phase diagram dilution takes place along a straight line from the initial values of the relative concentrations of BTB and TMA to the origin in Figure 2.

These experiments were carried out successfully with different starting solutions. For example, beginning with structure B at $c_{TMA} / c_{Sat,TMA} = c_{BTB} / c_{Sat,BTB} = 50$ %, moving along a "dilution-path" (c.f. Figure 2) towards the origin, first structure B was changed to C, to D and eventually to E. Upon further dilution TMA/BTB monolayers could not be detected on the surface. The time scale for this solvent mediated reorganization at room temperature is less than 30 sec., which is the minimum time needed to re-approach the STM tip and start the scanning process after deposition of additional solvent. Generally, it was possible to induce phase transitions between different networks and, therefore, to change the size of the surface monolayer cavities directly (*in-situ*) by just adding solvent.

5) Co-Adsorption of solvent molecules:

During the imaging experiments three different types of image contrast were observed within the BTB/TMA monolayer cavities: (I) the contrast presented in Table 1 corresponding to very blurry features inside the cavities; (II) the BTB/TMA network of molecules is clearly discernible, but protruding spots appear inside the cavities, which are aligned in rows, (c.f. Figure 5(b)); and (III) an 'inverted' structure with circular spots arranged inside the cavities almost obscuring the BTB/TMA network molecules (see Figure 5(c)). These three, clearly

---

[ii] The droplets spread out over the whole graphite surface (~10 x 10 mm²), and some solution creeps below the sample mounting clamp.

distinguishable, structures were reproducibly observed; all STM patterns were detected in different experimental runs with different probes, eliminating tip artifacts as a source of the image patterns. As depicted in Table 1, contrast type I was observed for all structures using both heptanoic and nonanoic acid as solvent. Contrast type II was only found for structure F with nonanoic acid solvents. Again contrast type III was observed for all structures when heptanoic acid was used as the solvent. On the other hand, for nonanoic acid solutions this image pattern was only observed for structures E and F.
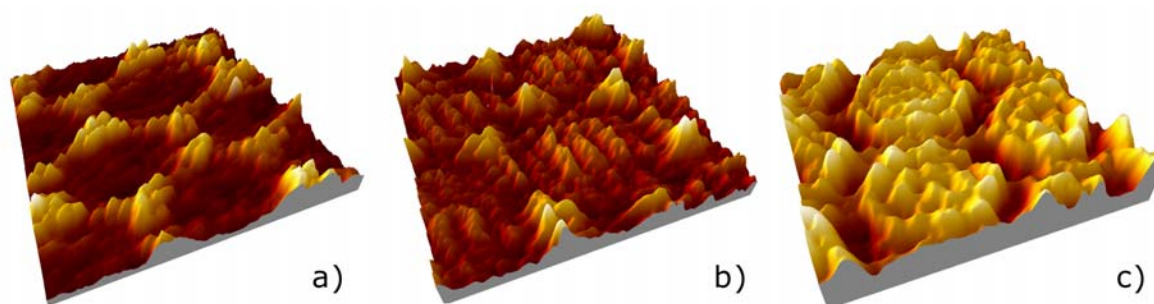
Figure 5: Three different types of contrast assigned to adsorption of solvent molecules inside the BTB/TMA cavities (a) no solvent molecules inside the cavities are discernible (contrast type I, structure E), (b) a row-like pattern appears within the cavities (contrast type II, structure F), and (c) adsorption in a circular pattern (contrast type III, network structure E).

In the case of contrast type I the apparent height of the cavities is about 0.2 nm lower than the TMA/BTB network. Since the apparent height of planar aromatic molecules lying flat on a graphite surface in STM images is normally on the order of 0.2-0.4 nm, depending on the particular system and the bias voltage, contrast I can be assigned to "empty" cavities. However, solvent molecules may either not adsorb within the cavities or adsorb/desorb on a rapid time scale, too fast for the STM to follow. Furthermore, interaction with the STM tip may contribute to the emptying of the cavities if the species are loosely bound.

The distance between adjacent maxima in the row like features of contrast type II amounts to ~0.26 nm, and coincides with the lattice constant of the graphite substrate (~0.25 nm)[iii]; however, the linear arrangement contradicts the hexagonal symmetry of the substrate. Furthermore, the similarity of the height of these features with the surrounding molecules renders the graphite substrate as the origin of these features very unlikely. The spot-spot distance of ~0.26 nm is in good agreement with both STM measurements and Molecular Mechanics simulations of aliphatic molecules lying flat on the surface, if the maxima are assigned to H-atoms of adjacent methyl groups.[14] On graphite, nonanoic acid is known to adsorb flat with the aliphatic backbone aligned to the high symmetry directions of the substrate[39-41]. Generally, extended aliphatic portions of molecules tend to align with the graphite axes, due to the almost perfect registry between surface and molecule. This can have a major impact on the adsorption site and orientation even of molecules with large macrocycles.[31,42,43] Another hint that these images correspond to adsorption of solvent molecules parallel to the surface is that the row-pattern was only observed for structures with

---

[iii] in STM measurements every second graphite atom is visible only, therefore the atom-atom distance appears enlarged

sufficiently large cavities (F). For structures with smaller cavities (e.g. structure B with a cavity diameter ~1.1 nm), the length of nonanoic acid molecules (~1.5 nm) makes adsorption with its axis parallel to the substrate impossible. Contrast III looks rather different: the bright spots are not aligned along rows, but arranged in concentric circles covering the whole cavity. This can clearly be seen in Figure 5(c) where the cavities of different size in structure E result in different spot patterns. The bigger cavities (such as the structure F cavity in the background of Figure 5(c)) have two concentric rings with spots in the center, whereas the smaller cavities exhibit just two, slightly distorted concentric rings (cf. the cavities in the front and on the right hand side of Figure 5(c)). The underlying BTB/TMA network structure is almost obscured by the large apparent height of the structures within the cavities. The distance between the maxima of the spots in these cavities varies between 0.45 nm and 0.55 nm. This is almost twice as large as the spot distance for contrast type II. (This spot separation is much bigger than both the H-H-distance in alkyl chains and the graphite lattice spacing of ~0.25 nm.) However, it is well known, that alkanoic acid molecules can adsorb upright on strongly interacting metal surfaces such as gold or platinum, with the terminal methyl (CH_3) group facing up, leading to an autophobic surface.[44,45] Although this behavior has never been reported for less reactive surfaces, such as graphite, the pattern in Figure 5(c) strongly suggests an upright adsorption geometry for heptanoic acid. Since the two kinds of network molecules (BTB and TMA) have a clearly distinguishable triangular shape when adsorbed flat, co-adsorption of these compounds within the cavities can be ruled out. Any other adsorption geometry of either BTB or TMA within the cavities can be excluded on energetic grounds, and moreover, would not explain the symmetry of the pattern.

Very recently, Hipps et al. have investigated the adsorption of coronene molecules in fatty acid solvents on a Au(111) surface.[46] Depending on the solvent used, different structures of non-densely packed coronene molecules were observed surrounded by concentric protrusions. The size of these satellite spots matches the area of solvent molecules adsorbed in an upright geometry, thus suggesting co-adsorption of solvent molecules with the carboxylic group binding to the substrate. These observations are consistent with our experiments, if the circular spots inside the cavities are assigned to be solvent molecules adsorbed with their axis perpendicular to the surface. The nearest neighbor distance of the spots within the cavity suggests a dense packing of upright solvent molecules, similar to the widely studied SAMs based on the interaction of gold surfaces with thiols. In this kind of arrangement an additional energy gain also results from interactions between the upright alkane backbones.

Conclusions:

The phase diagram of a binary solute system was probed at the liquid-solid (graphite) interface by means of in-situ STM. Depending on the concentrations of the two solutes, TMA and BTB, six different hydrogen-bonded monolayer structures were discovered with heptanoic acid as the solvent, three of these being mixed TMA/BTB phases. Although both species are always present in solution, the different molecular arrangements observed on the surface range from pure TMA networks to different hexagonal and rectangular mixed networks (containing BTB and TMA) to arrangements built up from just BTB molecules. All networks exhibit a periodic arrangement of large internal cavities of various sizes (1.1 nm – 2.8 nm) and shapes. The cavities are potential sites for the guided adsorption of appropriate guests by the TMA/BTB host networks. When using the slightly different molecule nonanoic acid as a solvent, similar network surface structures were found. Probing the 2D TMA/BTB

concentration space with pre-mixed solutions allowed a phase diagram of the system to be constructed. In addition, in-situ dilution of the solutions with pure solvent resulted in phase transitions as anticipated from and consistent with the phase diagram, thereby suggesting that the growth of these mixed networks is thermodynamically controlled. This in-situ switchablity of the networks provides an opportunity to construct monolayer host networks that offer a tunable cavity size, lattice constant, and composition.

The measured phase diagram was reproduced by means of a simple thermodynamic model, based upon a simulation of the concentration dependence of the chemical potential for TMA and BTB in solution. Measured unit cell parameters of the respective structures and the related molecular area densities of the two compounds were employed as experimental input to this model.

Different types of STM image contrast were observed inside the putatively "empty" cavities of the TMA/BTB networks providing experimental evidence for co-adsorption of solvent molecules. The different patterns of the solvent structures within the cavities suggest that either upright or parallel adsorption of the alkane solvent backbone can occur. This already suggests the possibility of incorporating other molecules or clusters – metallic or semi conducting – within the network host cavities. The BTB/TMA template structure can be used to introduce long range order among the guest species or immobilize them, e.g. for local spectroscopy. The remarkably rich phase diagram of this binary system makes six different surface structures readily accessible by simply varying the concentration of just two compounds.

References:

(1)   Whitesides, G. M.; Mathias, J. P.; Seto, C. T. *Science* 1991, *254*, 1312.

(2)   Sheats, J. R.; Smith, B. W. *Microlithography Science and Technology*, 1st edition ed.; Marcel Dekker, Inc: New York, 1998.

(3)   Chen, Q.; Frankel, D. J.; Richardson, N. V. *Langmuir* 2002, *18*, 3219.

(4)   Griessl, S.; Lackinger, M.; Edelwirth, M.; Hietschold, M.; Heckl, W. M. *Single Mol* 2002, *3*, 25.

(5)   Keeling, D. L.; Oxtoby, N. S.; Wilson, C.; Humphry, M. J.; Champness, N. R.; Beton, P. H. *Nano Lett* 2003, *3*, 9.

(6)   Macdonald, J. C.; Whitesides, G. M. *Chem Rev* 1994, *94*, 2383.

(7)   Weckesser, J.; De Vita, A.; Barth, J. V.; Cai, C.; Kern, K. *Phys Rev Lett* 2001, *8709*, art. no.

(8)   Yokoyama, T.; Yokoyama, S.; Kamikado, T.; Okuno, Y.; Mashiko, S. *Nature* 2001, *413*, 619.

(9)   de Wild, M.; Berner, S.; Suzuki, H.; Yanagi, H.; Schlettwein, D.; Ivan, S.; Baratoff, A.; Guentherodt, H. J.; Jung, T. A. *Chemphyschem* 2002, *3*, 881.

(10)   Berner, S.; Brunner, M.; Ramoino, L.; Suzuki, H.; Guntherodt, H. J.; Jung, T. A. *Chem Phys Lett* 2001, *348*, 175.

(11)   Lin, N.; Dmitriev, A.; Weckesser, J.; Barth, J. V.; Kern, K. *Angew Chem Int Edit* 2002, *41*, 4779.

(12) Jeffrey, G. A. *An introduction to hydrogen bonding*; Oxford University Press: New York ; Oxford, 1997.

(13) Frommer, J. *Angewandte Chemie-International Edition in English* 1992, *31*, 1298.

(14) Cyr, D. M.; Venkataraman, B.; Flynn, G. W. *Chem Mater* 1996, *8*, 1600.

(15) De Feyter, S.; De Schryver, F. C. *J Phys Chem B* 2005, *109*, 4290.

(16) EichhorstGerner, K.; Stabel, A.; Moessner, G.; Declerq, D.; Valiyaveettil, S.; Enkelmann, V.; Mullen, K.; Rabe, J. P. *Angewandte Chemie-International Edition in English* 1996, *35*, 1492.

(17) Qian, P.; Nanjo, H.; Yokoyama, T.; Suzuki, T. M. *Chem Commun* 1999, 1197.

(18) Qian, P.; Nanjo, H.; Yokoyama, T.; Suzuki, T. M.; Akasaka, K.; Orhui, H. *Chem Commun* 2000, 2021.

(19) Lei, S. B.; Wang, C.; Yin, S. X.; Bai, C. L. *J Phys Chem B* 2001, *105*, 12272.

(20) Venkataraman, B.; Breen, J. J.; Flynn, G. W. *J Phys Chem-Us* 1995, *99*, 6608.

(21) Stevens, F.; Dyer, D. J.; Walba, D. M. *Langmuir* 1996, *12*, 436.

(22) Hipps, K. W.; Lu, X.; Wang, X. D.; Mazur, U. *J Phys Chem-Us* 1996, *100*, 11207.

(23) Baker, R. T.; Mougous, J. D.; Brackley, A.; Patrick, D. L. *Langmuir* 1999, *15*, 4884.

(24) Padowitz, D. F.; Sada, D. M.; Kemer, E. L.; Dougan, M. L.; Xue, W. A. *J Phys Chem B* 2002, *106*, 593.

(25) De Feyter, S.; Larsson, M.; Schuurmans, N.; Verkuijl, B.; Zoriniants, G.; Gesquiere, A.; Abdel-Mottaleb, M. M.; van Esch, J.; Feringa, B. L.; van Stam, J.; De Schryver, F. *Chem-Eur J* 2003, *9*, 1198.

(26) De Feyter, S.; Miura, A.; Yao, S.; Chen, Z.; Wurthner, F.; Jonkheijm, P.; Schenning, A. P. H. J.; Meijer, E. W.; De Schryver, F. C. *Nano Lett* 2005, *5*, 77.

(27) Yang, X. Y.; Mu, Z. C.; Wang, Z. Q.; Zhang, X.; Wang, J.; Wang, Y. *Langmuir* 2005, *21*, 7225.

(28) Weber, E.; Hecker, M.; Koepp, E.; Orlia, W.; Czugler, M.; Csöregh, I. *J Chem Soc Perk T 2* 1988, 1251.

(29) Griessl, S. J. H.; Lackinger, M.; Jamitzky, F.; Markert, T.; Hietschold, M.; Heckl, W. M. *J Phys Chem B* 2004, *108*, 11556.

(30) Lackinger, M.; Griessl, S.; Heckl, W. A.; Hietschold, M.; Flynn, G. W. *Langmuir* 2005, *21*, 4984.

(31) De Feyter, S.; De Schryver, F. C. *Chem Soc Rev* 2003, *32*, 139.

(32) Yan, H. J.; Lu, J.; Wan, L. J.; Bai, C. L. *J Phys Chem B* 2004, *108*, 11251.

(33) Lei, S. B.; Wang, C.; Yin, S. X.; Wang, H. N.; Xi, F.; Liu, H. W.; Xu, B.; Wan, L. J.; Bai, C. L. *J Phys Chem B* 2001, *105*, 10838.

(34) Lu, J.; Zeng, Q. D.; Wang, C.; Zheng, Q. Y.; Wan, L. J.; Bai, C. L. *J Mater Chem* 2002, *12*, 2856.

(35) Kampschulte, L.; Griessl, S.; Heckl, W. M.; Lackinger, M. *J Phys Chem B* 2005, *109*, 14074.

(36) Griessl, S.; Lackinger, M.; Maier, A.-K.; Kalsani, V.; Kampschulte, L.; Schmittl, M.; Heckl, W. M. *Journal of Physical Chemistry B* 2005, *submitted*.

(37) Mayo, S. L.; Olafson, B. D.; Goddard, W. A. *J Phys Chem-Us* 1990, *94*, 8897.

(38) Gavezzotti, A. *Crystengcomm* 2002, 343.

(39) Hibino, M.; Sumi, A.; Hatta, I. *Jpn J Appl Phys 1* 1995, *34*, 610.

(40) Hibino, M.; Sumi, A.; Hatta, I. *Jpn J Appl Phys 1* 1995, *34*, 3354.

(41) Hibino, M.; Sumi, A.; Tsuchiya, H.; Hatta, I. *J Phys Chem B* 1998, *102*, 4544.

(42) Yablon, D. G.; Giancarlo, L. C.; Flynn, G. W. *J Phys Chem B* 2000, *104*, 7627.

(43) Yablon, D. G.; Guo, J. S.; Knapp, D.; Fang, H. B.; Flynn, G. W. *J Phys Chem B* 2001, *105*, 4313.

(44) Fox, H. W.; Hare, E. F.; Zisman, W. A. *J Phys Chem-Us* 1955, *59*, 1097.

(45) Hare, E. F.; Zisman, W. A. *J Phys Chem-Us* 1955, *59*, 335.

(46) Gyarfas, B. J.; Wiggins, B.; Zosel, M.; Hipps, K. W. *Langmuir* 2005, *21*, 919.

Dynamics of Grain Boundaries in
Two-Dimensional Hydrogen-Bonded Molecular Networks

Markus Lackinger, Stefan Griessl, Lorenz Kampschulte, Ferdinand Jamitzky, and
Wolfgang M. Heckl

Dynamics of Grain Boundaries in Two-Dimensional Hydrogen-Bonded Molecular Networks**

Markus Lackinger,* Stefan Griessl, Lorenz Kampschulte, Ferdinand Jamitzky, and Wolfgang M. Heckl

The temporal evolution of domain boundaries of hydrogen-bonded molecular monolayers at the liquid–solid interface is evaluated by recording series of subsequent scanning tunneling microscopy (STM) images. Comparison of dissimilar benzene carboxylic acids reveals a clear distinction between one- and two-dimensional H-bonded network structures. Trimesic acid forms a two-dimensionally H-bonded networked structure, whereas terephthalic acid organizes in a dense packing of H-bonded linear chains on a graphite surface. In addition, TMA forms a sixfold lattice on a threefold graphite substrate, whereas TPA exhibits only a twofold lattice, causing a high grain-boundary line energy for the latter. In the case of TMA the nanostructure was mostly stable during the observation time. For TPA, Ostwald ripening—that is, the growth of larger islands at the expense of smaller islands—was observed. To explain the various experimentally observed timescales of the dynamics occurring at grain boundaries, molecular mechanics simulations were applied to calculate the binding energy of edge molecules, that is, the line energy, of finite islands of both trimesic and terephthalic acid on a graphite substrate.

Keywords:
· hydrogen bonding
· molecular dynamics
· molecular mechanics
· self-assembly
· structure–property
  relationships

1. Introduction

Many technologically relevant materials are applied in a polycrystalline state, that is, the active region of the material consists of grains with a more- or less-defined size, shape, and orientation. Nucleation (the density and spatial distribution of the nuclei) as the first step of crystal growth determines the average size and distribution of the crystallites.[1] Given sufficient thermal energy, a reorganization of the nanostructure can still take place. For two-dimensional (2D) molecular layers on atomically clean substrates, homonucleation (nuclei comprised of at least a critical number of crystallizing species) generally occurs, and monolayer growth is terminated when grains touch one another. This process generates grain boundaries that limit the translational symmetry of the otherwise crystalline material. Hence, this kind of defect has a high impact on important physical properties, in particular transport properties such as electrical conductivity. STM has already proven its value for the investigation of inorganic grain boundaries,[2] and similarly for studies on the structure and dynamics of grain boundaries in organic monolayers.[3]

[*] Dr. M. Lackinger, Dr. S. Griessl, L. Kampschulte, Dr. F. Jamitzky,
    Prof. W. M. Heckl
    Ludwig-Maximilians-Universität München
    Departement für Geo- und Umweltwissenschaften & Center for
    NanoScience (CeNS)
    Theresienstr. 41, 80333 München (Germany)
    Fax: +49 89 2180 4331
    E-mail: markus@lackinger.org
    Prof. W. M. Heckl
    Deutsches Museum
    80306 München (Germany)
    Supporting information for this article is available on the WWW
    under http://www.small-journal.com or from the author.

Depending on the ratio between available thermal energy and binding energy of the building blocks of the crystal adjacent to the grain boundary, dynamics and reorganization can occur; particles can fluctuate between neighboring grains without generating a net flux. Alternatively, larger grains can grow at the expense of smaller ones—a process known as Ostwald ripening. Moreover, adjacent grains can coalesce and form a more extended island through the incorporation of additional material.

The subjects of this study are 2D hydrogen-bonded supramolecular structures at the liquid–solid interface. Here, organic molecules adsorb and self-assemble on a solid substrate with the liquid phase above. The liquid phase serves as a reservoir for molecules and is normally in a dynamic equilibrium with the molecular layer on the surface. Herein we focus on hydrogen-bonded molecular systems. Because of their relative strength in comparison to pure Van der Waals bonds, H-bonds are very important both in nature and in the design of supramolecular structures.[4] Another interesting aspect, which can be exploited for tailoring supramolecular structures, is the selectivity and directionality of H-bonds.[5] Herein, we compare networks of 1,3,5-benzene-tricarboxylic acid (trimesic acid; TMA) and 1,4-benzene-dicarboxylic acid (terephthalic acid; TPA) at the interface between the respective solution and the (0001) plane of highly oriented pyrolytic graphite with heptanoic acid as solvent. TPA forms densely packed molecular chains,[6] whereas TMA builds a 2D H-bonded network.[7] Models of both structures are depicted in Figure 1. In this work, in situ STM was used as a high-resolution real-space observation tool. By means of video-STM (that is, merging subsequent STM "snapshots" into a movie, similar to making a flipbook), changes in island size and shape on a timescale of ten minutes are visualized (for details see the Experimental Section). Likewise, Rabe and co-workers investigated Ostwald ripening in 2D molecular layers at the liquid–solid interface.[8] In one work two different systems exhibit Ostwald
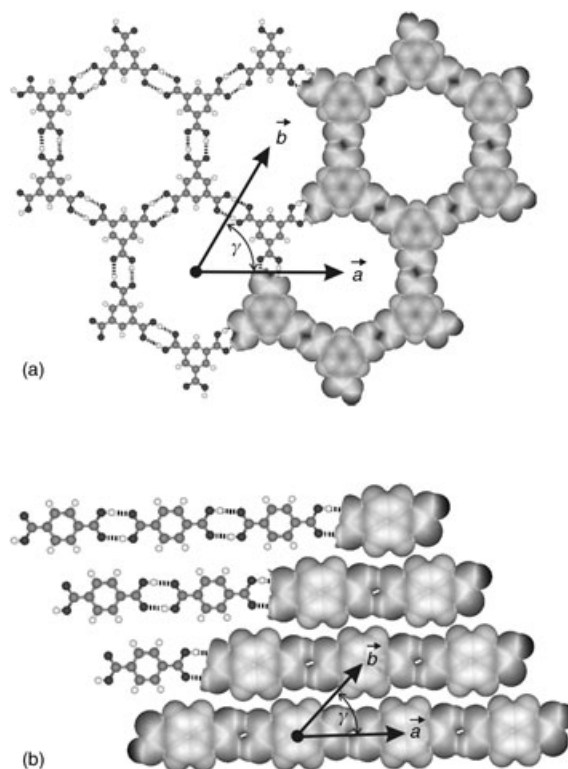
Figure 1. Models of the monolayer structures of a) trimesic acid (TMA) and b) terephthalic acid (TPA) on graphite; on the right-hand side the molecules are depicted with the Van der Waals radii of the atoms; the black dashed lines indicate hydrogen-bonds, where two H-bonds are formed between adjacent carboxylic groups; each TPA molecule within the monolayer is bound by a total of four H-bonds, whereas each TMA molecule forms six H-bonds. The lattice parameters for TMA and TPA are $a=b=1.6$ nm, $\gamma=60°$ and $a=1.0$ nm, $b=0.9$ nm and $\gamma=46°$, respectively.

ripening on slightly different timescales, whereas here TPA rearranges very rapidly and the TMA nanostructure remains almost unaffected, at least during the observation time.

2. Results and Discussion

In thermodynamic equilibrium both TMA and TPA molecules assemble in long-range-ordered monolayers at the interface between the heptanoic acid solution and the (0001) face of a highly oriented pyrolytic graphite substrate. The unit cells of the systems under investigation are already known from previous studies. TMA forms a sixfold-symmetric hydrogen-bonded network, with each TMA molecule bound to three neighboring molecules,[7] whereas TPA assembles in linear, 1D H-bonded chains, which are associated mainly through comparatively weak Van der Waals forces.[6] Since carboxylic groups can act as both a donor and acceptor for H-bonds, intermolecular bonding becomes possible without the need for further functional groups. Two H-bonds are formed per two adjacent carboxylic groups, and a straight configuration, that is, a bonding angle of 180°, is energetically most favorable. In contrast to TPA, TMA assembles in an open (that is, not densely packed) structure with

a periodic arrangement of voids, suitable for the incorporation of both TMA and different species as guest molecules. As shown previously, these voids are appropriate for the co-adsorption of coronene and buckminsterfullerenes.[9]

The dynamics at grain boundaries were analyzed by means of a series of subsequent STM images. In this paper only a few snapshots are shown, but whole series, packed into movies, are available as Supporting Information.[10]

For TMA, a series of 47 subsequent STM images was recorded; selected snapshots are presented in Figure 2a–c). The recording time for a single frame was approximately 20 s. Hence the whole movie (TMA1.mov, see Supporting Information) covers a time span of approximately 16 min. This series reveals fluctuations at domain boundaries between rotational and anti-phase domains. Rotational domains are characterized by different azimuthal orientations of the adsorbate lattice vectors (for example, the two domains at the left-hand side of Figure 2), whereas anti-phase domains are laterally translated by an integer number of substrate lattice vectors, although their extrapolated lattices do not coincide; an example is given by the two domains on

the right-hand side of Figure 2. It was found in previous studies that the primitive TMA lattice vectors, as sketched in Figure 1a, are tilted $\pm 5°$ with respect to the graphite $[\bar{1}2\bar{1}0]$ directions, which gives rise to two energetically equivalent rotational domains. The resulting incommensurability leads to a Moiré-like sixfold superstructure with a lattice constant of ≈ 10 nm, which can be recognized as a modulation of the apparent height in the STM images of Figure 2. The superstructure unit cell is marked by arrows in Figure 2b. To allow the superstructure to be discerned more easily, a different color coding was applied to the domain at the lower right side. Substrate-induced Moiré patterns are well known from other adsorbate–substrate combinations.[11] Since the graphite substrate exhibits a threefold symmetry and the adsorbate a sixfold symmetry only two different, equally favored rotational domains exist.

In the STM images of TMA grain boundaries, only fluctuations without a lasting exchange of molecules were observed. Single six-membered TMA rings build up and decay again at the domain boundaries; it essentially appears that the molecules are just going back and forth between adja-
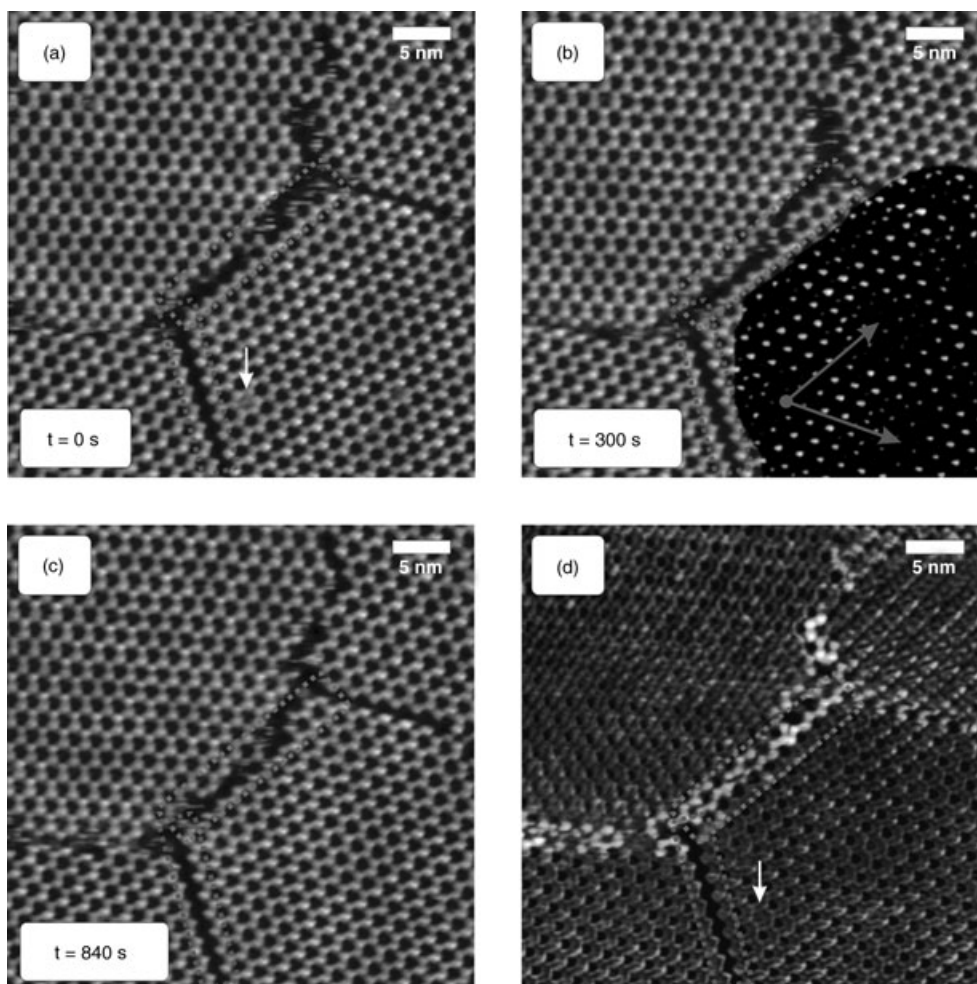

Figure 2. a–c) Selected snapshots of a series of STM images of TMA domain boundaries (40 × 40 nm²). Only slight changes happen directly at the domain edge and the domain size and shape is mainly preserved; d) standard deviation of all 47 images of the series. Brighter shading indicate larger values of the standard deviation, and therefore represents regions that exhibit enhanced molecular dynamics. The Moiré pattern in (b) is discerned by the color coding of the island at the lower right. Arrows indicate the vectors of the sixfold superstructure. See the Supporting Information for color images.[10]

cent domains. Single molecules cannot be tracked here, although in particular cases, this becomes possible through chemically marked molecules.[12] Thus, a mechanism with desorption at one domain boundary and adsorption at the other cannot be excluded. However, the observation that the uncovered area between the domains remains nearly constant throughout the observation time favors the hypothesis of an exchange between the domains, rather than correlated adsorption/desorption events. An example is marked in Figure 2a–c) by the dashed rectangle in the center of the image. For this reason the shape and size of the TMA islands (that is, the nanostructure) is mainly preserved throughout the observation time. The close-packed domain boundaries between the two translated domains (marked by the second dashed rectangle) in the lower part of the image do not show any fluctuations at all and are extraordinarily stable. Apparently, dense-packed edges of TMA domains without any kinks are stable at room temperature.

In order to illustrate the fluctuations occurring in all frames in a single image, the standard deviation of 47 aligned images is shown in Figure 2d. The color coding of each pixel represents the value of the standard deviation of this pixel from all STM images at this position. During image acquisition it was necessary to compensate for drift; details are given in the Experimental Section. In principle, this standard deviation image represents a mapping of the dynamics. It can be seen that those non-close-packed domain boundaries exhibit a high value of the standard deviation (bright in the image and marked by the dashed rectangle in the center) and therefore indicate molecular fluctuations. In contrast, the close-packed anti-phase domain boundary in the lower right part (marked by the second dashed rectangle) of the image does not show any fluctuations at all in the standard deviation image. This more condensed view of the dynamics in the standard deviation image is also consistent with the STM movie (TMA1.mov), where single six-membered TMA rings assemble and disassemble at the domain edge during the time of observation. As evident in Figure 2d the standard deviation mimics the TMA lattice as well. The reason for this is a residual misalignment, which can be attributed to an imperfect drift correction during the measurement. Due to changes in the drift and/or superimposed drift correction, the measured lattice parameters, both length and angles, are slightly distorted and cannot be compensated for just by lateral alignment.

In the STM movie (TMA1.mov) some TMA cavities within the network show a transient adsorption of a molecular guest from the liquid phase. An example is marked in Figure 2a by the white arrow. An occupation of a TMA cavity during a single scanning frame is sufficient to be recognized in the standard deviation, with the white arrow in Figure 2d pointing to the very same cavity. These guests are most likely TMA molecules, likewise observed within the cavities of evaporated TMA films.[7] They can interact with the TMA lattice by means of weak H-bonds. However, since they are observed so rarely, their stabilization energy must be considerably lower. A detailed analysis of TMA as a guest molecule in the TMA chicken-wire polymorph will be published elsewhere.

It is also obvious that fluctuations of the TMA structure are spatially limited to the region of the domain boundary up to the first dense-packed edge of the TMA domain, which results in conservation of the island shape and size. In a second STM movie of TMA (TMA2.mov) however, one island grows at the expense of a rather small one (diameter ≈ 20 nm, marked by the dashed black circle in the first frame of the movie). This might be explained by the high ratio of edge molecules in these small islands. In other words, the relatively high line-energy of small islands, that is, the high ratio of circumference to area, renders them thermodynamically unstable. This process can be understood in the framework of Ostwald ripening. However, in the case of TMA, it was only observed for rather small islands. A further event in this movie is the coalescence of two islands (the respective grain boundary is marked by black arrows in the first frame of the movie). This can only happen if these are true domains (with the same rotational orientation and no translational displacement, that is, their extrapolated lattices coincide) by adsorption of linking TMA molecules from the liquid phase, thereby filling the gap between these two domains. Otherwise the merger of these two islands would have to be accompanied by a 1D defect, such as a dislocation.

In comparison, the TPA nanostructure is not quite as stable as that of TMA at the same temperature on a comparable timescale. Experimental evidence is given in Figure 3a–d) and the movie TPA1.mov by a sequence of STM images, where a smaller island with different rotational orientation is incorporated into the surrounding domain. This event can be seen as an example for the more general concept of Ostwald ripening. Again, the driving force is the minimization of free energy by avoiding additional energy costs at grain boundaries due to line energy. The smaller island, because of its higher circumference-to-area ratio, is thermodynamically less stable. The small hole in the monolayer shown in Figure 3d, which was left after the island had disappeared, was observed for an additional ≈ 10 min (TPA2.mov) until it was entirely closed by adsorption from the liquid phase. Although there is a huge number of TPA molecules offered in the liquid phase above, it takes a considerable amount of time to adsorb enough TPA molecules to finally close the hole. The movie TPA2.mov shows that many adsorption and desorption processes are actually necessary until a stable configuration is reached. On average, approximately 14 TPA adsorption sites are unoccupied during the movie with a standard deviation of ≈ 4 adsorption sites. The number of free adsorption sites in the hole versus time is depicted in Figure 4. Because the number of unoccupied TPA adsorption sites varies non-monotonically, it is assured that adsorption and desorption actually happens, but rearrangement of the TPA molecules within the hole might play a role as well. The lifetime of this hole is remarkably long. One possible explanation is offered by the kinetics of the system. A low concentration and/or mobility of TPA in the liquid phase would explain an exceedingly long life time. However, since TPA desorption events are observed as well (compare Figure 4), it is more likely that the hole can be considered as a separate 2D molecular gas
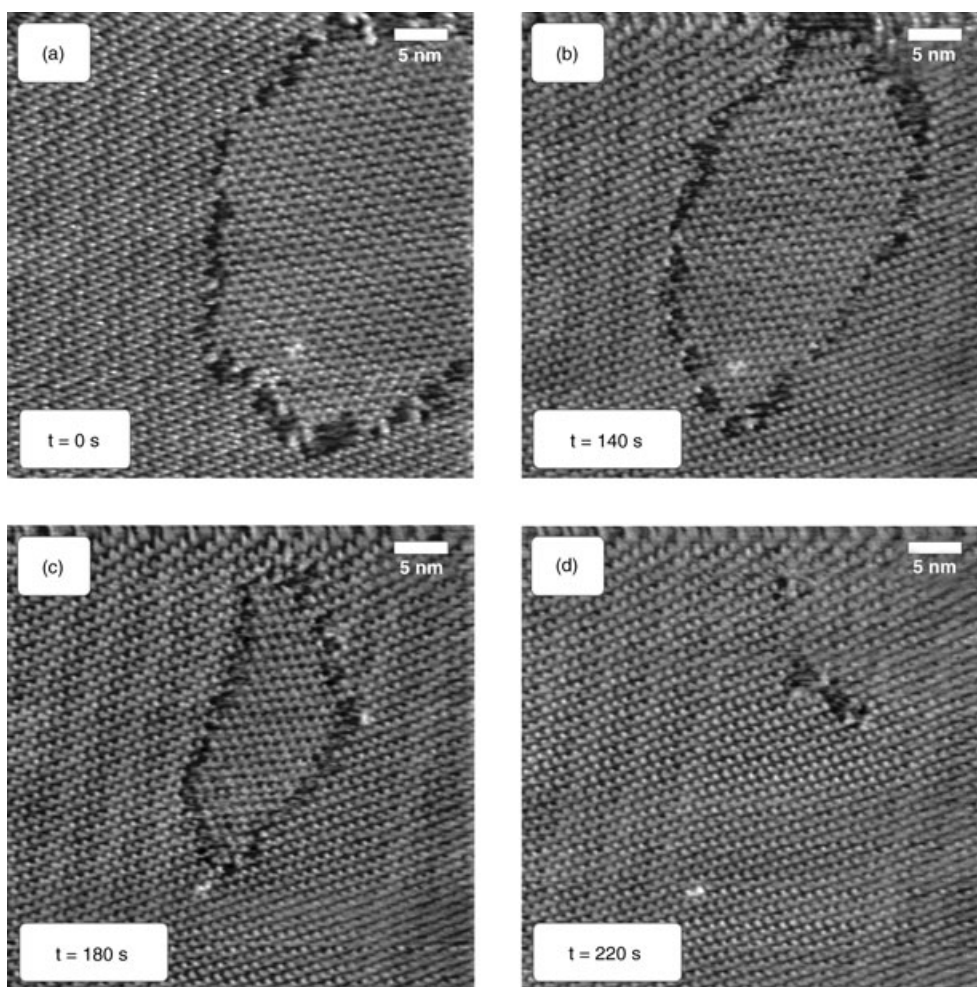
Figure 3. Series of STM topographs (43 × 43 nm²) of a TPA monolayer on graphite (0001). The images show a small island surrounded by a domain with different rotational orientation. From (a) to (c) the surrounding area is growing at expense of the small island until only a small hole with a size on the order of 10 TPA adsorption sites is left (d).
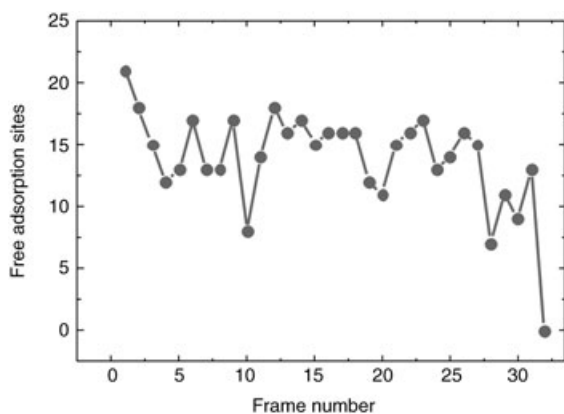

Figure 4. Number of free adsorption sites (corresponding to the size of the hole in Figure 3 d) versus frame number (one frame represents ≈ 20 s). The graph shows that adsorption (negative slope) and desorption (positive slope) events actually take place. Thus the number of free adsorption sites does not demonstrate a monotonic time dependence. The mean number of free adsorption sites amounts to ≈ 14 and the standard deviation to ≈ 4.

phase in equilibrium with the 2D crystalline phase. Because this separate phase has an average size of only 14 adsorption sites, it is too small to be thermodynamically stable and eventually disappears. STM images of the TPA monolayer on a larger scale and at different locations show both very large domains and small holes comparable to that shown in Figure 3d, which suggests the mechanism under discussion is important for reorganization processes in the TPA monolayer. Comparable small holes were found in domains of the equally 1D H-bonded networks of 2,6-naphthalene-dicarboxylic acid (NDA). Since the adsorption energy of NDA on graphite is larger due to its more extended π-electron system, the reorganization of the molecules takes place on a longer timescale. However, the appearance of comparable small holes within NDA islands might be a hint for a more general grain-coarsening mechanism in 1D H-bonded adsorbate layers.

The driving force for the disappearance of the smaller enclosed TPA island is of thermodynamic origin, namely the minimization of the free energy by the elimination of domain boundaries, which cause additional energy costs due to their line energy. But what is the physical reason that

domain boundaries of the TMA network are stable for several 10 min, whereas TPA domain boundaries reorganize and even vanish within several minutes? Apparently this experimental observation must be related to the line energies of both structures. From the models in Figure 1 it is evident that the sixfold symmetry of the TMA lattice results in three equivalent dense-packed domain boundaries with angles of 120° and 240° between each other, respectively. On the contrary, the TPA structure only has a twofold symmetry. This fact leads to two vastly different domain boundaries, where edge molecules differ in the number of formed H-bonds and consequently their binding energy. Thus, TPA domains exhibit facets with a considerably lower binding energy of the edge molecules, which gives rise to the observed highly dynamic behavior.

In order to obtain a quantitative estimate for the binding energies of edge molecules, molecular mechanics simulations with a Dreiding II force field,[13] which includes a specific term for H-bonding, were performed. First, the orientations of the molecules within the unit cells were determined by applying periodic boundary conditions and using the lattice parameters determined by calibrated STM measurements as a constraint.[6] The calibration was achieved by recording images with one half showing the adsorbate layer and the other half the substrate lattice, thereby using the atomic lattice of the substrate as an intrinsic ruler. The fast Fourier transform (FFT) of these split images allows for a precise determination of the superstructure matrix. The following energy minimization yields refined information about the orientation of the molecules within the unit cell. According to Figure 1 the TMA structure has two molecules per primitive unit cell, while TPA only has one. These optimized unit cells were used as a base to create finite islands as depicted in Figure 5. In order to include edge effects like structural relaxation due to the lower coordination of edge molecules, an additional energy minimization of the finite islands was performed. For this second minimization molecules within the island, which are sufficiently far away from the edge, were kept fixed. Finally, the binding energy of the various edge and corner molecules was calculated as the difference in total energies for configurations with the molecule under consideration in place and when "infinitely" far away. In this case the "binding energy" is comprised of the sum of lateral binding and desorption energies. In these calculations the influence of the liquid phase above is neglected. However, a comparison of TPA and TMA edge-binding energies is justified. The corresponding binding energies are depicted in Figure 5 for both TMA and TPA. The intuitively attributed higher stability of the TMA domain boundary is confirmed by the molecular mechanics simulations. One type of edge molecule exhibit a total of four H-bonds (two per carboxylic group) and a relatively high binding energy of 1.87 eV, while the second type of edge molecule is sixfold H-bonded, and the binding energy amounts to 2.21 eV due to the contribution of an additional two H-bonds. The situation is rather different for TPA on graphite, as shown in Figure 5b. Because of the molecular structure of TPA, a maximum of four H-bonds can be formed both within an island and at the edge, which results in a maximum binding energy
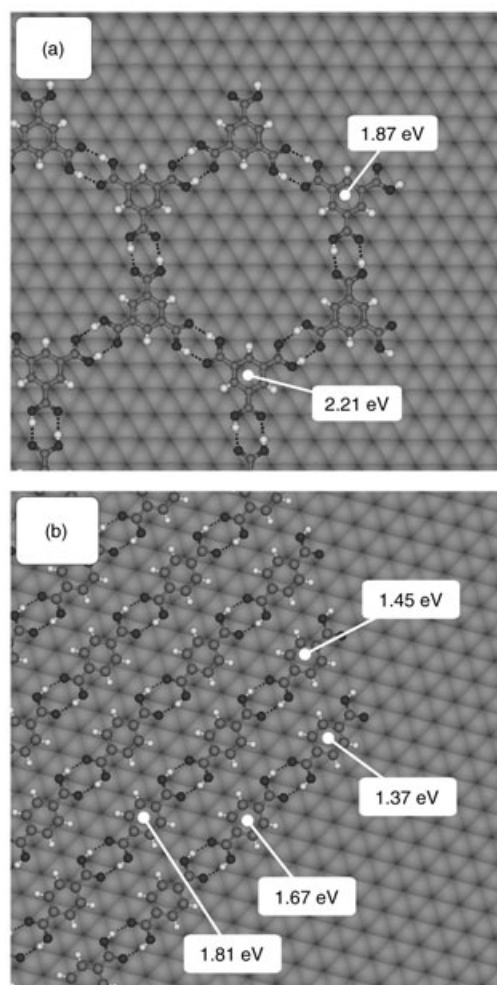

Figure 5. Molecular mechanics simulations of finite islands of a) TMA and b) TPA were utilized to obtain an estimate for the binding energy of edge molecules. Two adjacent carboxylic acid groups form two H-bonds, symbolized by black dotted lines. The corresponding binding energies of nonequivalent edge molecules are indicated within the models. TPA islands show two substantially differing facets with the edge molecules being bound by either two or four H-bonds, which results in a significant difference in binding energy of 1.67−1.45 eV = 0.22 eV.

of 1.87 eV and 1.67 eV, respectively. However, for a finite TPA domain only two facing edges can benefit from the stabilization through four H-bonds. On the other edges TPA molecules form only two H-bonds and their binding energy is considerably lower at 1.45 eV. The TPA corner molecule is the lowest-coordinated molecule of this island and lacks Van der Waals stabilization from a second next-nearest neighbor, which is expressed in the lowest observed binding energy of 1.37 eV. These huge differences in binding energies explain the experimentally observed differences in the timescale of domain-boundary dynamics.

Although the accuracy of the absolute values of binding energies determined by purely classical molecular mechanics simulations is highly questionable—for example, the liquid phase is neglected and important interactions like mirror charges in the semimetal graphite are not included—

they are suited for a direct comparison and confirm the intuitively obvious difference in binding energies of TMA and TPA edge molecules. Most of the binding energy differences of edge molecules can be attributed to a different number of H-bonds, owing to the molecular structures and symmetries of TMA and TPA respectively. Both the experimental results and the simulations unambiguously prove the dominating influence of H-bonds in supramolecular assemblies of these rather small molecules.

3. Conclusions

Room-temperature video-STM at the liquid–solid interface was utilized to compare the temporal evolution of the nanostructure (that is, the molecular dynamics at grain boundaries) of one-dimensionally (TPA) versus two-dimensionally (TMA) H-bonded supramolecular structures. The 1D-networked TPA structure is comprised of densely packed, H-bonded linear chains of molecules. By means of a series of STM images it was possible to show that larger TPA domains grow at the expense of smaller domains on a timescale of minutes. The coarsening of the nanostructure can be considered as an example of the more general concept of Ostwald ripening. Since the TPA lattice exhibits only a twofold symmetry, two vastly different facets exist, with the edge molecules exhibiting a remarkable variation in binding energies. Therefore, the domain boundaries, where edge molecules are bound by two H-bonds only, are the starting points for structural changes and reorganization respectively in the monolayer. Furthermore, adsorption and desorption events within a small hole in the TPA monolayer were tracked on a single-molecule level, until the hole eventually had been entirely closed by adsorption of TPA from the liquid phase.

In comparison, due to the sixfold symmetry of the structure, TMA islands have three equivalent domain boundaries where edge molecules have even larger binding energies than in the TPA structure. The main reason is that TMA edge molecules are bound by at least four H-bonds, whereas one facet of the TPA edge molecules exhibits only two H-bonds. Consequently the TMA domain boundaries are relatively stable at room temperature, and the shape and size of islands is mainly preserved, except for very small islands. This is also in accordance with the binding energy of edge molecules as estimated for both systems by molecular mechanics simulations. In summary, by the combination of experimental results from STM measurements with theoretical calculations of edge-molecule binding energies it was possible to consistently demonstrate the relationship between symmetry, the bonding scheme of the H-bonded supramolecular structure, and the molecular dynamics at grain boundaries.

4. Experimental Section

All experiments were conducted at room temperature with a home-built, pocket-sized STM under ambient conditions. The microscope was driven by a commercial SPM-100 control electronics unit from RHK. Mechanically cut Pt/Ir tips were used, which were conditioned in situ by short (20–150 ms) voltage pulses. All images were obtained in the constant-current mode of operation with tunneling voltages in the range 0.5–1.5 V and reference currents of around 100 pA. Since our STM is by no means optimized for high scanning speeds, large images were recorded with a speed of ≈ 20 s per frame and smaller images with ≈ 10 s per frame. The supramolecular structures were prepared by applying a droplet of saturated solution on a freshly cleaved graphite (0001) surface. Heptanoic acid was used as a solvent for both TMA and TPA. At typical tunneling voltages this fatty acid is an insulator, and its vapor pressure is low enough for stable STM experiments in the order of 1 h. For noise reduction all images were leveled and processed with a 3×3 Gaussian filter. In order to image the same sample area despite large drifts (mostly thermal drift) a drift-correction algorithm was essential during the measurement. For this purpose a feature of the control software, which stabilizes the position of a randomly chosen, unambiguously recognizable feature in subsequent scanning frames was used. Except for the TPA main movie (TPA1.mov), all images were additionally aligned during image processing before merging them into a movie. The maximum of the cross-correlation with a master image gives coordinates for the necessary lateral displacement. The duration of the observation period was mainly limited by the stability of the STM tip or by solvent evaporation.

In case of thermally activated processes the temperature is the most important adjustable parameter to match the timescale of the dynamics and the scanning speed. In contrast to UHV experiments the sample temperature cannot be varied greatly for experiments at the liquid–solid interface. However, for both systems under investigation the timescale of the dynamics at room temperature was appropriate to monitor changes with a scanning speed of 10–20 s per frame.

[1] a) C. V. Thompson, *Annu. Rev. Mater. Sci.* **1990**, *20*, 245–268; b) J. E. Taylor, J. W. Cahn, C. A. Handwerker, *Acta Metall. Mater.* **1992**, *40*, 1443–1474; c) F.-J. Meyer zu Heringdorf, M. C. Reuter, R. M. Tromp, *Nature* **2001**, *412*, 517–520.
[2] a) A. K. Kar, A. Dhar, S. K. Ray, B. K. Mathur, D. Bhattacharya, K. L. Chopra, *J. Phys. Condens. Matter* **1998**, *10*, 10795–10804; b) M. J. Rost, D. A. Quist, J. W. M. Frenken, *Phys. Rev. Lett.* **2003**, *91*, 026101–026104.
[3] a) J. P. Rabe, S. Buchholz, *Phys. Rev. Lett.* **1991**, *66*, 2096–2099; b) R. Heinz, J. P. Rabe, W. V. Meister, S. Hoffmann, *Thin Solid Films* **1995**, *264*, 246–249; c) M. Hibino, A. Sumi, I. Hatta, *Thin Solid Films* **1996**, *273*, 272–278; d) D. Wouters, S. Hoeppener, R. Lunkwitz, L. F. Chi, H. Fuchs, U. S. Schubert, *Adv. Funct. Mater.* **2003**, *13*, 277–280.
[4] a) W. M. Heckl, D. P. E. Smith, G. Binnig, H. Klagges, T. W. Hansch, J. Maddocks, *Proc. Natl. Acad. Sci. USA* **1991**, *88*, 8003–8005; b) J. V. Barth, J. Weckesser, C. Cai, P. Günter, L.

Bürgi, O. Jeandupeux, K. Kern, *Angew. Chem.* **2000**, *112*, 1285–1288; *Angew. Chem. Int. Ed.* **2000**, *39*, 1230–1234; c) M. Bohringer, K. Morgenstern, W. D. Schneider, R. Berndt, F. Mauri, A. De Vita, R. Car, *Phys. Rev. Lett.* **1999**, *83*, 324–327; d) T. Yokoyama, S. Yokoyama, T. Kamikado, *Nature* **2001**, *413*, 619–621; e) S. De Feyter, F. C. De Schryver, *Chem. Soc. Rev.* **2003**, *32*, 139–150.

[5] a) A. Dmitriev, N. Lin, J. Weckesser, J. V. Barth, K. Kern, *J. Phys. Chem. B* **2002**, *106*, 6907–6912; b) J. Lu, Q.-d. Zeng, C. Wang, Q.-y. Zheng, L. Wana, C. Bai, *J. Mater. Chem.* **2002**, *12*, 2856–2858.

[6] M. Lackinger, S. Griessl, T. Markert, F. Jamitzky, W. M. Heckl, *J. Phys. Chem. B* **2004**, *108*, 13652–13655.

[7] S. Griessl, M. Lackinger, M. Edelwirth, M. Hietschold, W. M. Heckl, *Single Mol.* **2002**, *3*, 25–31.

[8] a) A. Stabel, R. Heinz, F. C. De Schryver, J. P. Rabe, *J. Phys. Chem.* **1995**, *99*, 505–507; b) P. Samori, K. Müllen, J. P. Rabe, *Adv. Mater.* **2004**, *16*, 1761–1765.

[9] a) S. J. H. Griessl, M. Lackinger, F. Jamitzky, T. Markert, M. Hietschold, W. M. Heckl, *J. Phys. Chem. B* **2004**, *108*, 13652–13655; b) S. Griessl, M. Lackinger, F. Jamitzky, T. Markert, M. Hietschold, W. M. Heckl, *Langmuir* **2004**, *20*, 9403–9407.

[10] The movies (and further graphical information) are available as *.mov files for download as Supporting Information from the *Small* website: http://www.small-journal.com.

[11] a) J. P. Rabe, S. Buchholz, *Science* **1991**, *253*, 424–427; b) M. M. Reiter, F. Jamitzky, F. Trixler, W. M. Heckl, *Phys. Status Solidi A* **2001**, *187*, 171–176; c) F. Sellam, T. Schmitz-Hubsch, M. Toerker, S. Mannsfeld, H. Proehl, T. Fritz, K. Leo, C. Simpson, K. Müllen, *Surf. Sci.* **2001**, *478*, 113–121.

[12] A. Gesquière, M. M. Abdel-Mottaleb, S. De Feyter, F. C. De Schryver, M. Sieffert, K. Müllen, A. Calderone, R. Lazzaroni, J.-L. Brédas, *Chem. Eur. J.* **2000**, *6*, 3739–3746.

[13] S. L. Mayo, B. D. Olafson, W. A. Goddard, III, *J. Phys. Chem.* **1990**, *94*, 8897–8909.

2. Additional Material

Additional material to this thesis:

- Chapter 4.4: M4: Dynamics of Grain Boundaries in Two-Dimensional Hydrogen-Bonded Molecular Networks

  o movie1_TMA-1.mov
    47 subsequent STM images of TMA grain boundaries at the liquid solid interface (40 x 40 nm², ~20 s/frame). The movie covers a time span of ~16 min. Fluctuations of molecules in the vicinity of the grain boundaries can be seen, but the island size and shape is mainly preserved.

  o movie2_TMA-2.mov
    40 subsequent STM images of TMA grain boundaries at the liquid solid interface (125 x 125 nm², ~20 s/frame). The movie covers a time span of ~13 min.
    The drift compensation was not perfect for this movie, therefore the observed area is wandering. A small island (~ 20 nm) disappears (marked by the black dashed circle in the first frame) and two islands coalesce (marked by black arrows in the first frame).

  o movie3_TPA-1.mov
    23 subsequent STM images of TPA grain boundaries at the liquid solid interface (35 x 35 nm², ~20 s/frame). The movie covers a time span of ~8 min.
    A small island is incorporated into the surrounding domain, which differs in the rotational orientation of the TPA lattice with respect to the substrate. Eventually, only a small hole with a size in the order of 10 TPA adsorption sites remains.

  o movie4_TPA-2.mov
    32 subsequent STM images of TPA grain boundaries at the liquid solid interface (16 x 16 nm², ~10 s/frame). The movie covers a time span of ~6 min.
    Many adsorption and desorption processes occur until the hole in the TPA monolayer is completely closed.

- Chapter 4.5.2: Comparing Three Similar One-Dimensional H-bonded Molecules

  o movie5_NDA.avi
    36 subsequent STM images of an NDA monolayer at the liquid solid interface (54 x 54 nm², ~21 s/frame). The movie covers a time span of ~12 min.
    This movie shows the slow but steady growth of domains in an NDA monolayer.

o   movie6_BPDA.avi
     16 subsequent STM images of an BPDA monolayer at the liquid solid interface
     (54 x 54 nm², ~21 s/frame). The movie covers a time span of ~5 min.
     Starting from an impurity on the left bottom corner, and several point defects in
     the middle of the image, the whole BPDA monolayer is disassembling quickly.

o   movie7_SDA.avi
     94 subsequent STM images of an SDA monolayer at the liquid solid interface
     (80 x 80 nm², ~21 s/frame). The movie covers a time span of ~33 min.
     The drift compensation was not perfect for this movie, therefore the observed
     area is wandering. This movie shows the reorganization of domains and growth
     on behalf of smaller domains (Ostwald ripening). The second domain from the
     left is disassembled and overgrown by neighboring domains. After the
     reordering was finished and stable over several frames, a voltage pulse of 2.98V
     was applied after frame 59. In the following frame the structure is severely
     damaged in the upper right corner, but healing quickly in the subsequent frames.

The material can be found on the CD attached, or in the internet at
www.kampschulte.org/diss.

3. Acknowledgements

4. CV

since 10/06   scientific assistant at the Deutsches Museum, Munich

04/06 – 07/06 research stay in the group of Prof. E. Altman at Yale University / New Haven
Investigation of molecular adsorption on piezoelectric substrates
(fellowship of the German Academic Exchange Service (DAAD))

11/04 – 02/05 research stay in the group of Prof. G.W. Flynn at Columbia University / New York
Scanning tunneling microscopy at the liquid solid interface and in UHV
(fellowship of the German Academic Exchange Service (DAAD))

since 10/03   graduate student in the group of Prof. W.M. Heckl at the Ludwig-Maximilians-University, Munich

10/01 – 10/03 master studies "Micro- and Nanotechnology" at the University of Applied Sciences, Munich
- 9-month internship at the Dept. for Earth- and Environmental Sciences, Ludwig-Maximilians-University, Munich, assistance in setting up a UHV chamber
- 6-month internship at Infineon Technologies AG, Munich, physical failure analysis of semiconductors
master thesis: "TDS investigations of trimesic acid on gold(111) surfaces"
qualification: Master of Engineering, final grade 1.3

08/01 – 10/01 internships at the University of Applied Sciences, Munich
(vacuum and thin film technology laboratory, micro system technology laboratory)

10/00 – 07/01 consultant at MLP Finanzdienstleistungen AG / Rosenheim, a financial services company

10/96 – 02/01 undergraduate studies "Wood Technology" at the University of Applied Sciences, Rosenheim
6-month internship at Norservice Interiør, Støren, Norway
qualification: diploma, final grade 1.9

10/95 – 07/96 basic military service

09/82 – 07/95 primary and secondary school
qualification: "Abitur" (general qualification for university entrance), final grade 2.8